SUBTAIN RASOOL
01-244221-005

Optimal Position Fuzzy SMC Control for Movement Coordination of Two Finger Model

Masters of Science in Electrical Engineering

Supervisor: ENGR.MARYAM IQBAL

Department of Electrical Engineering
Bahria University, Islamabad

March 21,2022

MS-13
Thesis Completion Certificate

Student Name: **Subtain Rasool** Registration Number: **52793**
Program of Study: **Masters of Science in Electrical Engineering**
Thesis Title: **Optimal Position Fuzzy SMC Control for Movement Coordination of Two Finger Model**

It is to certify that the above student's thesis has been completed to my satisfaction and, to my belief, its standard is appropriate for submission for evaluation. I have also conducted plagiarism test of this thesis using HEC prescribed software and found similarity index at **10%** that is within the permissible set by the HEC. for MS/MPhil/PhD.

The thesis is also available in a format that the BU accepts for MS/MPhil/PhD thesis.

Principle Supervisor's Signature:_____
Principle Supervisor's Name: ENGR.MARYAM IQBAL
March 26, 2024

MS-14A
Author's Declaration

I, **Subtain Rasool** hereby state that my MS thesis titled **"Optimal Position Fuzzy SMC Control for Movement Coordination of Two Finger Model"** is my own work and has not been submitted previously by me for taking any degree from **"Bahria University, Islamabad"** or anywhere else in the country / world.

The university has the power to revoke and annul my MS degree at any time if it is discovered that my statement was false, even after I have graduated.

SUBTAIN RASOOL
01-244221-005
March 26, 2024

MS-14B
Plagiarism Undertaking

I, **Subtain Rasool** solemnly declare that research work presented in the thesis titled

Optimal Position Fuzzy SMC Control for Movement Coordination of Two Finger Model

is solely my research work with no significant contribution from any other person. Small contribution / help whenever taken has been duly acknowledged and that complete thesis has been written by me.

I understand the zero tolerance policy of Bahria University and the Higher Education Commission of Pakistan towards plagiarism. Therefore, I as an author of the above titled thesis declare that no portion of my thesis has been plagiarised and any material used is properly referred / cited.

I undertake that if I am found guilty of any formal plagiarism in the above titled thesis even after award of MS degree, the university reserves the right to withdraw / revoke my MS degree and HEC and the university has the right to publish my name on HEC / University Website on which name of students who submitted plagiarised thesis are placed.

SUBTAIN RASOOL
01-244221-005
March 26, 2024

Dedication

I dedicate this dissertation to my supervisor for her unconditional support and encouragement, my class fellows for their affection and patience.I am very thankful to my parents who gave me both the moral and financial support needed to achieve the milestone.

Acknowledgments

I thank Almighty Allah for all His blessings also giving me the best opportunity and providing me strength and potential to complete my master's degree with thesis.

I am deeply indebted to my esteemed supervisor, Engr. Maryam Iqbal, whose guidance,unwavering support, and insightful feedback have been invaluable in shaping this research. Her expertise, dedication, and passion for knowledge have inspired me to strive for excellence in every aspect of my work. Her effective and well-defined approach to work has paid off countless achievements in the completion of this research work.

My sincere appreciation to all the Professors for their immense knowledge, without their teachings, it wouldn't be possible to accomplish my work. It is not enough to give credit only to my parents. I am thankful to my teachers who supported my research in every way. My university fellows, who always helped me whenever needed.

Furthermore, I am immensely thankful to my loving parents for their unconditional love, encouragement, and unwavering belief in my abilities. Their constant support, sacrifices, and belief in me have been the cornerstone of my success. I am forever indebted to them for instilling in me the values of hard work, perseverance, and integrity, which have guided me on this academic journey.

Abstract

The movement and mobility of the hand fingers are affected by various degrees of freedom. As both the ring and little finger cannot move independently, this research focuses on the movement, orientation, and control of these fingers. Neural synchronization connects the central nervous system with finger movements. We used the fuzzy logic controller (FLC) technique and sliding mode controller (SMC) to construct a theoretical framework for the bio-mechanical model of a partially damaged human hand, including the dynamics of inertial effect, muscle, damping, and stiffness. This investigation begins with determining how the ring and little fingers move and coordinate. Each of the five fingers has three degrees of freedom. In order to design, develop, implement, and analyze the effective performance of the controlled motion for each prosthetic joint of the little and ring finger to move independently and behave robustly despite the availability of adjacent finger movements, there is a need and requirement to design and implement an effective and optimized controller to actuate the motion of the ring and little finger joints. As the hand finger has multiple degrees of freedom and coordinate axis motions like roll, pitch, yaw, angular coordinates motion, and translational axis motions as well, the main focus and concern design objectives related to control the single coordinate axis motion control of three joints of finger as Proximal InterPhalangeal (PIP), Distal InterPhalangeal (DIP), and MetaCarpoPhalangeal (MCP) joints for little and ring finger dynamics. Control of the angular motion for the above-mentioned joints of the little and ring finger will be the design requirements of this research. In order to design, develop, and implement a robust and effective control architecture for any biomedical dynamics and mechanics of system control, it is required to define the system and its components completely and comprehensively. Fuzzy logic and the SMC-FLC control architecture will be designed and developed to control the nonlinear dynamic behaviour of joint angular motion or angular position control for all the joints, angle of ring, and little finger movements.

Contents

List of Figures

List of Tables

Acronyms and Abbreviations

CNS	Central Nervous System
DP	Distal Phalenge
IP	Intermediate Phalange
PP	Proximal Phalange
EOMs	Equations Of Motions
EMG	ElectroMyoGraphic Signal
IMU	Inertial Measurement Unit
SS	State Space
PIP	Proximal InterPhalangeal
DIP	Distal InterPhalangeal
MCP	MetaCarpoPhalangeal
FLC	Fuzzy Logic Controller
SMC-FLC	Sliding Mode Control- Fuzzy Logic Controller
DOF	Degree Of Freedom
FIS	Fuzzy Inference System
AMD	Active Mass Dampers

Chapter 1

Introduction

1.1 Introduction

In today's time, As we build prototypes and their interactions with the environment, control development for robotic hands continues to be a topic of interest in our efforts to replicate human-hand contact with our surroundings. The research has main focus on the movement and orientation coordination and control of ring and little finger as these fingers cannot be independently moved. There exist the neural coordination's between central nervous system and finger movements. In this research project initially the movement and coordination as well as relation between the ring and little finger is determined [1]. Due to the intricate mechatronic systems that allow us to hold, move, and use a variety of objects and equipment, the robotic hands that are being controlled make this challenging to do. As a possible and obtainable solution, we have focused on improving controls task in order to generate robust grasp to hold any object [2]. The fingers on the hand depend on a large number of degrees of freedom for their movement and mobility. The research focuses on coordination and control of movement and orientation because the ring and little fingers are incapable of moving independently. Neural coordination exists between the central nervous system and finger motions. Initially, the movement and synchronization of the ring and little finger are determined in this study effort. There are five fingers and each has three degrees of freedom (DOF). The hand's remarkable capacity to morph and adjust to various things is facilitated by its 23 degrees of freedom (DOF) [3]. In service robots and other difficult fields, the robot hand is crucial. Several laboratories and businesses, including NASA, have created some nice robot hands [4].
In order to make sure the precise, accurate, exact, uniform, and mutually coordinated movements, and motion of the little and ring finger so that there are no disruptions, fluctuations in angular motion of the fingers, it is required to design and develop the intelligent based

feedback dynamic linear control system [5].
The Central Nervous System (CNS) provides orders to the muscles that control the contraction and relaxation of the fingers. There are multiple joints of fingers names as DIP, PIP, MCP. These joint angles must be controlled in order to govern finger movements [6]. Figure1.1 is the basic structure of human hand.

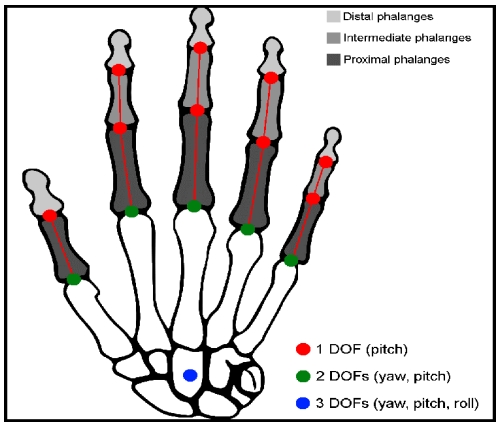

Figure 1.1: Kinematic Joints for hand Model

The DIP and PIP has single degree of freedom movement, so single actuator is required to acquire the movement, this movement is known as Pitch movement. The MCP has two degree of freedom motion, the motion is pitch and yaw motion [7] . In order to control the movement of MCP, there required two actuators. So, in order to design the feedback control system, it is required to define the dynamic model of joint actuators or identify the linear model of joint actuators so that the controlled signal must be applied to control the movement, and angular motion of actuators. The feedback commands and set reference commands will be obtained from EMG electromyography sensors [8].
The techniques employed to measure the range of motion of fingers have a major impact on the reporting of hand disabilities. Although the accuracy of the sensors used in data gloves from the literature has been determined thus far, more research is still necessary. In order to gather a variety of motion data for the distal interphalangeal, proximal interphalangeal, and metacarpophalangeal finger joints of an index finger, this research introduces an inertial measurement unit sensor-based data glove. The distal, proximal, and metacarpophalangeal finger joint sites on the glove were equipped with three inertial measurement sensors—the MPU-6050 and two flexible bend sensors—that can measure angle displacement in this research [9]. To achieve the intended, consistent, steady, efficient, and optimised output response of the concerned fingers, it is required to design and develop the robust and optimal controller that ensures the ability of disturbance rejections arise due to the dynamic movement effect of one finger over the other [10]. The generated dynamic biomedical system's nonlinear behaviour and characteristics must be linearized by the controller. To design, develop and implement the robust and optimal non-linear controller, initially the system mathematical model defining complete dynamics. As there exist three joints in

one finger so three degrees of freedom for little finger and three degrees of freedom for ring finger. The dynamic motion of these two fingers not independent, as there exist the dependency of moving one finger to the other.

1.2 Motivation and Problem Description

In the realm of rehabilitative robots, human hand motion control is a significant difficulty because of its many phalangeal joints, which offer excellent flexibility for completing a variety of tasks [11]. The basis of this research is a partial physical impairment. When a portion of the body is damaged and unable to function to its maximum potential at work, it is referred to as a partial handicap. As the movements of the little and middle fingers are not independent and cannot be moved independently rather than there exists the coordination between their movement and angular motion profile. For instance, a person unable to use two of their fingers cannot complete mundane tasks. A nonlinear controller governs the prosthetic hand's two-finger model in this investigation. The principle of superposition does not apply to nonlinear control. Since all systems in the real world are nonlinear, nonlinear controllers are applicable to real world systems. Using a controller that functions as an artificial brain to control these two fingers is difficult [12]. It is one of the challenges to design and develop the optimized controlled system that will be ensured the required mutually coordinated movements of the little and ring finger in precise, accurate and required angular motion profile should be achieved.

1.3 Research Objectives

The objectives include the following:

- To make sure the comprehensive dynamic mathematical modelling of fingers (ring and little finger) by using fundamental equations of motions (EOMs).
- Define and express the prosthetic hand fingers model in form of state space expressions or SS domain.
- Define and expressed the nonlinearity of finger motion dynamics in form of disturbance involved.
- Design, develop and implement the Fuzzy Logic controller with MATLAB to linearize the system and obtained the robust, effective, desired performance.
- Design and develop the fuzzy based Sliding mode control by proper defining of sliding surface with MATLAB-SIMULINK.

- Implement Sliding mode controller SMC integrated with Fuzzy logic controller FLC with developed prosthetic hand fingers to control the motion and obtained the desired and optimum results.
- Ensure the simulation based comprehensive analysis and make sure the comparison between the performances of developed controllers.

1.4 Limitations

The limitations always occur with some extension:

- Patients with mental disabilities should not utilize this procedure; severe partial impairment patients need to learn how to use a prosthesis [13].
- Individuals who have pacemakers, irrespective of the type of device they use, are not notified about it. In that scenario, they cannot use a two-finger prosthetic [14].
- It is improper to take it without FDA approval, yet as a pregnant lady, there are no adverse responses [15].
- It is not advisable to treat patients with brain, stroke, or transischemia using this technique as it can be lethal in these situations [16].

1.5 Thesis Organization

The thesis comprises of five chapters, Chapter 2 includes the literature work and comparative analysis of scholarly work done by researchers in terms of different controllers including linear and non-linear. Chapter 3 includes design and technical details of our proposed methodology and Chapter 4 comprises of experimental setup, the detailed discussion of different controller schemes and their results. The last chapter concludes our research work.

Chapter 2

Literature Review

The research is based on the development of transfer function models for touchless gesture-controlled movement of hands fingers. The concerned fingers are pointing finger, middle finger as well as thumb. The gesture pattern analyzed on the figures depending upon the pixels. The application of design is regarding to touchless system use like mouse pad etc [1]. The author published the article related to transferring the communis tendon of the index finger to the longus tendon and observe as well as analyze the movement of the finger with different orientation. The research ensures the successful approach of the index finger movements [2]. The article describes three-dimensional model identification, dynamic model consideration utilizing model prediction or model predictive controller implementation, and system identification for prosthetic hand long finger kinematics. Sliding mode control and model predictive control architectures were designed and developed to govern the dynamic movement of a system. The robust PID controllers are designed and implemented for each joint angle motion control of actuators with the desired motion control. Initially, the transfer function model for the actuators of the fingers of the gripper is determined, and then the controller and multiple input output robust PID controller are designed and implemented for the five-finger gripper design. The force muscle sensors are integrated for feedback measurements [3].

The research-based work is based on to design the bio mimetic prosthetic hand for human. The article investigates and analyzes comprehensively the study of the joint motion of the prosthetic hand. The IP, MP and CM joints movements are analyzed. The model of the hand and its components, like actuators, are developed. The angular orientations and movements of developed system results are plotted and analyzed [4]. Figure 2.1 is the basic structure of human hand finger exoskeleton.

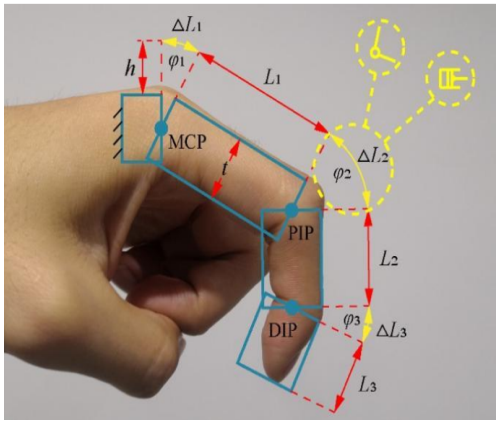

Figure 2.1: Basic design principle of hand finger exoskeleton

The research study describes and demonstrates an intelligent controller based on a Fuzzy logic infrastructure or control approach that is employed and applied to regulate the robust motion of PIP , MCP joints for the prosthetic hand finger under controlled conditions. The project is based on real time hand tracking for purpose of rehabilitation as well as character animations are ensured. The research is beneficiary for medically unfit or impartial people. The glove design is proposed to develop for motion and character animations for gaming etc. the IMU sensors are used to acquire the data of inertial measurements of coordinate axis movements. The real time movement of flexion as well as extension is ensured [5].
The research article related to develop the robotic system that has capability of hybrid impedance contact force tracking via adaptive hybrid control of Robot under uncertain external environment. The novelty of this project is to design the robust and adaptive control system based on impedance control for robot under dynamic forces of contact operations like painting etc. the older technique deals with control design for contact force without dynamic effects. The transient parameters are brought into considered like percentage overshoot, peak time, rise time etc [6].
The project is related to make sure the verification of joint of finger stiffness estimation via soft robotic actuator. Results are compared with SECA actuator response to obtained and estimate the stiffness model with designed mechatronic device and comparative analysis ensured [7].
The research-based article is related to develop the mathematical modelling and ensure the simulation-based analysis of finger movement via EMG sensor. The feedback sensory signals are obtained by electromyography sensor or EMG sensors to the controller. The Arduino micro-controller used as main control unit to acquire the data of EMG sensors and monitoring is ensured on display [8]. The article describes sophisticated control methods; however, the disruption impact owing to the availability of dependent nearby fingers movement is not considered [10]. This work introduces a novel hand exoskeleton rehabilitation equipment to facilitate tendon therapy exercises. The purpose of the exoskeleton is to support the fingers' natural flexion and extension movements. A direct-driven, optimally

tuned, and under-actuated serial linking mechanism with the capacity to apply extraordinarily high force levels perpendicularly to the finger phalanges makes up the suggested multi-degree-of-freedom (DOF) system. The suggested gadget has kinematic and dynamic models that have been developed. The multi-objective optimisation algorithm's output and a set of tests done to examine the capabilities of the human hand served as the foundation for the device's design [11].

Article describe the three-dimensional model identification and dynamic model consideration by using model prediction or model predictive controller implementation as well as system identification for the prosthetic hand long finger kinematics. Sliding mode control as well as Model predictive control architecture design and developed to control the dynamic movement for the dynamic system. Article describe the advanced control methods but the disturbance effect due to availability of dependency adjacent fingers movement does not consider [17]. Research article illustrate to design, develop as well as implemented the controlled scheme based on sliding Fuzzy logic controller algorithm to stabilize, regulate, controlled the transient as well as steady state performance of uncontrolled and non-stable prosthetic biomedical finger joint movement under controlled constraints. The research is novel but the disturbance effect due to the dependent movement of one finger over the other is not brought into considered [18]. Research work describe and demonstrate the intelligent controller based on Fuzzy logic infrastructure or control method used and practically applied to control the robust motion of PIP, MCP joints for the prosthetic hand finger under controlled constraints. The plant and kinematic manipulator dynamic and mechanic model exhibit the non-linear dynamics [19]. A wave variable-based control system was suggested by the author. In contrast to alternative approaches, the suggested strategy could reduce the performance deterioration brought on by time delay fluctuations. However, using this approach could lead to the system producing unlimited energy in certain unique circumstances and make it impossible to strictly ensure the system's stability. The technology is modified in this study by adding a monitoring mechanism for the energy input/output balance, which sets a limit on the amount of energy the system can produce. We worked with a single DOF system in several simulation studies. The findings of the simulation validate the suggested plan [20].

In order to stabilize, regulate, and control the transient as well as steady state performance for the uncontrolled and non-stable prosthetic biomedical finger joint movement under controlled constraints, research articles demonstrate how to design, develop, and implement a controlled scheme based on sliding fuzzy logic controller algorithm. Although the research is new, It ignores the interference that results from one finger moving dependently over the other [21, 22]. The human hand has been utilised to establish communication channels for a wide range of human-machine systems because of its numerous degrees of freedom and close ties to the brain. The purpose of this study is to offer quantitative evidence of the hand's efficiency as a communication medium. The authors have ensured

communication between the information capacity of thumb as well as the index finger. As there are a large number of degrees of freedom for hand motion, there are wide variety of communication with the brain. The research has ensured effective communication and cooperation between the movements of thumb and index finger [23].
The research work is related human finger independency, limitation to passive mechanical coupling versus active neuro muscular control. The research analyzes the thumb, index, middle, ring as well as little finger movement in form of angular position. the movements of DIP, PIP, MCP joints angle of finger is analyzed and observed [24]. In this article there is research about design and development of five finger robotic gripper. The plant and kinematic manipulator dynamic and mechanic models display nonlinear dynamics. The phase portraiture as well as controller effort energy reduction are not assured and taken into consideration, demonstrating the limits of the suggested study [25].
Working with lower-order models as opposed to high-order models can significantly simplify system analysis and control design. This research examines a biomechanical model with the minimum realisation of finger's reactive action when the pinky or little finger is bent. This model simulates the movements of two fingers and is of the sixth-order minimal state space realisation. To get the system to respond steadily, we created a H_2 robust controller. The answers of the minimal state space realisation model and the full-order state space model were compared. To improve the controller, exogenous inputs known as parametric uncertainty were included, and the values were adjusted [26]. This work presents an analysis of the impact of structured uncertainty on a model based on the involuntary flexion of the human ring finger when the little finger is bent. The performance of the controller is adjusted to reduce the impact of structural uncertainties and to limit their impacts. Additionally, there is less of an impact from input and measurement noise. The final model is demonstrated to be fully programmable, and the simulation's outcomes are entirely stable [27].
The project focuses on developing and implementing a time-varying sliding surface control algorithm for a SMC architecture designed to govern non-linear prosthetic hand and finger joint movement [28]. The established model and kinematic structure for system and plant dynamics represent nonlinear dynamic behavior, with feedback linearization providing system stability [29]. This study uses the 33-story Riverside Sumida Central Tower in Tokyo, Japan, which was designed and built by Obayashi Corporation, to test the resilient H_∞ state feedback control theory presented in Part 1. This structure's two active mass dampers (AMDs), which are situated on the roof, can regulate vibrations brought on by light disturbances. For these AMDs, study creates robust $H\infty$ controllers that take actuator saturation and structural uncertainty into consideration. The trade-offs between expected peak actuator effort and robust, worst-case closed-loop system performance are presented, and several H_∞ controllers are constructed. When small-magnitude loadings are applied to the structure/control model utilised in this study, robust H_∞ controllers perform better at

reducing transient vibrations of the structure than conventionally constructed LQR controllers. The parameters obtained, both transient and steady state, are robust and effective. The phase profiles, actuator force, and torque values are not investigated in this study, and control efforts are not lowered; these are the research article's shortcomings [30, 31]. Research-based work is related to designing and implementing the time-varying sliding surface control algorithm of sliding mode controller architecture developed for non-linear prosthetic hand-finger joint movement control. The obtained model and kinematic structure for the system and plant dynamics represent the non-linear dynamic behavior, and feedback linearization is ensured to stabilize the non-linear system. transient as well as steady state parameters obtained are robust and effective [32]. The phase portraits, actuator force, and torque values are not considered in this research, and control efforts are not minimized; these are the deficiencies of the research article [33].

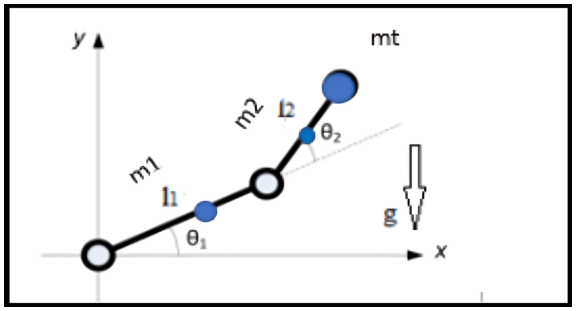

Figure 2.2: 2-DOF Single finger Model.png

Technical based research article demonstrated the Bjørngaard. The Hunt Study examined changes in health during a five-year period prior to and following disability payment. The way the joints move physically over time is tracked, examined, and the effectiveness of the created model is examined and researched [34].

The research-based article describes the technical and effective algorithm regarding to pattern recognition and movement profile analysis for the prosthetic hand [35]. The movement of the hand according to recognized and machine-oriented pattern generated is tracked as reference. The saturation's and limits applied to restrict the movement are not failures and confined pattern for the prosthetic hand analyzed as well as investigated [36, 37].

According to the research-based paper, an artificial leg model is subjected to a hybrid learning process known as adaptive neuro fuzzy inference system in order to determine the proper locations of the servomotors that actuate the leg joints. Efficiently calculating the correct joint angles for a space trajectory is a critical control problem for mechanical arms and legs. The usefulness of ANFIS for these kinds of mechanical systems is confirmed, despite the fact that Only the most basic model is represented by this software with two degrees of freedom. ANFIS is used to translate the experimental planar motion of the ankle joint into joint angles, which are then roughly represented by polynomial functions

in the gait model of the proposed mechanism. The chosen servomotors are run by a hybrid control system that consists of a PD controller and an FLC controller. On Sim-Mechanics, the control system's precision is further confirmed [38]. The article describes that one option for assisting an amputee in regaining their capacity to walk is a prosthetic leg. As a result, the majority of the knee components that are now in use are still unable to generate active body propulsion. Thus, in order for the amputee to move, a larger metabolic energy expenditure is needed. Therefore, the concept of creating an ANFIS knowledge-based control system and mechanical structure for the active actuated knee joint of a transfemoral (TF) prosthetic limb was put forth in this study. While the actuated knee joint was constructed using Inventor CAD software, ANFIS was adopted utilising Matlab software to analyse human gait phase recognition required for cadence and torque management required by the knee joint mechanism. In terms of the knee mechanism, the physical simulation of the controller offered a realistic simulation of the actuated knee joint [39]. Robotic hands that are dexterous must have a strong neural-machine interface that can recognise and interpret various finger actions. Previous research focuses mainly on single-finger movement or largely depends on multi-finger data for training the decoder, which necessitates large processing demands and large datasets. In order to train a neural decoder that can predict the forces of unknown multi-finger combinations, we examined in this study the viability of employing limited single-finger surface electromyogram (sEMG) data. Methods: To forecast the extension and flexion forces of the index, middle, and ring-little fingers simultaneously, we used a deep forest-based neural decoder. With constrained conditions (i.e., single-finger data), we used different quantities of high-density EMG data to train the model. Conclusions: Our findings demonstrated that the deep forest decoder could consistently outperform the convolutional neural network approach and conventional EMG amplitude method, with 7.0% of force prediction errors and an R^2 value of 0.874 [40]. The 2-dimensional matrix stiffness method, which the author utilised, makes it simple to perform numerical estimations using software. They can now identify the force applied in a certain direction on a finger and perform various stiffness tasks, such as finger flexion and extension, using 2-D analysis. The end product of this modelling provides manipulators with a deeper comprehension of mechanical impedance [41]. Underactuated mechanical systems present unique challenges in terms of meeting the control requirement. An underactuated truss-like robotic finger (UTRF) is a specific and intricate underactuated mechanical device that is explored by defining its dynamic model. High nonlinearity, model inaccuracy, and uncertainty are among the control issues. Given that type-2 fuzzy logic control is capable of handling uncertainties and does not require an accurate description of the controlled object, it is thought to be an appropriate solution to these challenges. For UTRF to achieve stabilisation at its equilibrium point, an interval type-2 fuzzy logic controller is constructed based on a brief overview of type-2 fuzzy logic systems [42] .

The objective of this research is to provide an adaptive fuzzy hierarchical sliding mode control approach to address the uncertain under-actuated switching nonlinear systems with actuator defect control problems. First, for the actuator problems, both the bias fault and the loss of efficacy are taken into account. Next, using fuzzy logic systems' (FLSs) approximation capability, the unknown, uncertain functions of the under-actuated switching nonlinear system are approximated. The upper bound of the actuator faults' bias signal and the error terms resulting from FLSs are combined into a function, the upper bound of which is estimated online. Moreover, the introduction of the projection algorithm can effectively handle the unique problem of denominators. By using the Lyapunov stability theory, we can confirm the boundedness of all the signals in the closed-loop system based on our suggested control approach [43].

In this paper, the author coupled fuzzy logic systems with nonlinear techniques in order to create adaptive control systems. The author suggested using an FLC in conjunction with a sliding-mode method to regulate systems that are underactuated. To demonstrate the effectiveness of the closed-loop system, the authors included a thorough stability study as well as a numerical example of a non-specified system. The fuzzy system isn't optimised, though. Optimisation techniques have proven beneficial in tackling the intricate task of determining suitable parameter values and structure for fuzzy systems [44].

In this paper author presents the ideal position control of a robotic finger that is underactuated. To mimic the flexion and extension movements of the finger, two trajectories are proposed: one for the proximal and another for the medial phalanx. Because the system does not have a clear dynamical model, Mandani fuzzy control is suggested. An optimisation technique based on the membership functions is used to acquire the control parameters. In various applications, genetic algorithms (GA) are frequently employed as an optimisation technique. Nevertheless, in this instance, an autoadaptive differential evolution method is suggested to achieve improved convergence behaviour [45].

Chapter 3

Methodology

On the basis of kinematics and biomechanics numerical information on finger movements, It is possible to identify the finger dynamic motion model with the use of a system identification tool. Depending upon the profile motion, the transfer function or state space expression of the ring and little finger dynamic model is determined and identified.

3.1 Algorithm / Design procedure

Initially, the movement or angular motion profile as analyzed in [46, 47] for the ring and little finger is analyzed completely and comprehensively.

1. Motion profile of ring and little finger angular movement is observed with the muscle sensors Inertial measurement unit IMU [9] and extract the finger joint data and develop the respective angular movement profile of little and ring finger.

2. Design the intelligent based Fuzzy logic controller for the system. Figure 3.1 is the block diagram for the proposed model.

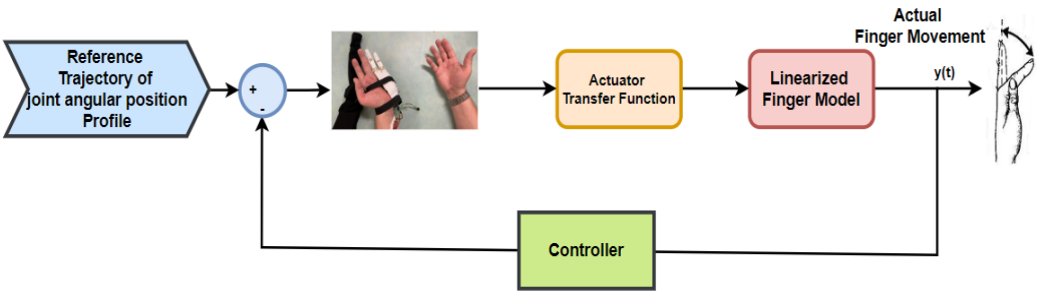

Figure 3.1: Fuzzy Logic Architecture.

3. Develop the mathematical linear model for finger joints actuators in from of transfer function expressions or state space model expressions.

4. Make sure to develop the feedback control linearized system via intelligent based fuzzy logic controller for dynamic movement of fingers and obtain the required motion profile or angular movement of little and ring finger.

5. Ensure the simulation-based analysis of system and obtain the dynamic behavior results of rehabilitee hand finger movement outcomes and also ensure the comparative analysis of designed and developed system model.

3.2 Mathematical Modelling

The mathematical expression for the dynamic model of finger is developed with all joint dynamic movements and motion in form of transfer function or state space model expression. The ring and little finger have multiple joints to move and acquire the required motion of hand. Each joint has respective actuator. The two degree of freedom movements required two actuators.

3.2.1 Ring finger dynamics

The Freebody diagram of Ring finger along inertia, damping and stiffness components can be developed in form of figure below. Figure 3.2 is the block diagram for the proposed model.

The damper offered the resistive effect, spring offered the stiffness as well as inertia

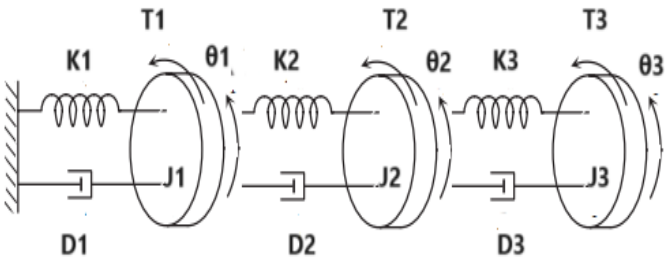

Figure 3.2: Freebody Diagram of ring finger.

offered the rotational angular movement for joints named as PIP, DIP and MCP of finger dynamics.

Rotational torque offered by first MCP joint.

$$T = J_1 \frac{\mathrm{d}^2\theta}{\mathrm{d}t^2} \tag{3.1}$$

Nonlinear Inertial Effect [48]:

$$T = ml^2 \sin\theta \frac{d^2\theta}{dt^2} \tag{3.2}$$

Damping effect on MCP joint movement [49]:

$$T = D\theta' \tag{3.3}$$

Stiffness of MCP joint due to torque [50]:

$$T = k(\theta + \theta^2) \tag{3.4}$$

Inertial effect, damping as well as stiffness offered by PIP and DIP joints will be considered as same.

Equation of motion:

We extend our formulation of an equation of motion for finger movement with the help of the principle of equivalency. None of the challenges associated with the covariant extension of the Lorentz-Dirac equation [51, 52] are present in the suggested equation of motion.

$$m_1 l_1^2 \sin(\theta_1)\frac{d^2\theta_1}{dt^2} + D_1\frac{d\theta_1}{dt} + k_1(\theta_1 + \theta_1^2) + k_2(\theta_1 + \theta_1^2) - k_2(\theta_2 + \theta_2^2) + D_2\frac{d\theta_1}{dt} - D_2\frac{d\theta_2}{dt} = 0 \tag{3.5}$$

$$m_2 l_2^2 \sin(\theta_2)\frac{d^2\theta_2}{dt^2} + D_2\frac{d\theta_2}{dt} + k_2(\theta_2 + \theta_2^2) + k_3(\theta_2 + \theta_2^2) - k_3(\theta_3 + \theta_3^2) + D_3\frac{d\theta_2}{dt} - D_3\frac{d\theta_3}{dt} = 0 \tag{3.6}$$

$$m_3 l_3^2 \sin(\theta_3)\frac{d^2\theta_3}{dt^2} + D_3\frac{d\theta_3}{dt} + k_3(\theta_3 + \theta_3^2) - k_3(\theta_2 + \theta_2^2) + D_3\frac{d\theta_2}{dt} = 0 \tag{3.7}$$

$$\frac{\mathrm{d}\theta_1}{\mathrm{d}t} = \omega_1 \tag{3.8}$$

$$\frac{\mathrm{d}\theta_2}{\mathrm{d}t} = \omega_2 \tag{3.9}$$

$$\frac{\mathrm{d}\theta_3}{\mathrm{d}t} = \omega_3 \tag{3.10}$$

$$\frac{\mathrm{d}^2\theta_1}{\mathrm{d}t^2} = \alpha_1 \tag{3.11}$$

$$\frac{\mathrm{d}^2\theta_2}{\mathrm{d}t^2} = \alpha_2 \tag{3.12}$$

$$\frac{\mathrm{d}^2\theta_3}{\mathrm{d}t^2} = \alpha_3 \tag{3.13}$$

Using expression (3.5)

$$m_1 l_1^2 \sin(\theta_1)\alpha_1 + D_1\theta_1' + k_1(\theta_1 + \theta_1^2) + k_2(\theta_1 + \theta_1^2) - k_2(\theta_2 + \theta_2^2) + D_2\theta_1' - D_2\theta_2' = 0 \tag{3.14}$$

$$m_1 l_1^2 \sin(\theta_1)\alpha_1 + D_1\omega_1 + k_1(\theta_1 + \theta_1^2) + k_2(\theta_1 + \theta_1^2) - k_2(\theta_2 + \theta_2^2) + D_2\omega_1 - D_2\omega_2 = 0 \tag{3.15}$$

$$\sin(\theta_1)\alpha_1 = -\frac{D_1}{m_1 l_1^2}\omega_1 - \frac{k_1}{m_1 l_1^2}(\theta_1 + \theta_1^2) - \frac{k_2}{m_1 l_1^2}(\theta_1 + \theta_1^2) + \frac{k_2}{m_1 l_1^2}(\theta_2 + \theta_2^2) - \frac{D_2}{m_1 l_1^2}\omega_1 + \frac{D_2}{m_1 l_1^2}\omega_2 \tag{3.16}$$

Using expression (3.6)

$$m_2 l_2^2 \sin(\theta_2)\alpha_2 + D_2\theta_2' + k_2(\theta_2 + \theta_2^2) + k_3(\theta_2 + \theta_2^2) - k_3(\theta_3 + \theta_3^2) + D_3\theta_2' - D_3\theta_3' = 0 \tag{3.17}$$

$$m_2 l_2^2 \sin(\theta_2)\alpha_2 + D_2\omega_2 + k_2(\theta_2 + \theta_2^2) + k_3(\theta_2 + \theta_2^2) - k_3(\theta_3 + \theta_3^2) + D_3\omega_2 - D_3\omega_3 = 0 \tag{3.18}$$

$$\sin(\theta_2)\alpha_2 = -\frac{k_2}{m_2 l_2^2}(\theta_2 + \theta_2^2) - \frac{D_2}{m_2 l_2^2}\omega_2 - \frac{k_3}{m_2 l_2^2}(\theta_2 + \theta_2^2) + \frac{k_3}{m_2 l_2^2}(\theta_3 + \theta_3^2) - \frac{D_3}{m_2 l_2^2}\omega_2 + \frac{D_3}{m_2 l_2^2}\omega_3 \tag{3.19}$$

$$\sin(\theta_2)\alpha_2 = (-\frac{k_2}{m_2 l_2^2} - \frac{k_3}{m_2 l_2^2})(\theta_2 + \theta_2^2) + (\frac{k_3}{m_2 l_2^2})(\theta_3 + \theta_3^2) + (-\frac{D_3}{m_2 l_2^2} - \frac{D_2}{m_2 l_2^2})\omega_2 + \frac{D_3}{m_2 l_2^2}\omega_3 \tag{3.20}$$

Using expression (3.7)

$$m_3 l_3^2 \sin(\theta_3)\alpha_3 + k_3(\theta_3 + \theta_3^2) + D_3\theta_3' - k_3(\theta_2 + \theta_2^2) - D_3\theta_2' = 0 \tag{3.21}$$

$$m_3 l_3^2 \sin(\theta_3)\alpha_3 + k_3(\theta_3 + \theta_3^2) + D_3\omega_3 - k_3(\theta_2 + \theta_2^2) - D_3\omega_2 = 0 \tag{3.22}$$

$$\sin(\theta_3)\alpha_3 = -\frac{k_3}{m_3 l_3^2}(\theta_3 + \theta_3^2) - \frac{D_3}{m_3 l_3^2}\omega_3 + \frac{k_3}{m_3 l_3^2}(\theta_2 + \theta_2^2) + \frac{D_3}{m_3 l_3^2}\omega_2 \tag{3.23}$$

Rearranging above equation, we get

$$\sin(\theta_3)\alpha_3 = \frac{k_3}{m_3 l_3^2}(\theta_2 + \theta_2^2) - \frac{k_3}{m_3 l_3^2}(\theta_3 + \theta_3^2) + \frac{D_3}{m_3 l_3^2}\omega_2 - \frac{D_3}{m_3 l_3^2}\omega_3 \tag{3.24}$$

State Space Representation of Ring Finger

$$X' = Ax + Bu \tag{3.25}$$

$$Y = Cx + Du \tag{3.26}$$

where;
A $\Rightarrow$ is system model matrix that defines the dynamics of system
B $\Rightarrow$ is the matrix of inputs
C $\Rightarrow$ matrix of output
D $\Rightarrow$ is the decoupling matrix
State vector for the Ring finger defined as

$$X' = \begin{bmatrix} \theta_1' \\ \theta_2' \\ \theta_3' \\ \omega_1' \\ \omega_2' \\ \omega_3' \end{bmatrix}$$

State variables for the Ring finger are defined and expressed as

$$\begin{bmatrix} x_1 \\ x_2 \\ x_3 \\ x_4 \\ x_5 \\ x_6 \end{bmatrix} = \begin{bmatrix} \theta_1 \\ \theta_2 \\ \theta_3 \\ \omega_1 \\ \omega_2 \\ \omega_3 \end{bmatrix} \tag{3.28}$$

Nonlinear state space model [53, 54, 55] for ring finger can be expressed as:

$$X' = \begin{bmatrix} \omega_1' \\ \omega_2' \\ \omega_3' \\ \frac{-k_1-k_2}{m_1 l_1^2 \sin(\theta_1)}(\theta_1+\theta_1^2) + \frac{K_2}{m_1 l_1^2 \sin(\theta_1)}(\theta_1+\theta_1^2) + \frac{-D_1-D_2}{m_1 l_1^2 \sin(\theta_1)} + \frac{D_2}{m_1 l_1^2 \sin(\theta_1)} \\ \frac{-k_2-k_3}{m_2 l_2^2 \sin(\theta_2)}(\theta_2+\theta_2^2) + \frac{K_3}{m_2 l_2^2 \sin(\theta_2)}(\theta_2+\theta_2^2) + \frac{-D_2-D_3}{m_2 l_2^2 \sin(\theta_2)} + \frac{D_3}{m_2 l_2^2 \sin(\theta_2)} \\ \frac{K_3}{m_3 l_3^2 \sin(\theta_3)}(\theta_2+\theta_2^2) + \frac{-K_3}{m_3 l_3^2 \sin(\theta_3)}(\theta_3+\theta_3^2) + \frac{D_3}{m_3 l_3^2 \sin(\theta_3)} + \frac{-D_3}{m_3 l_3^2 \sin(\theta_3)} \end{bmatrix}$$

$$y = g(x,u) \text{ [56]} \tag{3.30}$$

Jacobian Matrices:

Jacobian linearization matric [57, 58] can be expressed as:

$$J_f(x,y) = \begin{bmatrix} \frac{\partial f_1}{\partial x_1} & \frac{\partial f_1}{\partial x_2} & \frac{\partial f_1}{\partial x_3} & \frac{\partial f_1}{\partial x_4} & \frac{\partial f_1}{\partial x_5} & \frac{\partial f_1}{\partial x_6} \\ \frac{\partial f_2}{\partial x_1} & \frac{\partial f_2}{\partial x_2} & \frac{\partial f_2}{\partial x_3} & \frac{\partial f_2}{\partial x_4} & \frac{\partial f_2}{\partial x_5} & \frac{\partial f_2}{\partial x_6} \\ \frac{\partial f_3}{\partial x_1} & \frac{\partial f_3}{\partial x_2} & \frac{\partial f_3}{\partial x_3} & \frac{\partial f_3}{\partial x_4} & \frac{\partial f_3}{\partial x_5} & \frac{\partial f_3}{\partial x_6} \\ \frac{\partial f_4}{\partial x_1} & \frac{\partial f_4}{\partial x_2} & \frac{\partial f_4}{\partial x_3} & \frac{\partial f_4}{\partial x_4} & \frac{\partial f_4}{\partial x_5} & \frac{\partial f_4}{\partial x_6} \\ \frac{\partial f_5}{\partial x_1} & \frac{\partial f_5}{\partial x_2} & \frac{\partial f_5}{\partial x_3} & \frac{\partial f_5}{\partial x_4} & \frac{\partial f_5}{\partial x_5} & \frac{\partial f_5}{\partial x_6} \\ \frac{\partial f_6}{\partial x_1} & \frac{\partial f_6}{\partial x_2} & \frac{\partial f_6}{\partial x_3} & \frac{\partial f_6}{\partial x_4} & \frac{\partial f_6}{\partial x_5} & \frac{\partial f_6}{\partial x_6} \end{bmatrix}$$

By small angle approximation:

$$\sin(\theta = 0) \approx 0 \tag{3.32}$$

$$\sin(\theta = 90) \approx \theta \tag{3.33}$$

Or

$$\sin(\pi + 0) \approx 0 \tag{3.34}$$

$$\sin(\pi + \theta) \approx \theta \tag{3.35}$$

System Model Matrix is defined and expressed for ring finger dynamics expressed as:

$$A_1 = \begin{bmatrix} 0 & 0 & 0 & 1 & 0 & 0 \\ 0 & 0 & 0 & 0 & 1 & 0 \\ 0 & 0 & 0 & 0 & 0 & 1 \\ \frac{-k_1-k_2}{m_1 l_1^2} & \frac{K_2}{m_1 l_1^2} & 0 & \frac{-D_1-D_2}{m_1 l_1^2} & \frac{D_2}{m_1 l_1^2} & 0 \\ 0 & \frac{-k_2-k_3}{m_2 l_2^2} & \frac{K_3}{m_2 l_2^2} & 0 & \frac{-D_2-D_3}{m_2 l_2^2} & \frac{D_3}{m_2 l_2^2} \\ 0 & \frac{K_3}{m_3 l_3^2} & -\frac{K_3}{m_3 l_3^2} & 0 & \frac{D_3}{m_3 l_3^2} & -\frac{D_3}{m_3 l_3^2} \end{bmatrix}$$

System Input Matrix is defined and expressed for ring finger dynamics expressed as:

$$B_1 = \begin{bmatrix} 0 \\ 0 \\ 0 \\ \frac{1}{m_1 l_1^2} \\ \frac{1}{m_2 l_2^2} \\ \frac{1}{m_3 l_3^2} \end{bmatrix}$$

System output Matrix is defined and expressed for ring finger dynamics expressed as:

$$C_1 = \begin{bmatrix} 1 & 0 & 0 & 0 & 0 & 0 \\ 0 & 1 & 0 & 0 & 0 & 0 \\ 0 & 0 & 1 & 0 & 0 & 0 \end{bmatrix}$$

Decoupling matrix D will be:

$$D_1 = \begin{bmatrix} 0 \\ 0 \\ 0 \end{bmatrix} \quad (3.39)$$

The state space model for ring finger will be expressed as:

$$\begin{bmatrix} \theta_1' \\ \theta_2' \\ \theta_3' \\ \omega_1' \\ \omega_2 \\ \omega_3 \end{bmatrix} = \begin{bmatrix} 0 & 0 & 0 & 1 & 0 & 0 \\ 0 & 0 & 0 & 0 & 1 & 0 \\ 0 & 0 & 0 & 0 & 0 & 1 \\ \frac{-k_1-k_2}{m_1 l_1^2} & \frac{K_2}{m_1 l_1^2} & 0 & \frac{-D_1-D_2}{m_1 l_1^2} & \frac{D_2}{m_1 l_1^2} & 0 \\ 0 & \frac{-k_2-k_3}{m_2 l_2^2} & \frac{K_3}{m_2 l_2^2} & 0 & \frac{-D_2-D_3}{m_2 l_2^2} & \frac{D_3}{m_2 l_2^2} \\ 0 & \frac{K_3}{m_3 l_3^2} & -\frac{K_3}{m_3 l_3^2} & 0 & \frac{D_3}{m_3 l_3^2} & -\frac{D_3}{m_3 l_3^2} \end{bmatrix} \begin{bmatrix} \theta_1 \\ \theta_2 \\ \theta_3 \\ \omega_1 \\ \omega_2 \\ \omega_3 \end{bmatrix} + \begin{bmatrix} 0 \\ 0 \\ 0 \\ \frac{1}{m_1 l_1^2} \\ \frac{1}{m_2 l_2^2} \\ \frac{1}{m_3 l_3^2} \end{bmatrix} u$$

State Output expression for the ring finger:

$$y = \begin{bmatrix} 1 & 0 & 0 & 0 & 0 & 0 \\ 0 & 1 & 0 & 0 & 0 & 0 \\ 0 & 0 & 1 & 0 & 0 & 0 \end{bmatrix} \begin{bmatrix} \theta_1 \\ \theta_2 \\ \theta_3 \\ \omega_1 \\ \omega_2 \\ \omega_3 \end{bmatrix} + \begin{bmatrix} 0 \\ 0 \\ 0 \end{bmatrix} u$$

3.2.2 Non linearity in system dynamics

As two fingers little and ring fingers are mutually coordinated so angular motion also effected due to interlinked dynamic behavior. The nonlinear disturbance effect on the ring finger considered as system input disturbances added to the applied rotational torque. The applied disturbance effect on the little finger offered by input applied torque added with sine function.

Nonlinear applied input disturbance is offered as:

$$D=[\tau + A sin\omega t] \tag{3.42}$$

where;
D $\Rightarrow$ applied disturbance to system
$\tau \Rightarrow$ applied torque input applied by actuator
A $\Rightarrow$ amplitude of added input disturbance
$\omega \Rightarrow$ frequency of applied disturbance signal
$\sin\theta \Rightarrow$ non-linear function

3.2.3 Little finger dynamics

The Freebody diagram [59] of Little finger along inertia, damping and stiffness components [60] can be developed in form of following figure. Figure3.3 is the block diagram for the proposed model.

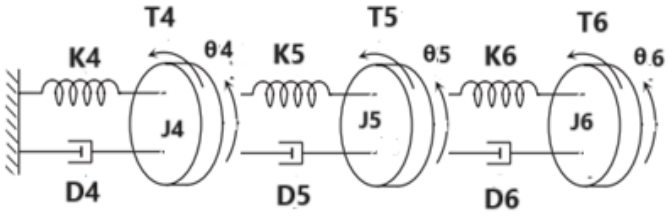

Figure 3.3: Freebody Diagram of little finger.

The damper offered the resistive effect, spring offered the stiffness as well as inertia offered the rotational angular movement for the joints named as PIP, DIP and MCP of finger dynamics.

Rotational torque offered by first MCP joint.

$$T = J_4 \frac{\mathrm{d}^2\theta}{\mathrm{d}t^2} \tag{3.43}$$

Nonlinear Inertial Effect:

$$T = m_4 l_4^2 \sin\theta \frac{d^2\theta}{dt^2} \tag{3.44}$$

Damping effect on MCP joint movement:

$$T = D\theta' \tag{3.45}$$

Stiffness of MCP joint due to torque:

$$T = k(\theta + \theta^2) \tag{3.46}$$

Inertial effect, damping as well as stiffness offered by PID and DIP joints will be considered as same.

Equation of motion:

$$m_4 l_4^2 \sin(\theta_4)\frac{d^2\theta_4}{dt^2} + D_4\frac{d\theta_4}{dt} + k_4(\theta_4+\theta_4^2) + k_5(\theta_4+\theta_4^2) - k_5(\theta_5+\theta_5^2) + D_5\frac{d\theta_4}{dt} - D_5\frac{d\theta_5}{dt} = 0 \tag{3.47}$$

$$m_5 l_5^2 \sin(\theta_5)\frac{d^2\theta_5}{dt^2} + D_5\frac{d\theta_5}{dt} + k_2(\theta_5+\theta_5^2) + k_6(\theta_5+\theta_5^2) - k_6(\theta_6+\theta_6^2) + D_6\frac{d\theta_5}{dt} - D_6\frac{d\theta_6}{dt} = 0 \tag{3.48}$$

$$m_6 l_6^2 \sin(\theta_6)\frac{d^2\theta_6}{dt^2} + D_6\frac{d\theta_6}{dt} + k_6(\theta_6+\theta_6^2) - k_6(\theta_5+\theta_5^2) + D_6\frac{d\theta_5}{dt} = 0 \tag{3.49}$$

$$\frac{d\theta_4}{\mathrm{d}t} = \omega_4 \tag{3.50}$$

$$\frac{\mathrm{d}\theta_5}{\mathrm{d}t} = \omega_5 \tag{3.51}$$

$$\frac{\mathrm{d}\theta_6}{\mathrm{d}t} = \omega_6 \tag{3.52}$$

$$\frac{\mathrm{d}^2\theta_4}{\mathrm{d}t^2} = \alpha_4 \tag{3.53}$$

$$\frac{\mathrm{d}^2\theta_5}{\mathrm{d}t^2} = \alpha_5 \tag{3.54}$$

$$\frac{\mathrm{d}^2\theta_6}{\mathrm{d}t^2} = \alpha_6 \tag{3.55}$$

Using expression (3.47)

$$m_1 l_1^2 \sin(\theta_1)\alpha_1 + D_1\theta_1' + k_1(\theta_1+\theta_1^2) + k_2(\theta_1+\theta_1^2) - k_2(\theta_2+\theta_2^2) + D_2\theta_1' - D_2\theta_2' = 0 \tag{3.56}$$

$$m_1 l_1^2 \sin(\theta_1)\alpha_1 + D_1\omega_1 + k_1(\theta_1+\theta_1^2) + k_2(\theta_1+\theta_1^2) - k_2(\theta_2+\theta_2^2) + D_2\omega_1 - D_2\omega_2 = 0 \tag{3.57}$$

$$\sin(\theta_4)\alpha_4 = -\frac{D_4}{m_4 l_4^2}\omega_4 - \frac{k_4}{m_4 l_4^2}(\theta_4+\theta_4^2) - \frac{k_5}{m_4 l_4^2}(\theta_4+\theta_4^2) + \frac{k_5}{m_4 l_4^2}(\theta_5+\theta_5^2) - \frac{D_5}{m_4 l_4^2}\omega_4 + \frac{D_5}{m_4 l_4^2}\omega_5 \tag{3.58}$$

$$\alpha_4 = \frac{-D_4 - D_5}{m_4 l_4^2 \sin(\theta_4)}\omega_4 + \frac{-k_4 - k_5}{m_4 l_4^2 \sin(\theta_4)}(\theta_4 + \theta_4^2) + \frac{k_5}{m_4 l_4^2 \sin(\theta_4)}(\theta_5 + \theta_5^2) + \frac{D_5}{m_4 l_4^2 \sin(\theta_4)}\omega_5 \tag{3.59}$$

Using expression (3.48)

$$m_5 l_5^2 \sin(\theta_5)\alpha_5 + D_5\theta_5' + k_5(\theta_5 + \theta_5^2) + k_6(\theta_5 + \theta_5^2) - k_6(\theta_6 + \theta_6^2) + D_6\theta_5' - D_6\theta_6' = 0 \tag{3.60}$$

$$m_5 l_5^2 \sin(\theta_5)\alpha_5 + D_5\omega_5 + k_5(\theta_5 + \theta_5^2) + k_6(\theta_5 + \theta_5^2) - k_6(\theta_6 + \theta_6^2) + D_6\omega_5 - D_6\omega_6 = 0 \tag{3.61}$$

$$\sin(\theta_5)\alpha_5 = -\frac{k_5}{m_5 l_5^2}(\theta_5 + \theta_5^2) - \frac{D_5}{m_5 l_5^2}\omega_5 - \frac{k_6}{m_5 l_5^2}(\theta_5 + \theta_5^2) + \frac{k_6}{m_5 l_5^2}(\theta_6 + \theta_6^2) - \frac{D_6}{m_5 l_5^2}\omega_5 + \frac{D_6}{m_5 l_5^2}\omega_6 \tag{3.62}$$

$$\sin(\theta_5)\alpha_5 = (-\frac{k_5}{m_5 l_5^2} - \frac{k_6}{m_5 l_5^2})(\theta_5 + \theta_5^2) + (\frac{k_6}{m_5 l_5^2})(\theta_6 + \theta_6^2) + (-\frac{D_6}{m_5 l_5^2} - \frac{D_5}{m_5 l_5^2})\omega_5 + \frac{D_6}{m_5 l_5^2}\omega_6 \tag{3.63}$$

Rearranging Equation

$$\alpha_5 = (\frac{-k_5 - k_6}{m_5 l_5^2 \sin(\theta_5)})(\theta_5 + \theta_5^2) + (\frac{k_6}{m_5 l_5^2 \sin(\theta_5)})(\theta_6 + \theta_6^2) + \frac{-D_5 - D_6}{m_5 l_5^2 \sin(\theta_5)} + \frac{D_6}{m_5 l_5^2 \sin(\theta_5)}\omega_6 \tag{3.64}$$

Using expression (3.49)

$$m_6 l_6^2 \sin(\theta_6)\alpha_6 + k_6(\theta_6 + \theta_6^2) + D_6\theta_6' - k_6(\theta_5 + \theta_5^2) - D_6\theta_5' = 0 \tag{3.65}$$

$$m_6 l_6^2 \sin(\theta_6)\alpha_6 + k_6(\theta_6 + \theta_6^2) + D_6\omega_6 - k_6(\theta_5 + \theta_5^2) - D_6\omega_5 = 0 \tag{3.66}$$

$$\sin(\theta_6)\alpha_6 = -\frac{k_6}{m_6 l_6^2}(\theta_6 + \theta_6^2) - \frac{D_6}{m_6 l_6^2}\omega_6 + \frac{k_6}{m_6 l_6^2}(\theta_5 + \theta_5^2) + \frac{D_6}{m_6 l_6^2}\omega_5 \tag{3.67}$$

Rearranging above equation, we get

$$\sin(\theta_6)\alpha_6 = \frac{k_6}{m_6 l_6^2}(\theta_5 + \theta_5^2) - \frac{k_6}{m_6 l_6^2}(\theta_6 + \theta_6^2) + \frac{D_6}{m_6 l_6^2}\omega_5 - \frac{D_6}{m_6 l_6^2}\omega_6 \tag{3.68}$$

$$\alpha_6 = \frac{k_6}{m_6 l_6^2 \sin(\theta_6)}(\theta_5 + \theta_5^2) - \frac{k_6}{m_6 l_6^2 \sin(\theta_6)}(\theta_6 + \theta_6^2) + \frac{D_6}{m_6 l_6^2 \sin(\theta_6)}\omega_5 - \frac{D_6}{m_6 l_6^2 \sin(\theta_6)}\omega_6 \tag{3.69}$$

State Space Representation of Little Finger

$$X' = Ax + Bu \tag{3.70}$$

$$Y = Cx + Du \tag{3.71}$$

where;
A $\Rightarrow$ is system model matrix that define the dynamics of system
B $\Rightarrow$ is the input matrix
C $\Rightarrow$ output matrix
D $\Rightarrow$ is the decoupling feed forward matrix

State vector for the little finger defined as

$$X' = \begin{bmatrix} \theta_4' \\ \theta_5' \\ \theta_6' \\ \omega_4' \\ \omega_5' \\ \omega_6' \end{bmatrix} \tag{3.72}$$

State variables for the Ring finger are defined and expressed as

$$\begin{bmatrix} x_7 \\ x_8 \\ x_9 \\ x_{10} \\ x_{11} \\ x_{12} \end{bmatrix} = \begin{bmatrix} \theta_4 \\ \theta_5 \\ \theta_6 \\ \omega_4 \\ \omega_5 \\ \omega_6 \end{bmatrix} \tag{3.73}$$

Nonlinear state space model for ring finger can be expressed as:

$$X' = \begin{bmatrix} \omega_4' \\ \omega_5' \\ \omega_6' \\ \frac{-k_4-k_5}{m_4 l_4^2 \sin(\theta_4)}(\theta_4+\theta_4^2) + \frac{K_5}{m_4 l_4^2 \sin(\theta_4)}(\theta_4+\theta_4^2) + \frac{-D_4-D_5}{m_4 l_4^2 \sin(\theta_4)} + \frac{D_5}{m_4 l_4^2 \sin(\theta_4)} \\ \frac{-k_5-k_6}{m_5 l_5^2 \sin(\theta_5)}(\theta_5+\theta_5^2) + \frac{K_6}{m_5 l_5^2 \sin(\theta_5)}(\theta_5+\theta_5^2) + \frac{-D_5-D_6}{m_5 l_5^2 \sin(\theta_5)} + \frac{D_6}{m_5 l_5^2 \sin(\theta_5)} \\ \frac{K_6}{m_6 l_6^2 \sin(\theta_6)}(\theta_6+\theta_6^2) \pm \frac{-K_6}{m_6 l_6^2 \sin(\theta_6)}(\theta_6+\theta_6^2) + \frac{D_6}{m_6 l_6^2 \sin(\theta_6)} + \frac{D_6}{m_6 l_6^2 \sin(\theta_6)} \end{bmatrix}$$

$$y = g(x,u) \tag{3.75}$$

Jacobian Matrices:
Jacobian linearization matric can be expressed as:

$$J_f(x,y) = \begin{bmatrix} \frac{\partial f_7}{\partial x_7} & \frac{\partial f_7}{\partial x_8} & \frac{\partial f_7}{\partial x_9} & \frac{\partial f_7}{\partial x_{10}} & \frac{\partial f_7}{\partial x_{11}} & \frac{\partial f_7}{\partial x_{12}} \\ \frac{\partial f_8}{\partial x_7} & \frac{\partial f_8}{\partial x_8} & \frac{\partial f_8}{\partial x_9} & \frac{\partial f_8}{\partial x_{10}} & \frac{\partial f_8}{\partial x_{11}} & \frac{\partial f_8}{\partial x_{12}} \\ \frac{\partial f_9}{\partial x_7} & \frac{\partial f_9}{\partial x_8} & \frac{\partial f_9}{\partial x_9} & \frac{\partial f_9}{\partial x_{10}} & \frac{\partial f_9}{\partial x_{11}} & \frac{\partial f_9}{\partial x_{12}} \\ \frac{\partial f_{10}}{\partial x_7} & \frac{\partial f_{10}}{\partial x_8} & \frac{\partial f_{10}}{\partial x_9} & \frac{\partial f_{10}}{\partial x_{10}} & \frac{\partial f_{10}}{\partial x_{11}} & \frac{\partial f_{10}}{\partial x_{12}} \\ \frac{\partial f_{11}}{\partial x_7} & \frac{\partial f_{11}}{\partial x_8} & \frac{\partial f_{11}}{\partial x_9} & \frac{\partial f_{11}}{\partial x_{10}} & \frac{\partial f_{11}}{\partial x_{11}} & \frac{\partial f_{11}}{\partial x_{12}} \\ \frac{\partial f_{12}}{\partial x_7} & \frac{\partial f_{12}}{\partial x_8} & \frac{\partial f_{12}}{\partial x_9} & \frac{\partial f_{12}}{\partial x_{10}} & \frac{\partial f_{12}}{\partial x_{11}} & \frac{\partial f_{12}}{\partial x_{12}} \end{bmatrix}$$

By small angle approximation:

$$\sin(\theta = 0) \approx 0 \tag{3.77}$$

$$\sin(\theta = 90) \approx \theta \tag{3.78}$$

Or

$$\sin(\pi+0) \approx 0 \tag{3.79}$$

$$\sin(\pi+\theta) \approx \theta \tag{3.80}$$

System Model Matrix is defined and expressed for ring finger dynamics expressed as:

$$A_2 = \begin{bmatrix} 0 & 0 & 0 & 1 & 0 & 0 \\ 0 & 0 & 0 & 0 & 1 & 0 \\ 0 & 0 & 0 & 0 & 0 & 1 \\ \frac{-k_4-k_5}{m_4 l_4^2} & \frac{K_5}{m_4 l_4^2} & 0 & \frac{-D_4-D_5}{m_4 l_4^2} & \frac{D_5}{m_4 l_4^2} & 0 \\ 0 & \frac{-k_5-k_6}{m_5 l_5^2} & \frac{K_6}{m_5 l_5^2} & 0 & \frac{-D_5-D_6}{m_5 l_5^2} & \frac{D_6}{m_5 l_5^2} \\ 0 & \frac{K_6}{m_6 l_6^2} & -\frac{K_6}{m_6 l_6^2} & 0 & \frac{D_6}{m_6 l_6^2} & -\frac{D_6}{m_6 l_6^2} \end{bmatrix}$$

System Input Matrix is defined and expressed for ring finger dynamics expressed as:

$$B_2 = \begin{bmatrix} 0 \\ 0 \\ 0 \\ \frac{1}{m_4 l_4^2} \\ \frac{1}{m_5 l_5^2} \\ \frac{1}{m_6 l_6^2} \end{bmatrix} \tag{3.82}$$

System output Matrix is defined and expressed for ring finger dynamics expressed as:

$$C_2 = \begin{bmatrix} 1 & 0 & 0 & 0 & 0 & 0 \\ 0 & 1 & 0 & 0 & 0 & 0 \\ 0 & 0 & 1 & 0 & 0 & 0 \end{bmatrix}$$

Decoupling matrix D will be:

$$D_2 = \begin{bmatrix} 0 \\ 0 \\ 0 \end{bmatrix}$$

The state space model for ring finger will be expressed as:

$$\begin{bmatrix} \theta_4' \\ \theta_5' \\ \theta_6' \\ \omega_4 \\ \omega_5 \\ \omega_6 \end{bmatrix} = \begin{bmatrix} 0 & 0 & 0 & 1 & 0 & 0 \\ 0 & 0 & 0 & 0 & 1 & 0 \\ 0 & 0 & 0 & 0 & 0 & 1 \\ \frac{-k_4-k_5}{m_4 l_4^2} & \frac{K_5}{m_4 l_4^2} & 0 & \frac{-D_4-D_5}{m_4 l_4^2} & \frac{D_5}{m_4 l_4^2} & 0 \\ 0 & \frac{-k_5-k_6}{m_5 l_5^2} & \frac{K_6}{m_5 l_5^2} & 0 & \frac{-D_5-D_6}{m_5 l_5^2} & \frac{D_6}{m_5 l_5^2} \\ 0 & \frac{K_6}{m_6 l_6^2} & -\frac{K_6}{m_6 l_6^2} & 0 & \frac{D_6}{m_6 l_6^2} & -\frac{D_6}{m_6 l_6^2} \end{bmatrix} \begin{bmatrix} \theta_4 \\ \theta_5 \\ \theta_6 \\ \omega_4 \\ \omega_5 \\ \omega_6 \end{bmatrix} + \begin{bmatrix} 0 \\ 0 \\ 0 \\ \frac{1}{m_4 l_4^2} \\ \frac{1}{m_5 l_5^2} \\ \frac{1}{m_6 l_6^2} \end{bmatrix} u$$

State Output expression for the ring finger:

$$y = \begin{bmatrix} 1 & 0 & 0 & 0 & 0 & 0 \\ 0 & 1 & 0 & 0 & 0 & 0 \\ 0 & 0 & 1 & 0 & 0 & 0 \end{bmatrix} \begin{bmatrix} \theta_4 \\ \theta_5 \\ \theta_6 \\ \omega_4 \\ \omega_5 \\ \omega_6 \end{bmatrix} + \begin{bmatrix} 0 \\ 0 \\ 0 \end{bmatrix} u$$

3.3 Simulink model

A SIMULINK/MATLAB toolbox called Sim-Mechanics offers a simulation environment for multi-body bio-mechanical models, robotics, vehicle components, and even landing gears. Since the user must implement the model without creating equations of motion, the simulation environment facilitates the realisation of the model. Building pieces that represent bodies, joints, constraints, force elements, and sensors or actuators can be used to create a multi-body system. Using these elements, Sim-Mechanics automatically creates and resolves equations of motion. In addition, the environment aids in the testing and development of control at the system level. The toolbox's seamless integration with Simulink and MATLAB allows for the parameterization of models using MATLAB variables and the use of all Simulink features to create the final controlled system.

3.3.1 Simulink Block model of Ring finger

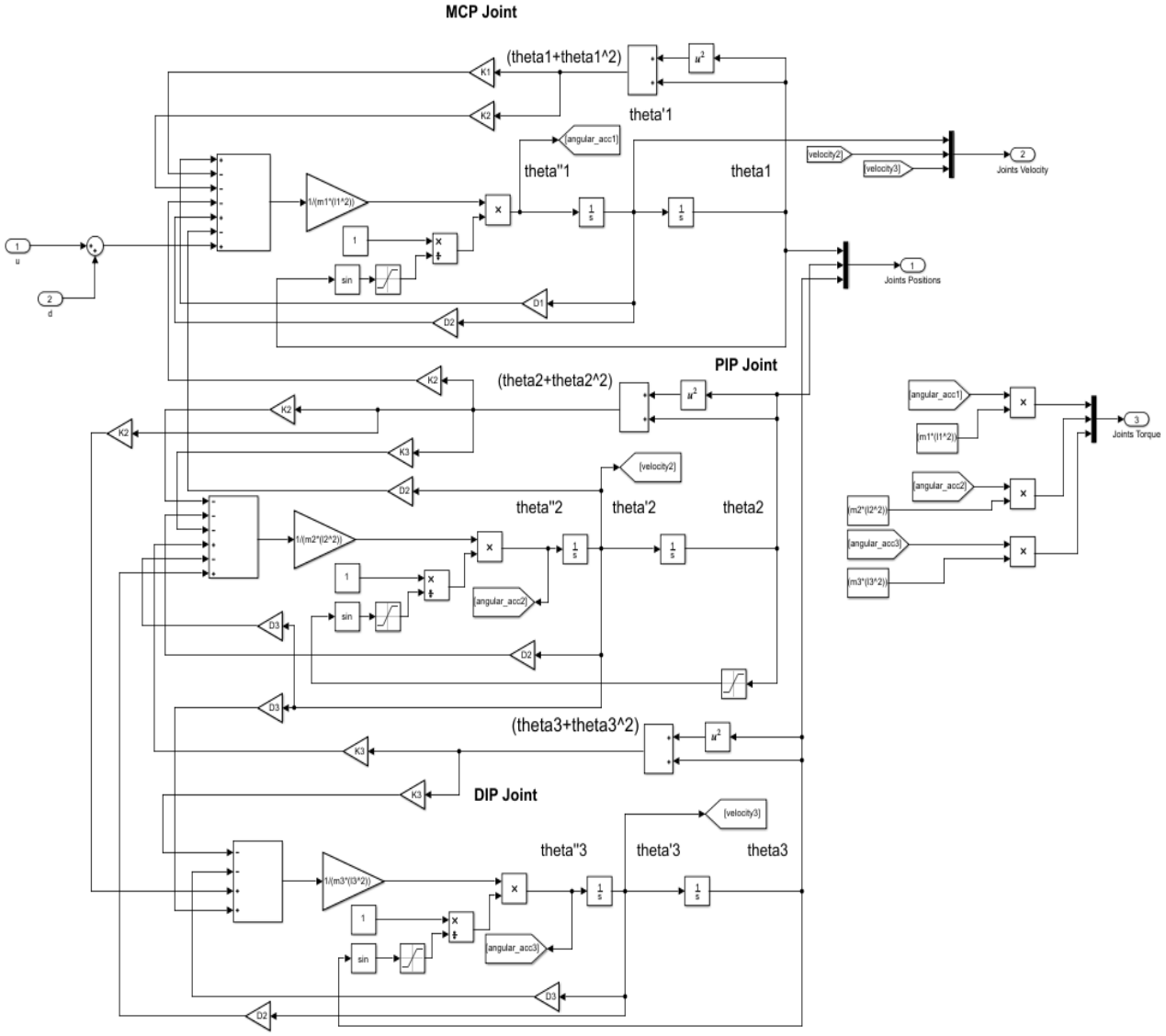

Figure 3.4: Simulink Block model of Ring finger

3.3.2 Simulink Components

• Gain block: Mathematics, multiplication in forward path ensured with the help of gain block.

• Sum / Add block: all the sum of expressions as well as differences or subtraction ensured with the help of sum /add block.

• Goto: To transport the signal value from one place to another place of Simulink window will be ensured by go-to block

- From: the from block acquired the signal value from Goto block.
- Mux: the decoding of multiple signals to one single line is ensured by MUX block.
- Scope: To visualize the output response, curves, graph and results displayed by scope block.
- Display: To monitor the measured value of the system in numerical form is ensured by display block.
- Saturation Block: to limit the signal value with saturation of upper limit as well as lower limit is ensured by saturation block.

3.3.3 Simulink Block model of Little finger

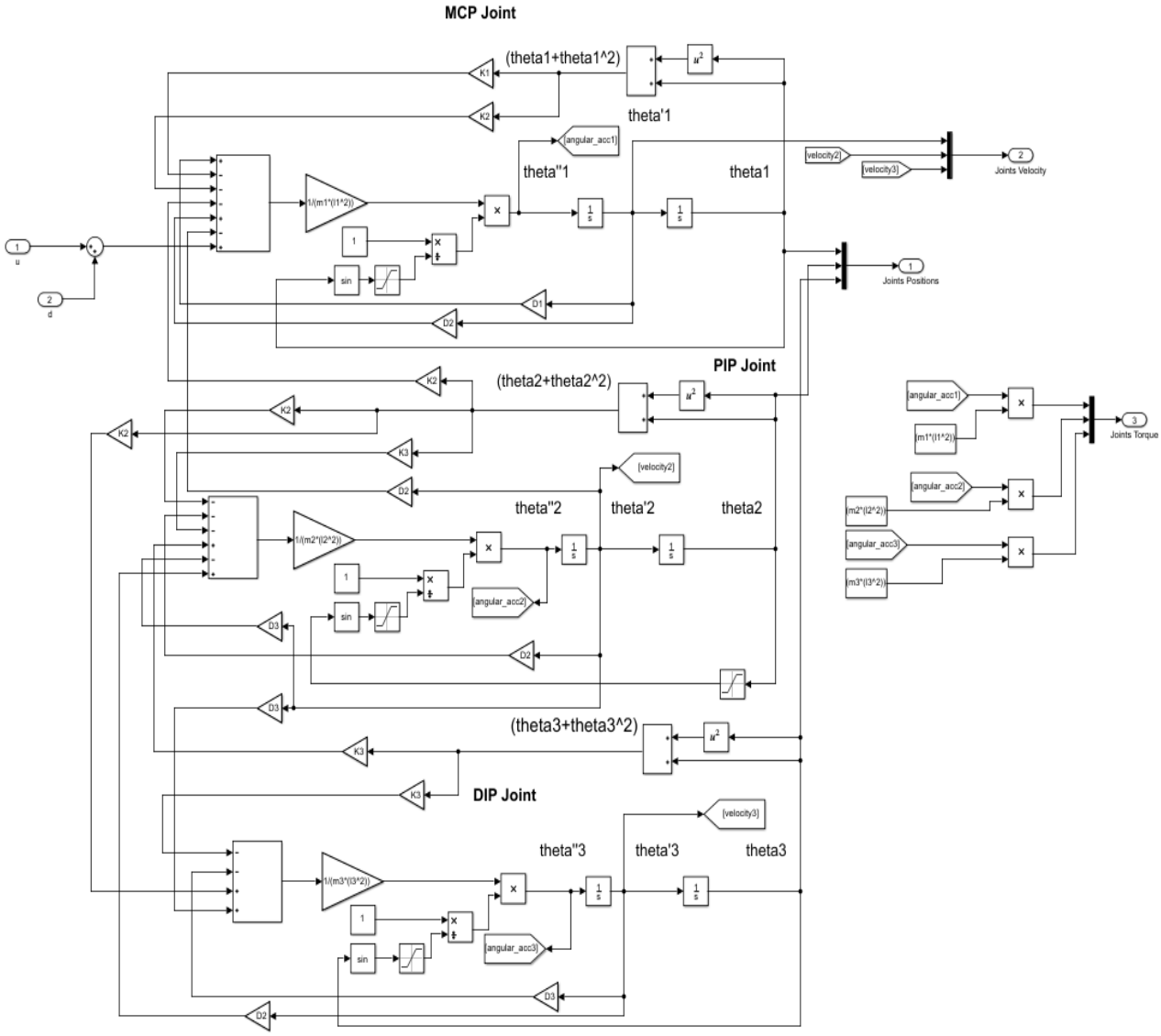

Figure 3.5: Simulink Block model of Little finger

3.3.4 Summarized and comprehensive Simulink model

We must linearize the model in order to create a model-based linear controller, which can then be used in conjunction with the human bio-mechanical model that Sim Mechanics has created with the help of non-linear statespace matrices and actuators for finger joints, as seen in Figure 3.6.

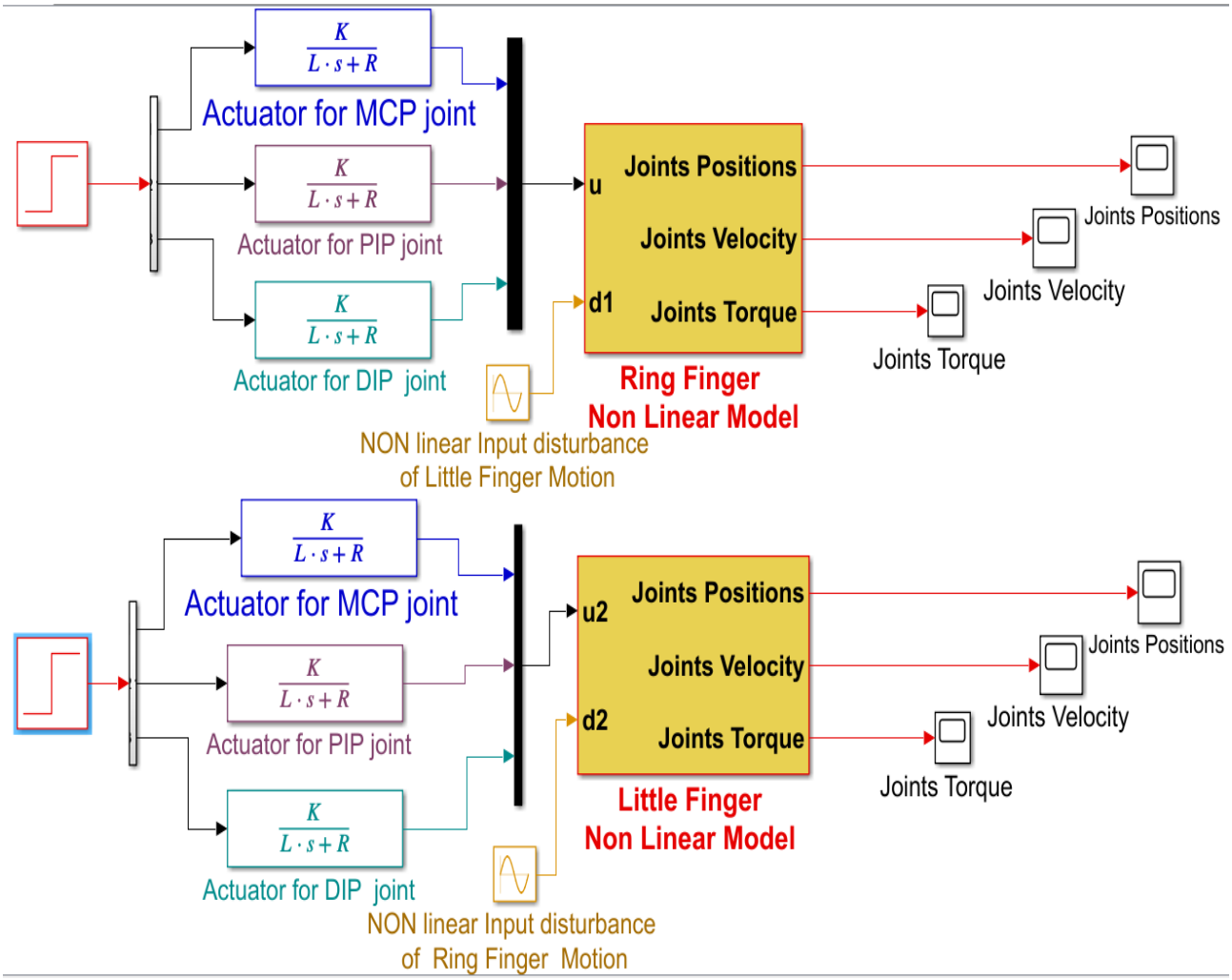

Figure 3.6: Comprehensive Simulink model

Simulink Components of a developed system:

- Step Block: The reference input supplied to the system is applied by the step input block.
- De-Mux: To encode the multiple information scattered to multiple lines obtained from a single line.
- Transfer function block: to define the system in Laplace transformation domain or in form of numeration and denominator expression of s-domain for system dynamics.

• Subsystem block: This block includes the non linear system dynamic model developed in previous section.

In MATLAB Simulink, we can add an icon image to a subsystem by making sure the image file location is accurately entered in the Image block attributes, and then we can adjust the details to suit our needs. Adding an icon image to the Simulink subsystem can be seen in the Figure 3.7.

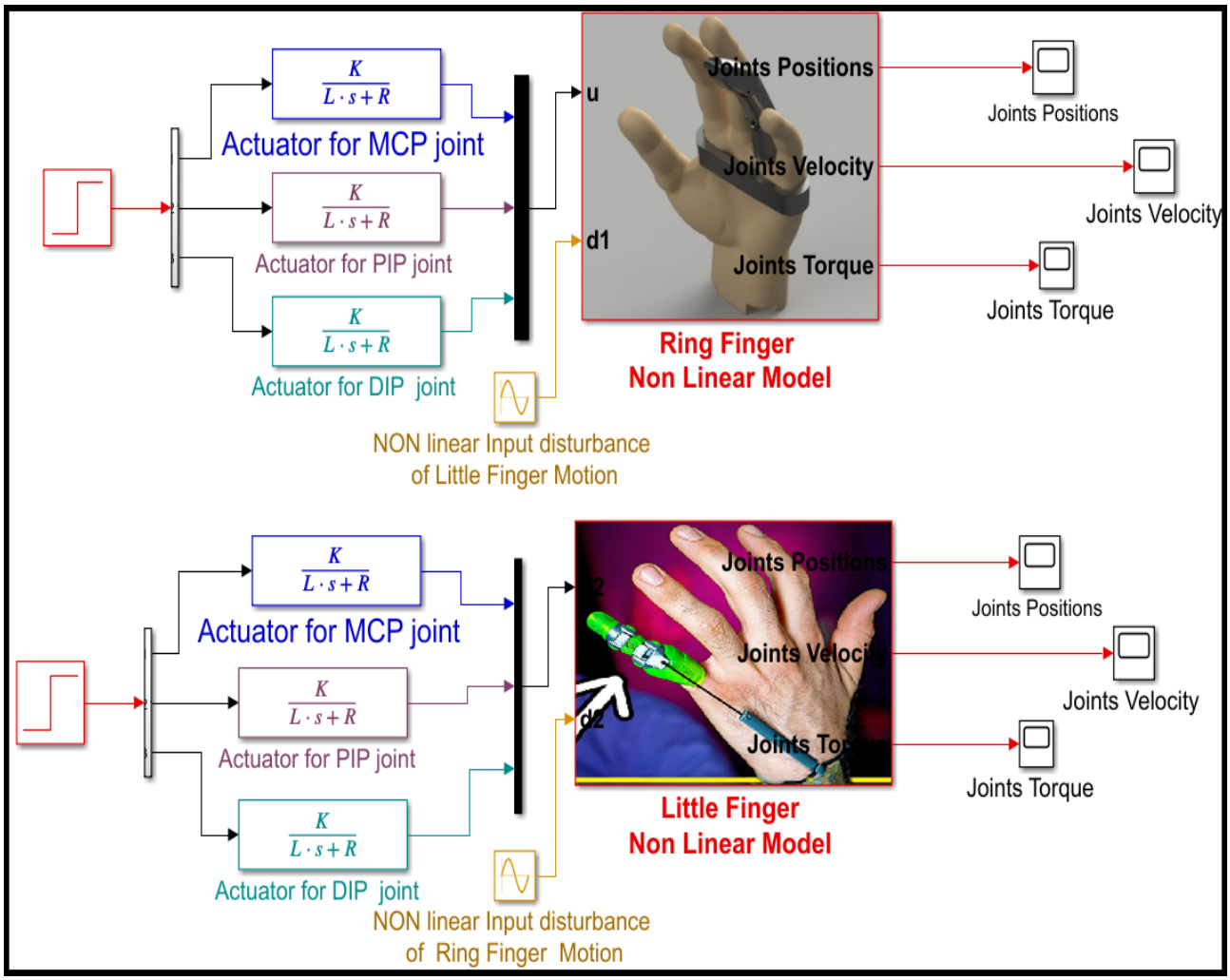

Figure 3.7: Comprehensive Simulink model

3.4 Controller Design

3.4.1 FLC based controller design and implementation

3.4.1.1 Fuzzy Inference System (FIS)

Fuzzy logic is the foundation of fuzzy inference systems. These systems perform best in situations where significance should take precedence over accuracy. An easy method for mapping an input space to an output space is to use fuzzy logic. It is one of several solutions that resemble "black boxes," such as lookup tables, differential equations, and linear systems. However, fuzzy logic can be used to model and control nonlinear systems and is more straightforward and adaptable. Membership functions (MF) are a series of curves that map input and output data. MFs are typically built in the shapes of bells, triangles, trapeziums, etc. To map the entire input space(s) to the output space for a collection of n input variables, n sets of such MFs are used. Defining FLC's precise inputs and outputs is the basic and necessary part for any controller. Fuzzy system has 3 variables error is the first crisp input; Change in Error is the second crisp input; and Control output is the output for FLC.

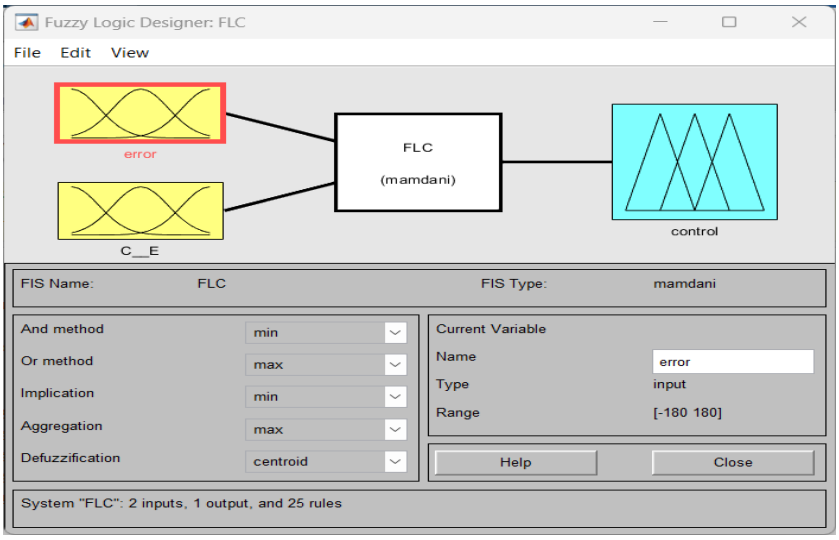

Figure 3.8: Fuzzy logic editor

MAMDANI type inference model is developed and applied in which there is ensured the AND and OR operations are performed or in other words initially the maximum operation is performed and then minimum of the resultant function is obtained. Output is defined in form of triangular or trapezoidal form membership function not in form of singleton or constant function. Defuzzification method is centroid method that is also known as center of gravity method. Five membership functions are defined for error inputs with triangular and sigmoidal type membership functions used with maximum overlapping

so that the uniform and smooth output surface plot and response should be obtained. In order to provide a consistent and smooth output surface plot and response, five membership functions of the triangular and sigmoidal types are defined for error inputs and employed with maximum overlap.

Similarly for the controller output, there are five membership function assigned with maximum overlapping to get uniform and smooth output surface plot.
The name of membership function defined as:
BN $\Rightarrow$ Big Negative
N $\Rightarrow$ Negative
Z $\Rightarrow$ Zero
P $\Rightarrow$ Positive
BP $\Rightarrow$ Big Positive

The Number of rules assigned for the system depends on number of membership functions for each input.

$$Numberofrules = n\mu_A * n\mu_B \tag{3.87}$$

n$\mu_A \Rightarrow$ number of membership function for first input
n$\mu_A \Rightarrow$ number of membership function for second input
Number of rules=5*5
Number of rules=25

3.4.2 Rules Table

Assign the rules to define the relation between the inputs and output membership functions.

Table 3.1: Rule Table

ez-1 e	**BN**	**N**	**Z**	**P**	**BP**
BN	BN	Z	BN	Z	Z
N	Z	N	N	Z	Z
Z	BN	N	Z	P	BP
P	Z	Z	P	P	Z
BP	Z	Z	BP	Z	BP

Big Negative, Negative, Zero, Positive, and Big Positive are the output membership functions together with the error and integration of error.

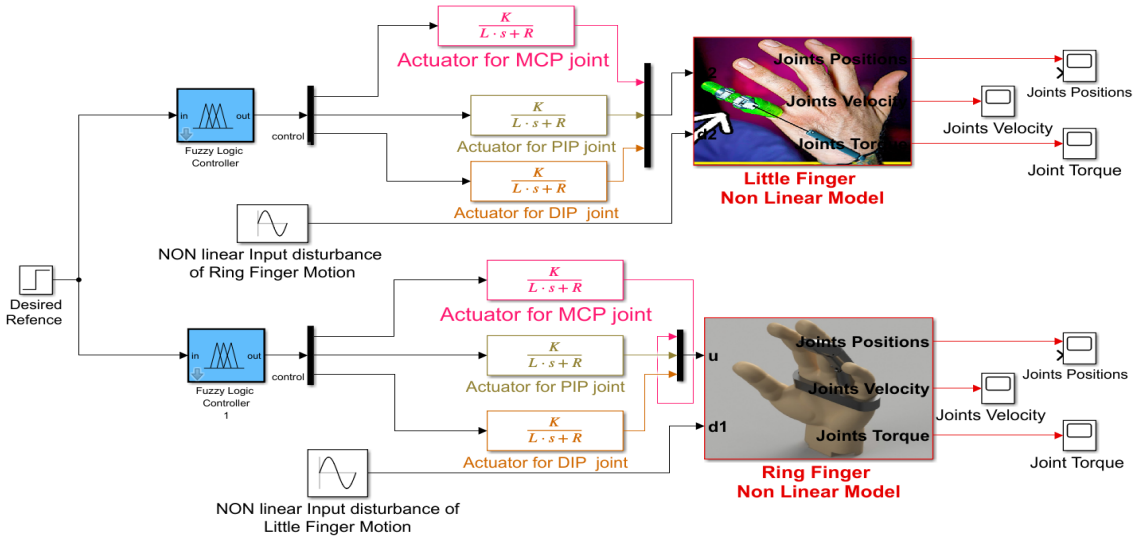

Figure 3.9: Simulink block Model of linearized system with developed linearized fuzzy logic model

3.4.3 Linearized System with Fuzzy logic Model

3.4.3.1 Simulink block Model of linearized system with developed linearized fuzzy logic model

System developed above represented the controlled architecture developed by using Fuzzy logic controller along three actuators dynamic transfer function expression and the non linear summarized little as well as ring finger dynamics.

3.4.3.2 Simulink Model for Ring Finger with Fuzzy logic controller

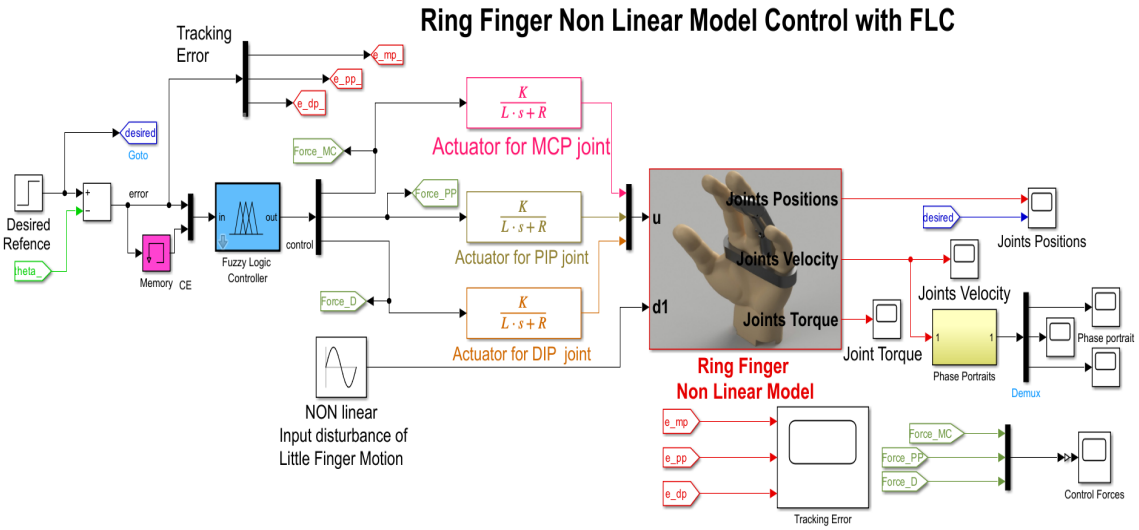

Figure 3.10: Simulink Model for individual Ring Finger with Fuzzy logic controller

Above Simulink block model has the dynamics including the FLC with crisp inputs and controller output obtained from FLC delivered to the actuators of joints of ring finger dynamic

3.4.3.3 Simulink Model for Little Finger with Fuzzy logic control architecture

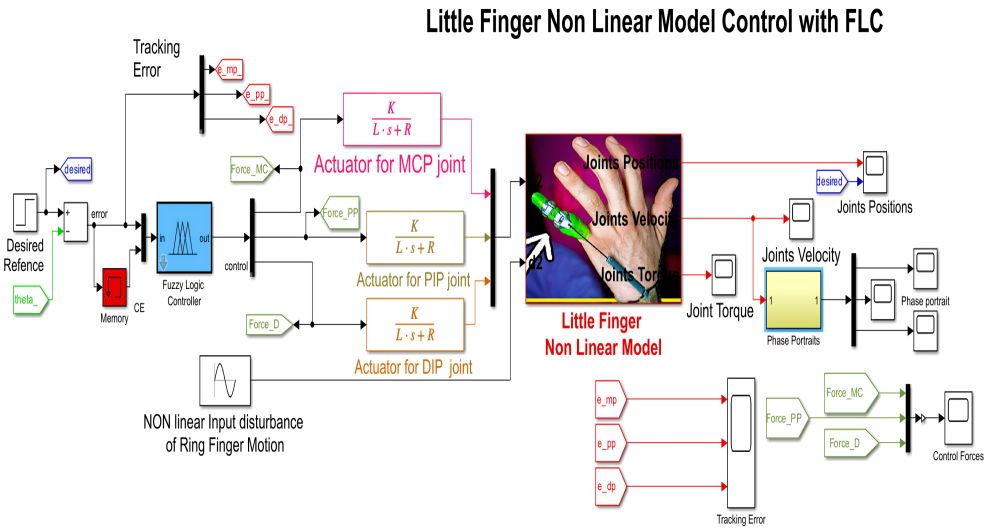

Figure 3.11: Simulink Model for Little Finger with Fuzzy logic controller

Simulink model developed for little finger joint movement-controlled system along fuzzy logic control architecture is shown in above figure. The MCP, PIP and DIP joints actuators received the controlled input signal obtained from FLC and actuate the Little finger joints as menntioned above.

3.4.4 Sliding Mode control with Fuzzy logic architecture design and implementation

Generic block schematic of FLC-SMC control structure is shown below

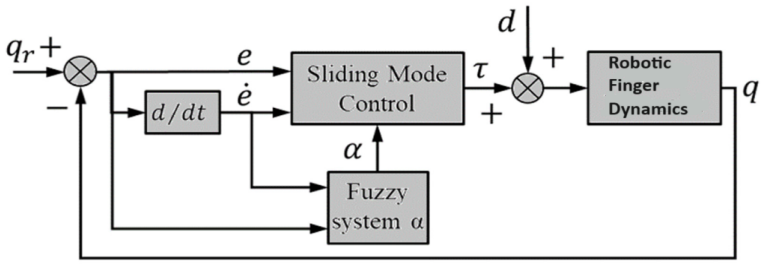

Figure 3.12: Generic block diagram of FLC-SMC control structure

Sliding surface expression:

$$S = e' + c_1 e \tag{3.88}$$

$$S = e' + Ke \tag{3.89}$$

$$S = e'' + c_1 e' \tag{3.90}$$

$$s'_\theta = -k_1 \sqrt{\theta} \, \mathrm{sgn}(s_\theta) k_2 \int \mathrm{sgn}(s_\theta) dt + \varphi_1(t) \tag{3.91}$$

Alternatively, the sliding surface P can be expressed by position and velocity expression expressed as:

$$p = \left[\frac{d}{dt} + \lambda \right] \tilde{x} \tag{3.92}$$

$$p = [\tilde{x'} + \lambda] \tilde{x} \tag{3.93}$$

Implement Sliding mode control architecture in Simulink:

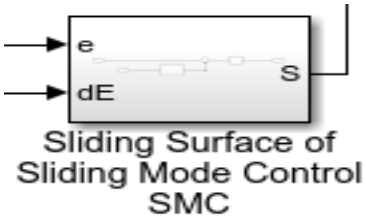

Figure 3.13: SMC architecture in Simulink

Defining the block model for sliding surface

Sliding surface for Sliding mode controller along discrete time differentiation block shown as below.

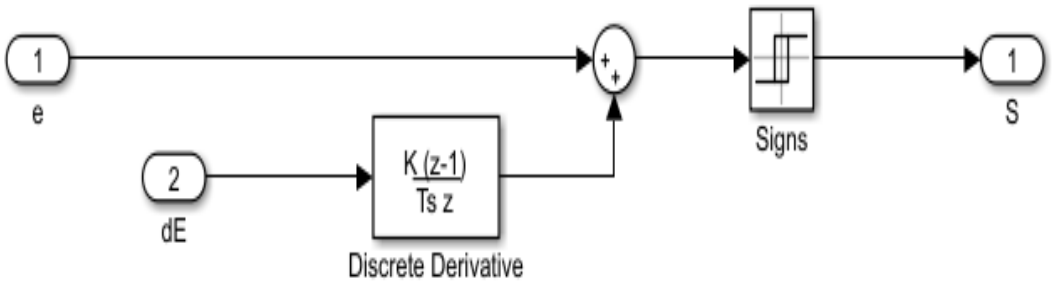

Figure 3.14: Block model for sliding surface

SMC control structure with Fuzzy logic controller

The complete Sliding mode control architecture along Fuzzy logic controller dynamics Simulink block model is shown below.

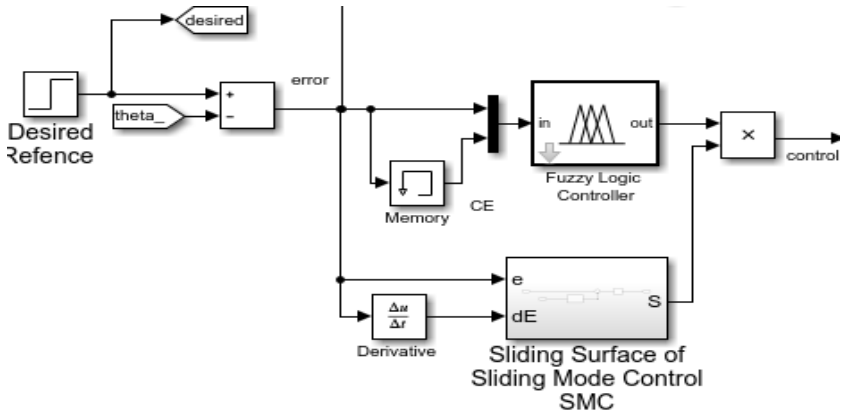

Figure 3.15: SMC control structure with Fuzzy logic controller

3.4.5 Simulink block model with SMC FLC control architecture for Ring Finger motion control

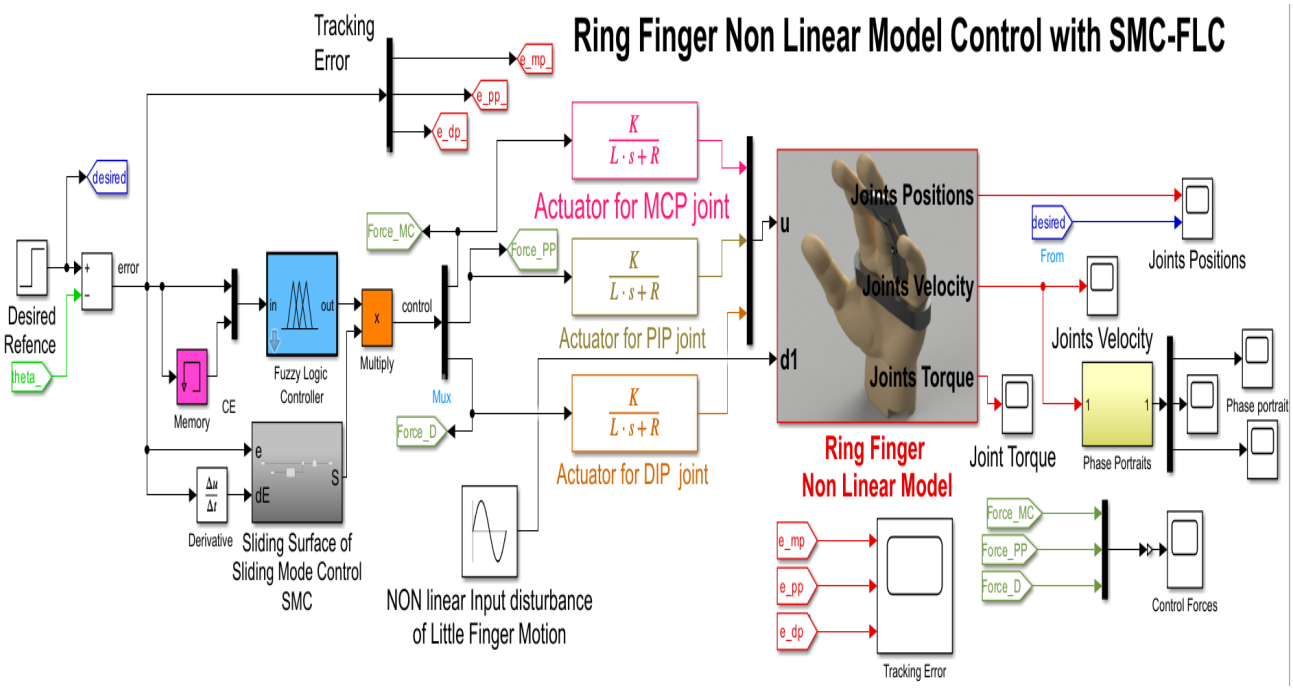

Figure 3.16: Simulink block model with SMC FLC control architecture for Ring Finger motion control

Simulink Model block diagram represented the SMC along Fuzzy logic control architecture to control the joint angle movements of ring finger is shown in above figure.

3.4.6 Simulink block mode with SMC FLC control architecture for Little Finger motion control

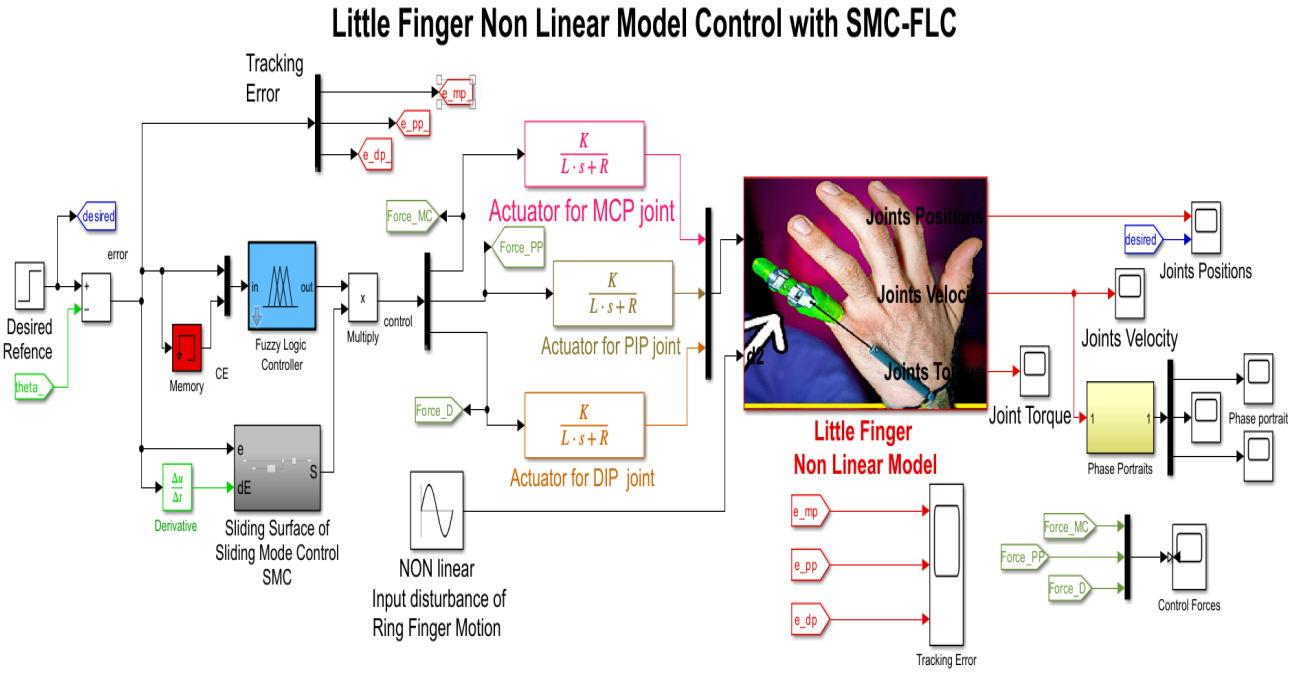

Figure 3.17: Simulink block model with SMC FLC control architecture for Little Finger motion control

Simulink Model block diagram representing the SMC along with FLC architecture to control the joint angle movements of little finger is shown in above figure.

Architecture has non linear dynamic model of little finger along Fuzzy SMC controller. Three actuators installed to control the non-linear movements of joints of the little finger.
Simulink Components of developed system:

Step Block: The reference input supplied to system is applied by step input block.

De-Mux: To encode the multiple information scattered to multiple line obtained from single line.

Transfer function block: To define the system in Laplace transformation domain or in form of numeration and denominator expression of s-domain for system dynamics.

Subsystem block: This block includes the nonlinear system dynamic model developed in previous section.

3.4.6.1 System Identification:

If the kinematics, biomechanics mathematical data for the finger motion not provided then there will be determination of finger dynamic motion model with the use of system

identification tool.
Depending upon the profile motion we will definitely determine and identify the transfer function or state space expression of ring and little finger dynamic model.

3.4.6.2 Novelty:

There are following innovative and novel prospective of this research-based work:

1. To develop the system that will be capable to obtain uniform, great flexible motion of ring and little finger that are unable to move independently.

2. The intelligent based fuzzy logic control ensures the optimized, required, effective motion control of little and ring finger with desired and uniform manner.

3. The fuzzy logic-based control ensures the linearization, if biomechanics model of finger is nonlinear in nature.

4. Desired transient response parameters as well as steady state parameters like settling time and steady state value will be achieved for dynamic angular motions of finger with more robust and effective control.

Chapter 4

Experiments and Results

4.1 Simulations Results for Ring Finger Nonlinear System

4.1.1 Nonlinear joint Position of ring finger

Obtained simulation results shows the non-linear joint position output response under uncontrolled behavior or without any controller design and implementation for ring finger joint motion control of MCP, PIP and DIP joints, the steady state value is not stable and transient response is also very slow. The obtained simulation results for joint positions of ring finger for Nonlinear System is shown in Figure 4.1.

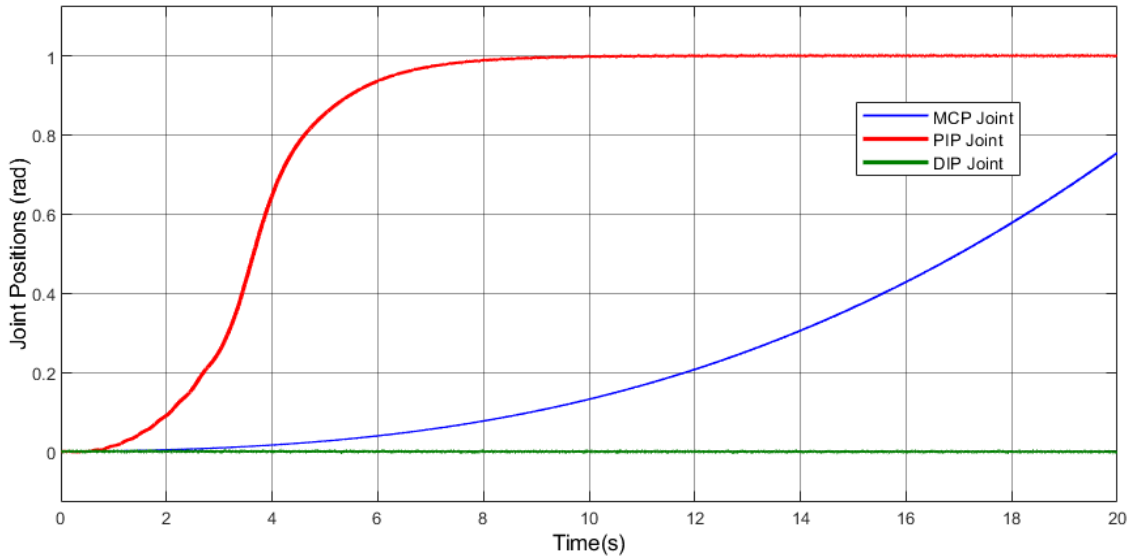

Figure 4.1: Nonlinear joint Position of ring finger

4.1.2 Nonlinear joint Velocity of ring finger

Obtained simulation results shows the uncontrolled nonlinear behavior for the ring finger joint velocities curves. The non stable and non-stationary steady state observed for the joint velocities of ring finger movement without any implementation of control scheme. The simulation results for joint velocity of ring finger is shown in Figure 4.2.

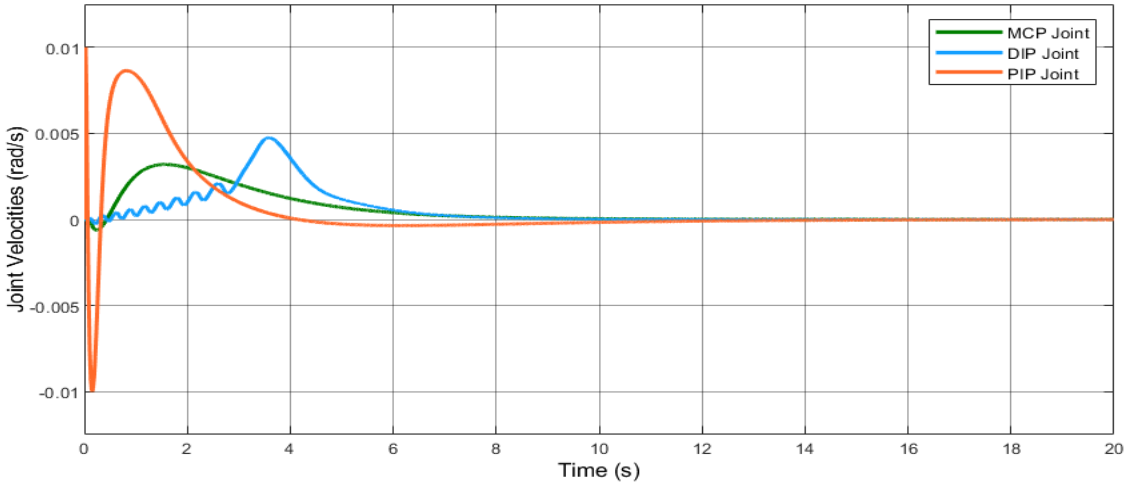

Figure 4.2: Nonlinear joint Velocity of ring finger

4.1.3 Nonlinear joint torque of ring finger

The output response or joint torque graph are displayed in the figure below. The steady state results demonstrate the actuator movement's uncontrollably oscillatory behaviour for the output torque of ring finger joint. The obtained simulation results for joints torque of ring finger for Nonlinear System is shown in Figure 4.3.

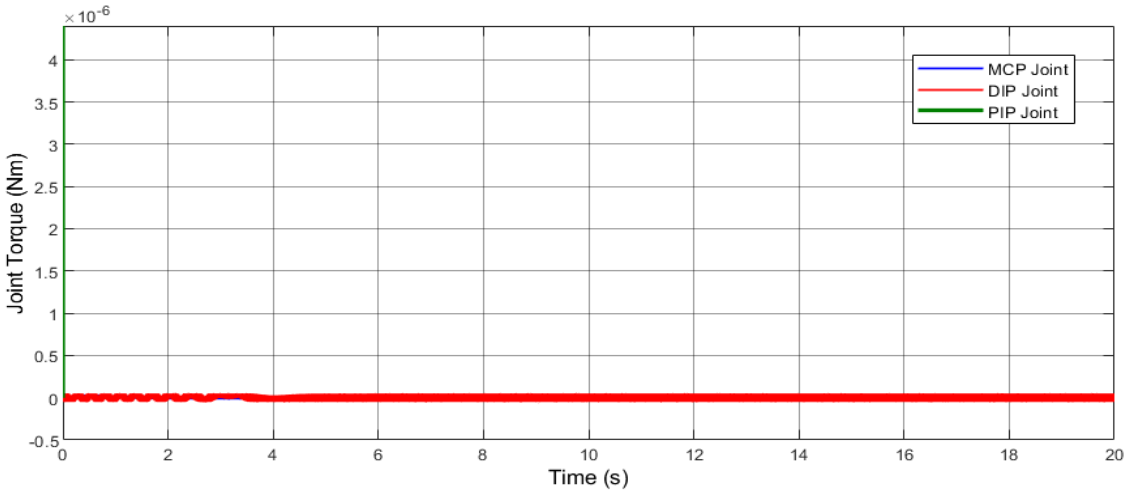

Figure 4.3: Nonlinear joint torque of ring finger

4.2 Simulations Results for Little Finger Nonlinear System

4.2.1 Nonlinear joint Position of little finger

Obtained simulation results show the non-linear joint position output response under uncontrolled behavior or without any controller design and implementation for little finger joint motion control of MCP, PIP and DIP joint. The steady state value is not stable and transient response is also very slow. The obtained simulation results for joints position of little finger for nonlinear system is shown in Figure 4.4.

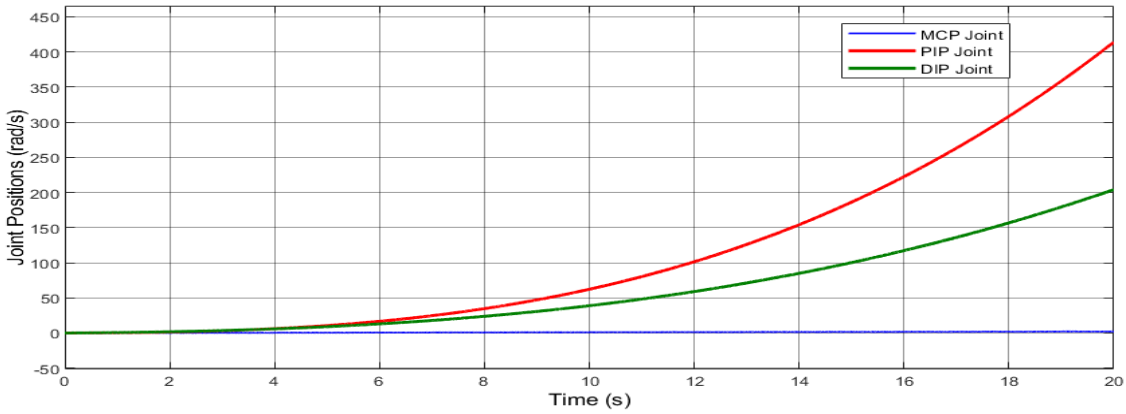

Figure 4.4: Nonlinear joint Position of little finger

4.2.2 Nonlinear joint Velocity of little finger

The obtained simulation response demonstrates the uncontrolled nonlinear nature of the little finger joint velocities curves in the absence of any implementation of control scheme. The simulation results for joint velocity of little finger is shown in Figure 4.5.

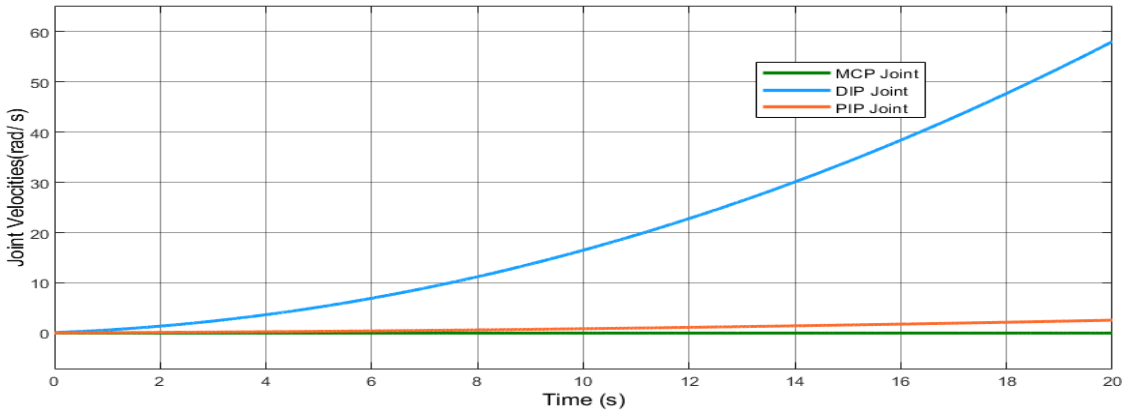

Figure 4.5: Nonlinear joint Velocity of little finger

4.2.3 Nonlinear joint torque of little finger

Initial values for the joint torque response not so much of high magnitude and steady state value for the torque values for each of the actuators attached for PIP, MCP and DIP joints is not zero rather than greater than zero shows the energy loss by actuator for little finger dynamic motion control. The obtained simulation results for joints torque of little finger for nonlinear System is shown in Figure 4.6.

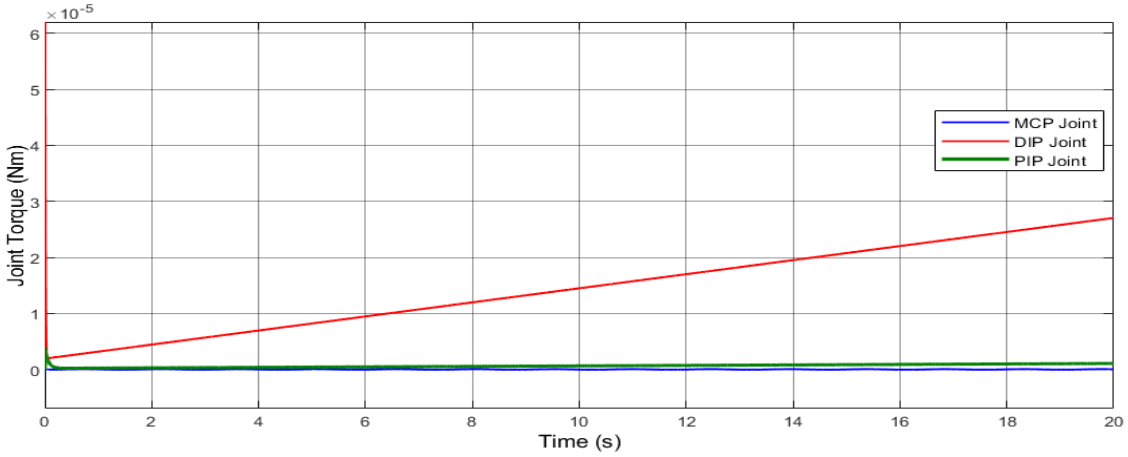

Figure 4.6: Nonlinear joint torque of little finger

4.3 Simulations Results for Ring Finger with Fuzzy Logic Controller

4.3.1 Ring Finger Joint Positions

The controlled position response obtained for the system developed with FLC shown below is stable, robust and effective. Controlled transient as well as steady state parameters achieved for the system developed to control the joint position control of ring finger. When discussing the step response, refers to the %overshoot that the system reaction exceeds the final steady-state value prior to reaching a stable level. The results display a rising time of 0.35 seconds with peak time that is 0.4 second with an approximate overshoot of 18% and stabilize approximately from 2 to 2.5 seconds for MCP joint. Rise time of 0.2 second and peak time of 0.3 seconds with the % overshoot of 21% and also settling time of 1.5 second approximately for PIP joint and the 0.3 second of rise time and peak time of 0.6 seconds with an approximate overshoot of 15% and settling time of 4 seconds for DIP joint. While rest of results are shown in performance parameters of ring finger joints control motion. Simulation results for joints position of ring finger is shown in Figure 4.7.

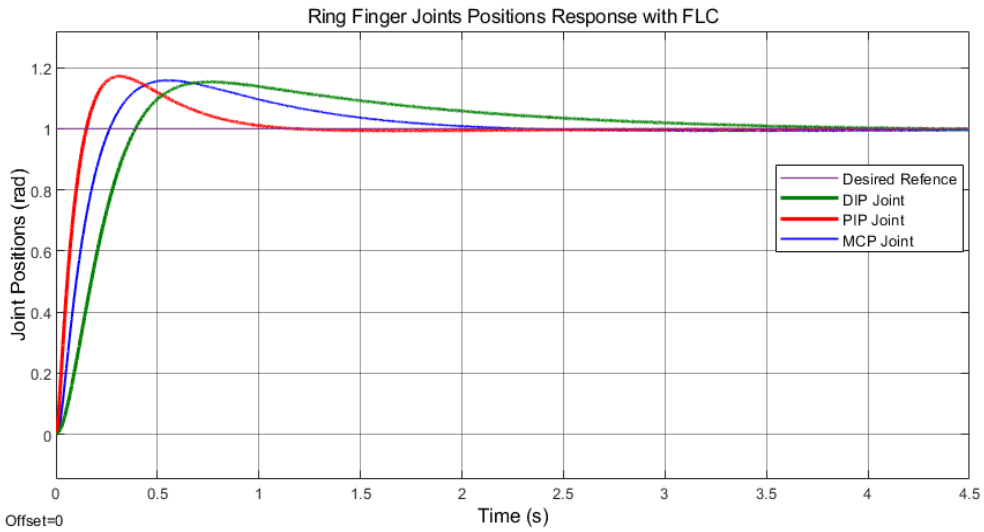

Figure 4.7: Joint Position for Ring finger motion Response

4.3.2 Ring Finger Joint Velocity

The controlled velocity response shows the controlled angular velocity response for ring finger joint movement control of MCP, PIP and DIP joints with fuzzy logic control architecture. The output results display a rise time 0% to 100% of its final value that is 0.04 seconds with an approximate settling time of 0.6 second for MCP. The rise time of 0.1 seconds can be seen in Figure 4.8 with the approximately settling time of 0.9 second for PIP joint and 0.05-second rise time with an approximate settling time of 0.7 second for DIP joint. The plant's output stabilises after about one second of simulation time for all joints. Simulation results for joints velocity of ring finger is shown in Figure 4.8.

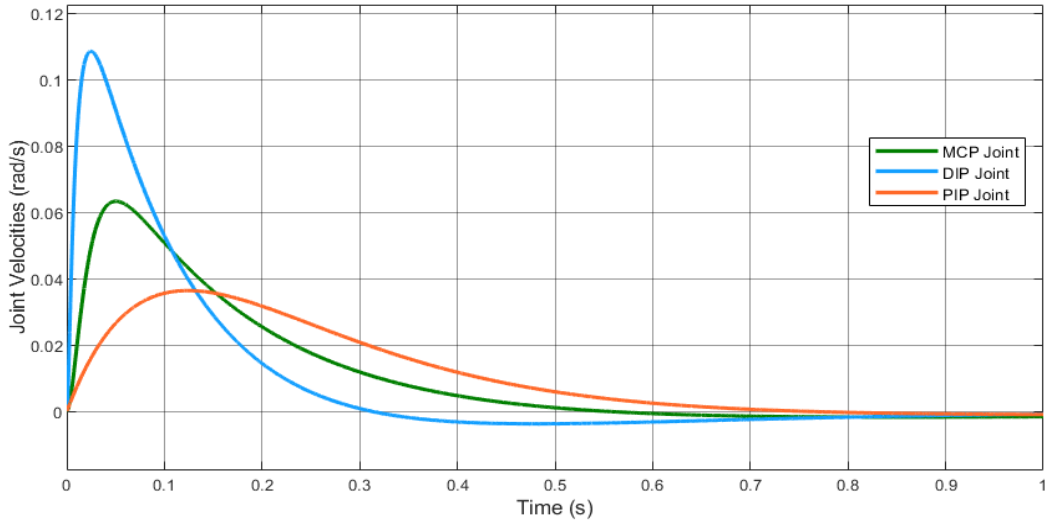

Figure 4.8: Joint Velocity for Ring finger motion Response

4.3.3 Ring Finger Joint Torque

The uniform smooth and optimized response obtained represented the controlled torque behavior for the joint actuator motion control with Fuzzy logic control architecture. The Controlled system with FLC control architecture exhibit the stable, optimized output response with minimum steady state value of joint actuator torque obtained by FLC. The output results display a rise time that is 0.01 second with an approximate settling time of 0.2 second for MCP. The rise time of 0.02 second can be seen in Figure 4.9 with the approximately settling time of 0.2 second for PIP joint and 0.04 second rise time with an approximate settling time of 0.3 second for DIP joint. Simulation results for joints torque of ring finger is shown in Figure 4.9.

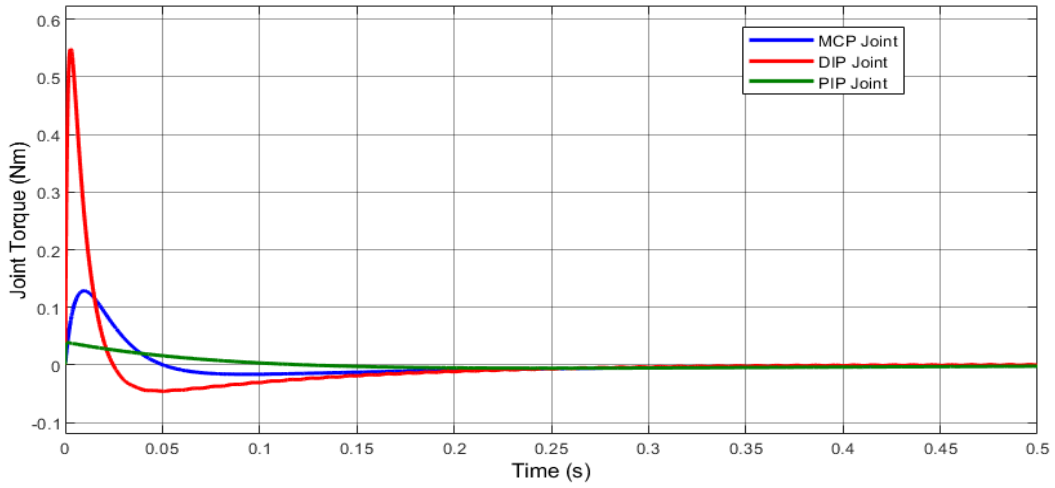

Figure 4.9: Joint Torque for Ring finger motion Response

4.4 Control / Contact forces for Finger Joints

4.4.1 Control forces for ring finger joints

The response of each joint linear actuator to actuator control is achieved through the design and application of a flc controller, as depicted in figure below. At a steady state, the control effort forces for every joint response are stable, minimised, and reach a stable value. Control forces for ring finger joints is shown in Figure 4.10.

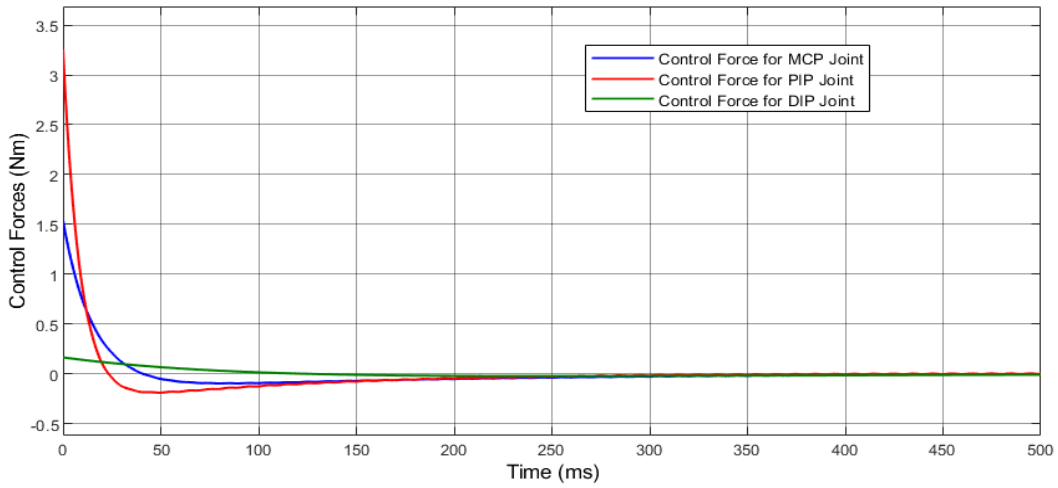

Figure 4.10: Control forces for ring finger joints with FLC

4.5 Tracking Error History for Finger Joints

4.5.1 Tracking error history for ring finger joint position control

Mentioned figure shows that there is tracking error present at the start but after approximately 3 seconds tracking error approaches to zero which shows that the controller track the perfect trajectory. Tracking error(rad) is eliminated at steady state response for the joint motion control of little finger MCP, PIP and DIP joints actuator and dynamic process control. Tracking error history for little finger joints is shown in Figure 4.19.

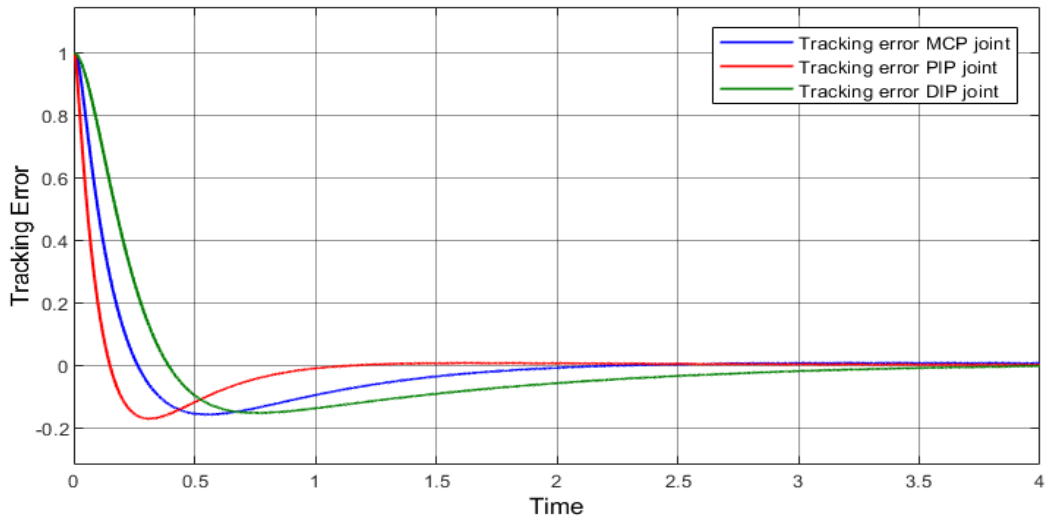

Figure 4.11: Tracking error history for ring finger joint position control with FLC

4.6 Phase portrait for Finger Joints

4.6.1 Phase portrait for ring finger MCP joint

Position along y-axis with respect to x-axis change observed or phase portraits for the ring finger movement in geometrical view observed in below figure is constrained and confined for MCP joint of ring finger. Phase portraits for ring finger MCP joint is shown in Figure 4.12.

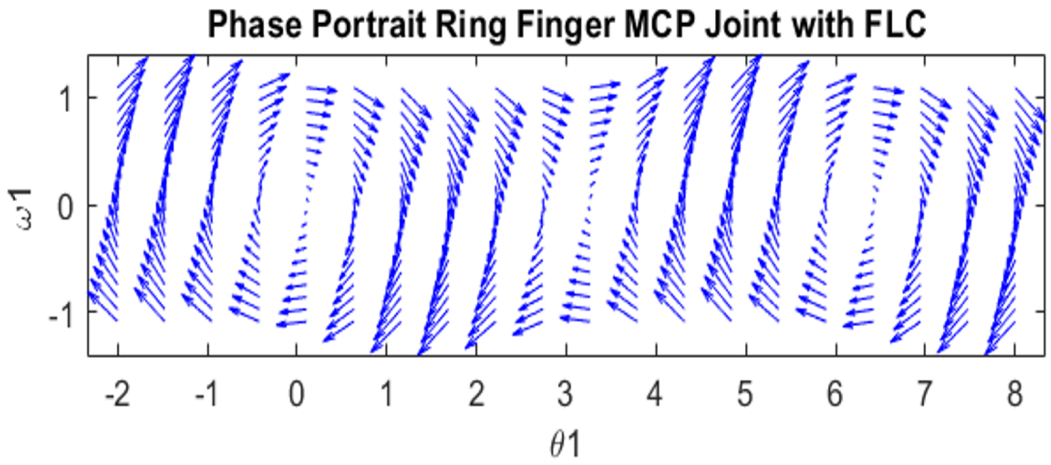

Figure 4.12: Phase portrait for ring finger MCP joint with FLC

4.6.2 Phase portrait for ring finger PIP joint

For the ring finger movement in the geometrical view shown in the below figure, position along the y-axis with regard to the observed x-axis change, or phase portraits, are constrained and circumscribed, restricted and uniform for the PIP joint of the ring finger. Phase portrait for ring finger PIP joint is shown in Figure 4.13.

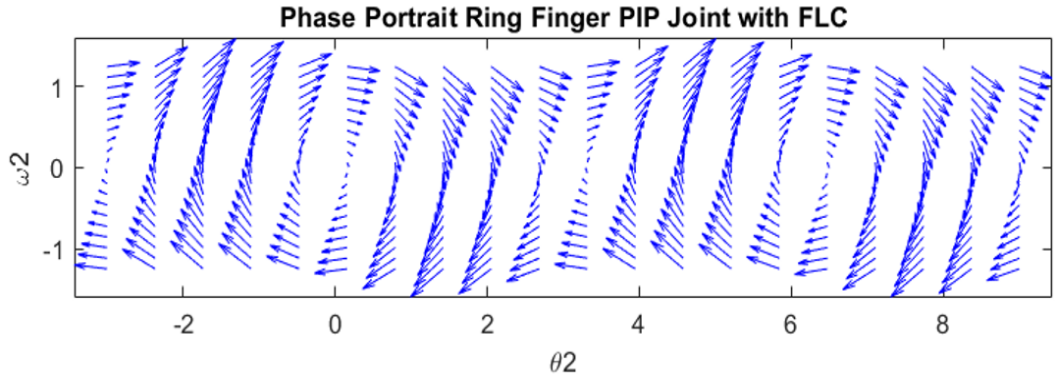

Figure 4.13: Phase portrait for ring finger PIP joint with FLC

4.6.3 Phase portrait for ring finger DIP joint

For the ring finger's DIP joint, position along the y-axis with respect to the observed shift in the x-axis, or phase portraits for the ring finger's movement in the geometrical view displayed in the figure below, are uniformly restricted and circumscribed. Phase portrait for ring finger DIP joint is shown in Figure 4.14.

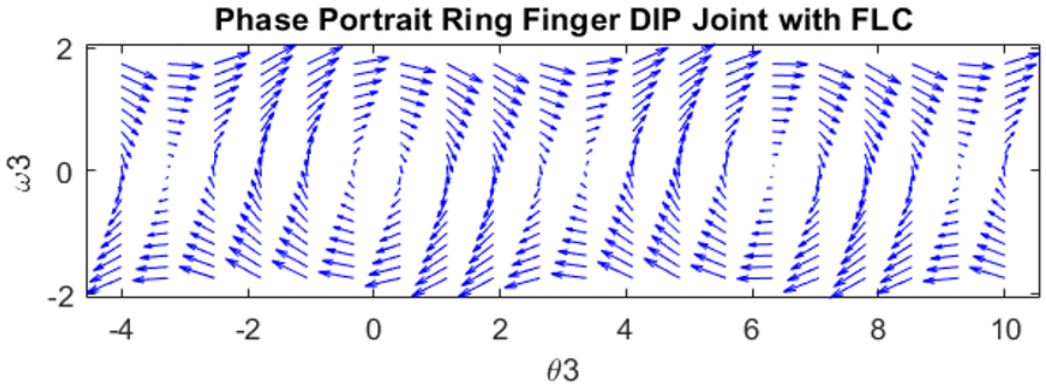

Figure 4.14: Phase portrait for ring finger DIP joint with FLC

4.7 Performance parameters of Ring Finger joints control motion

The output of the plant shows how applicable FLC control system for the 12-th order minimal state space realisation model. When discussing the step response, refers to the %overshoot that the system reaction exceeds the final steady-state value prior to reaching a stable level. The chart displays a rising time of 0.5 seconds with an approximate overshoot of 18%. The plant output stabilises after the simulation lasts for about three seconds. The plant's reaction is depicted in the Figure 4.7 when the ring finger's PIP deflects; the response stabilises after around 3.5 seconds of simulation time. The rise time of 0.9 seconds can be seen in above mention figure with the % overshoot of 21% approximately. After approximately 3 seconds of simulation time, the plant's output becomes stable. The Figure 4.7 shows the 0.6 second rise time with an approximate overshoot of 15%. The plant's output stabilises after about three and a half seconds of simulation time.

Transient as well as steady state performance parameters observed above for the MCP, PIP and DIP joint motion performance parameters are optimized, robust, effective and desired.

4.8 Simulations Results for Little Finger with Fuzzy Logic Controller

4.8.1 Little Finger Joint Positions

The obtained response for little finger joint position under Fuzzy logic controller design and implementation observed in above figure. The response is smooth, uniform and steady state stable behavior also controlled transient as well as steady state performance parameters achieved. For the MCP joint, the result shows a settling time of 1.6 seconds with an approximate overshoot of 0.6% and rise time of 0.2 second with approximately peak time of 0.4 second. The PIP joint has a settling time of 2.8 seconds with an approximate overshoot of 0.5% as well as rise time of 0.3 second, and the DIP joint had a settling time of 1 second with an approximate overshoot of 0.6% along with rise time of 0.1 second which is more shorter tie as compared to other joints. The remaining outcomes, however,rest of results are displayed in the ring finger joints' control motion performance characteristics. Simulation results for joints position of little finger is shown in Figure 4.15.

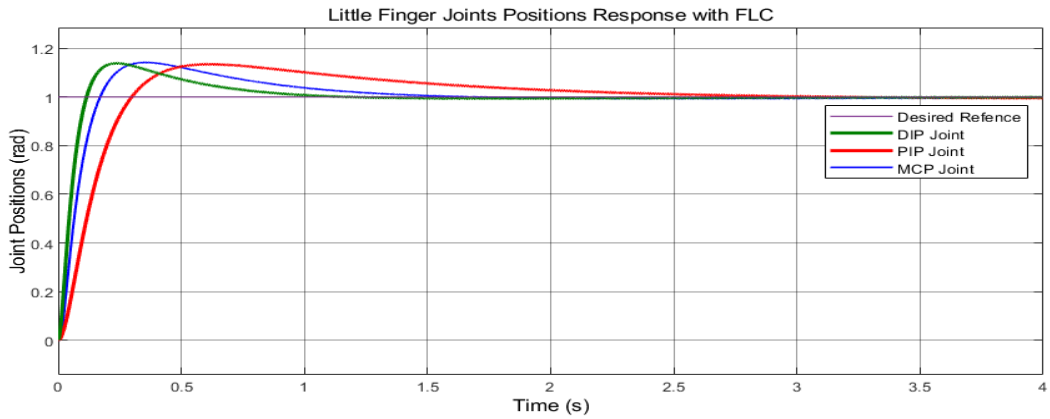

Figure 4.15: Little finger Joint position Response with FLC

4.8.2 Little Finger Joint Velocity

Fuzzy logic-controlled output response for joint velocities of joints for little finger dynamic motion controlled for joints observed. The output results display a rise time that is 0.08 seconds with an approximate settling time of 0.3 second for MCP. The rise time of 0.1 second can be seen in Figure 4.16 with the approximately settling time of 0.5 second for PIP joint and 0.04 second rise time with an approximate settling time of 0.8 second for DIP joint. Simulation results for joints velocity of little finger is shown in Figure 4.16.

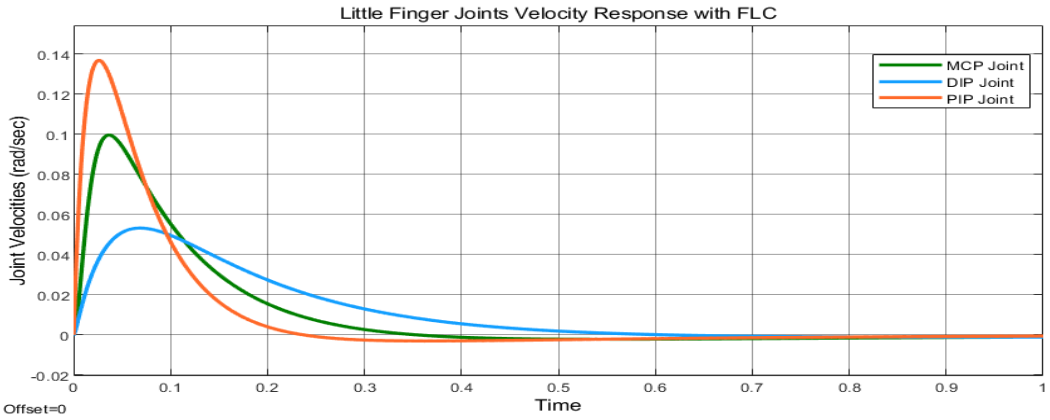

Figure 4.16: Little finger joint velocity response with FLC

4.8.3 Little Finger Joint Torque

Little finger joint actuators torque response-controlled behavior obtained by FLC control architecture observed. The transient minimized value obtained for the system torque response as well as steady state zero value achieved with design and implementation of FLC architecture. The output results display a rise time that is 0.1 seconds with an approximate settling time of 0.3 second for MCP. The rise time of 0.7 second can be seen in Figure 4.17 with the approximately settling time of 0.3 second for PIP joint and 0.03 second rise time with an approximate settling time of 0.2 second for DIP joint. Simulation results for joints velocity of little finger is shown in Figure 4.17.

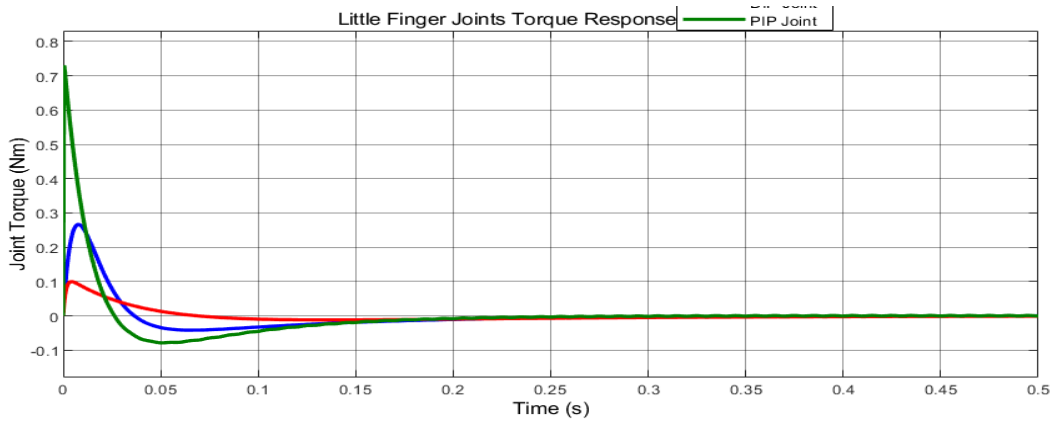

Figure 4.17: Joint Torque for little finger motion Response

4.9 Control / Contact forces for Finger Joints

4.9.1 Control forces for little finger joints

Actuator control forces response for each joint linear actuator obtained by design and implementation of Fuzzy logic controller shown in below figure. The control effort forces for each joint response are stable and minimized and stable value achieved at steady state. Control forces for little finger joints is shown in Figure 4.18.

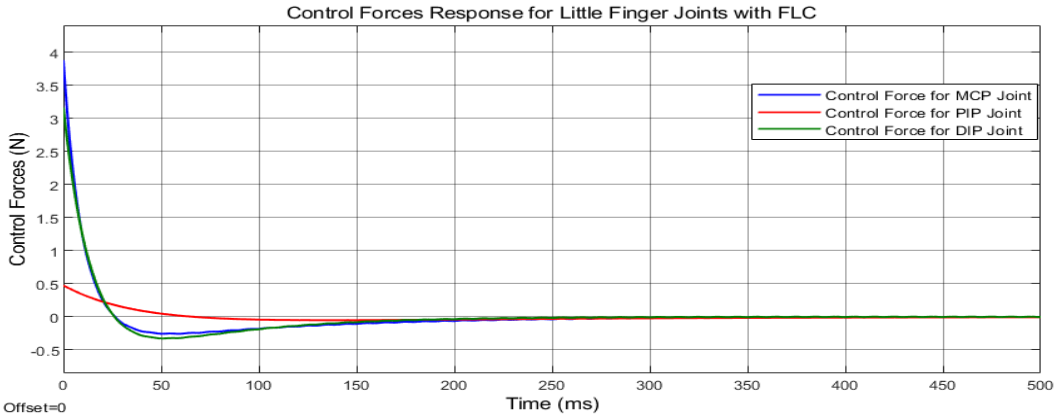

Figure 4.18: Control forces for little finger joints

4.10 Tracking Error History for Finger Joints

4.10.1 Tracking error history for little finger joint position control

Tracking error(rad) is eliminated at steady state response for the joint motion control of little finger MCP, PIP and DIP joints actuator and dynamic process control. Tracking error history for little finger joints is shown in Figure 4.19.

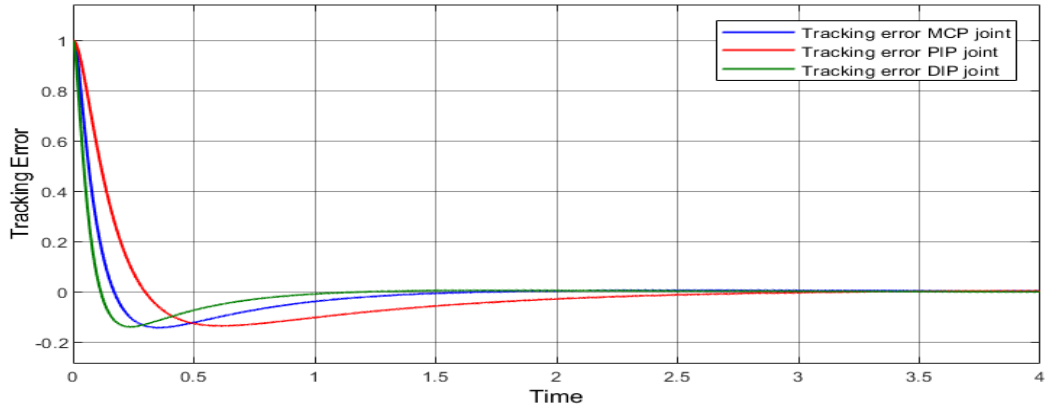

Figure 4.19: Tracking error history for little finger joint position control with FLC

4.11 Phase portrait for Finger Joints

4.11.1 Phase portrait for little finger MCP joint

Position along y-axis with respect to x-axis change observed or phase portraits for the ring finger movement in geometrical view observed in below figure is constrained and confined for MCP joint of ring finger. Phase portrait for little finger MCP joint is shown in Figure 4.20.

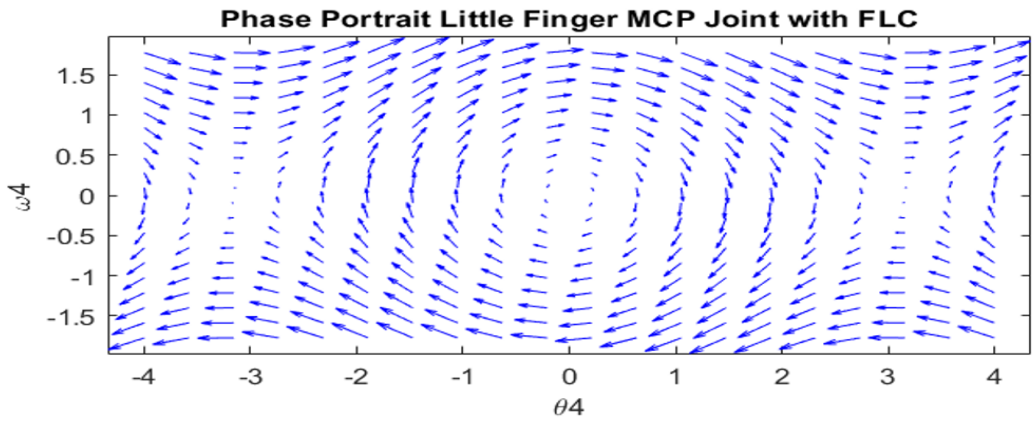

Figure 4.20: Phase portrait for little finger MCP joint with FLC

4.11.2 Phase portrait for little finger PIP joint

Position along y-axis with respect to x-axis change observed or phase portraits for the little finger movement in geometrical view observed in above figure is constrained and confined, restricted and uniform for PIP joint of little finger. Phase potrait for little finger PIP joint is shown in Figure 4.21.

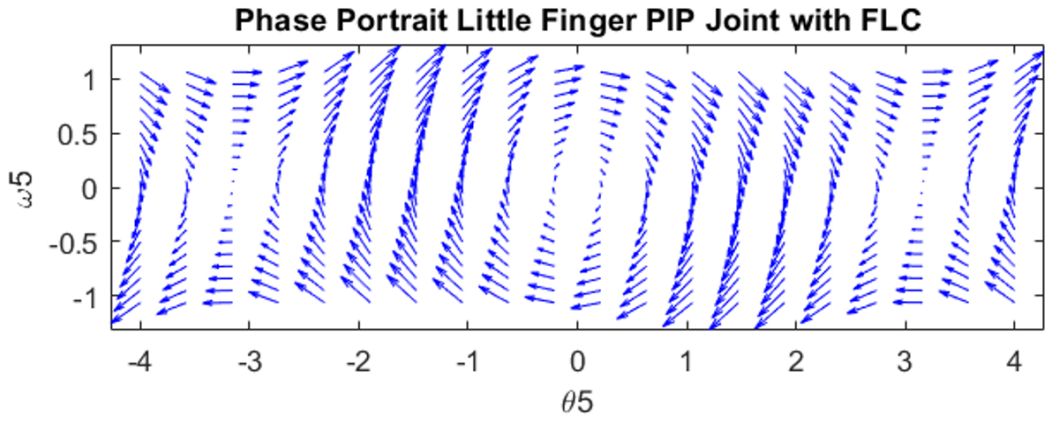

Figure 4.21: Phase portrait for little finger PIP joint with FLC

4.11.3 Phase portrait for little finger DIP joint

Position along y-axis with respect to x-axis change observed or phase portraits for the little finger movement in geometrical view observed in below figure is constrained and confined, restricted and uniform for DIP joint of little finger. Phase portrait for little finger DIP joint is shown in Figure 4.22.

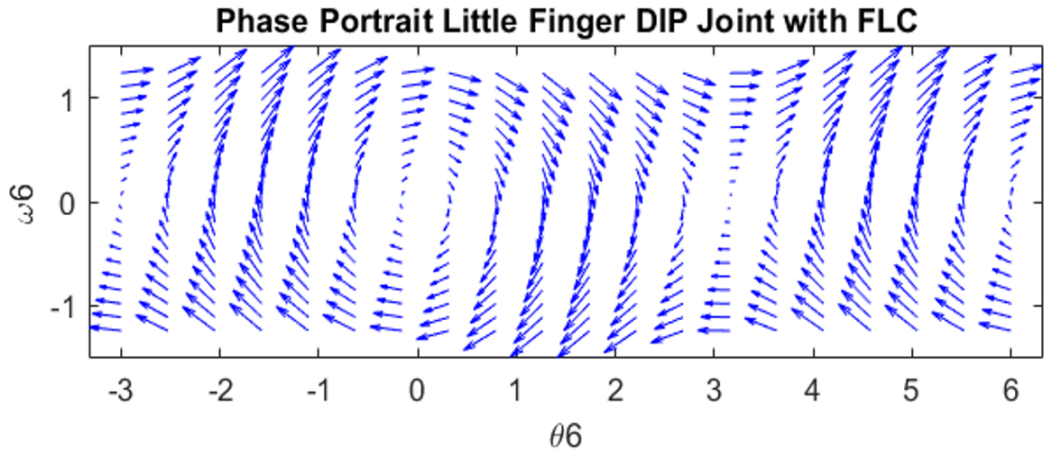

Figure 4.22: Phase portrait for little finger DIP joint with FLC

4.12 Performance parameters of Little Finger joints control motion

The little finger's positions of DIP, MCP,PIP are depicted in Figure 4.15, where the little finger's DIP initially deflects by 0.3 - 05 radian. In the simulation time, the response stabilises after about three second. The response following the introduction of a FLC controller shows that the outcomes are more consistent. In above mentioned figure the little finger's PIP initially deflects by 0.1 - 0.3 radian. In the simulation time, the response stabilises after about one and half second. The findings demonstrate the creation of a reliable controller for the two-finger bio-mechanical model, which includes the human hand's little and ring fingers. The mentioned figure shows the little finger's DIP initially deflects by 0.1 radian overall and stabilises after about one second.

Transient as well as steady state performance parameters observed above for the MCP, PIP and DIP joint motion performance parameters are optimized, robust, effective and desired.

4.13 Ring Finger Simulations with SMC-FLC

4.13.1 Joints Position Response for Ring finger with SMC-FLC control

The obtained response for ring finger joint position under sliding mode with fuzzy logic controller design and implementation is observed in the Figure 4.23. The response is smooth, uniform, and steady state stable behavior, as well as controlled transient and steady state performance parameters achieved as compared to just FLC control structure. The graph shows that the MCP joint has rise time of 0.04 seconds along peak time of 0.05 second and an approximate overshoot of 18% and a settling time of roughly 0.5 second. The PIP joint has an estimated overshoot of 21% during the 0.3-second settling time with peak time of 0.03 second, and the DIP joint has rise time of 0.02 second with an approximate overshoot of 15% during the 0.15 second of settling time . Additionally, the remaining results are displayed in the performance parameters of ring Finger joints control motion with SMC-FLC. Joints position response for ring finger with SMC-FLC control is shown in Figure 4.23.

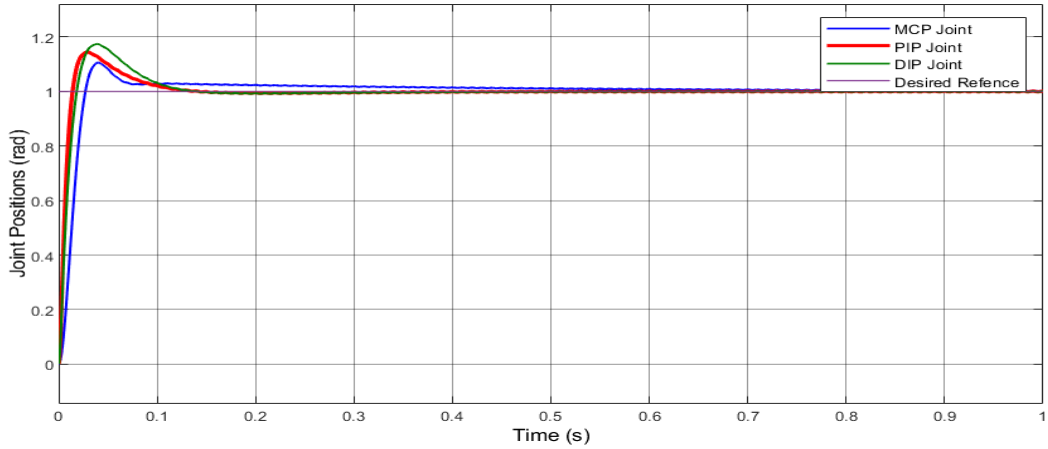

Figure 4.23: Joints Position Response for Ring finger with SMC-FLC control

4.13.2 Joint velocity Response for Ring finger with SMC-FLC control

SMC- Fuzzy logic-controlled output response for joint velocities of MCP, PIP and DIP joints for ring finger dynamic motion controlled for joints observed. The output results display a rise time that is 0.03 second with an approximate settling time of 0.1 second for MCP. The rise time of 0.02 second approximately can be seen in Figure 4.24 with the approximately settling time of 0.15 second for PIP joint and 0.01 second rise time with an approximate settling time of 0.09 second for DIP joint. Joints velocity response for ring finger with SMC-FLC control is shown in Figure 4.24.

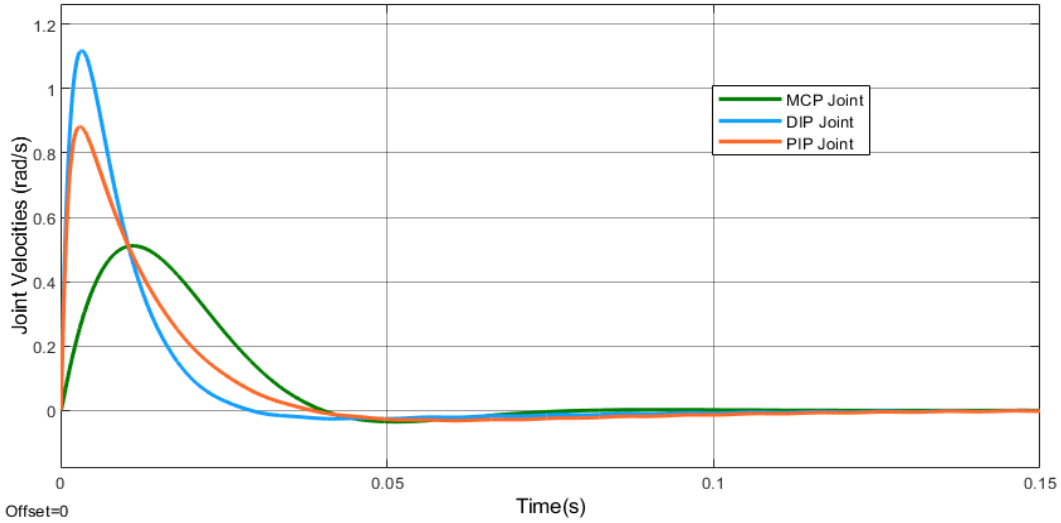

Figure 4.24: Joint velocity Response for Ring finger with SMC-FLC control

4.13.3 Joint Torque Response for Ring finger with SMC-FLC control

Less torque offered by actuators controlled by SMC -FLC control architecture developed and implemented for ring finger joint motion control as compared to simple FLC controller. The output results display a rise time that is 0.002 second with an approximate settling time of 0.04 second for MCP. The rise time of 0.0012 second approximately can be seen with the approximately settling time of 0.015 second for PIP joint and 0.0015 second rise time with an approximate settling time of 0.025 second for the DIP joint. Joints torque response for ring finger with SMC-FLC control is shown in Figure 4.25.

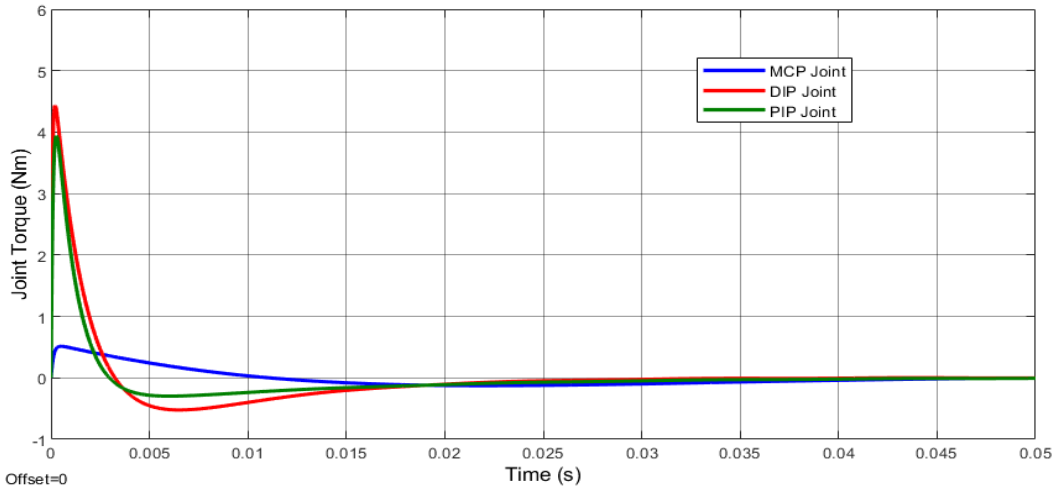

Figure 4.25: Joint Torque Response for Ring finger with SMC-FLC control

4.14 Control / contact forces for finger joints with SMC-FLC

4.14.1 Control forces of joint position for Ring finger with SMC-FLC

Control efforts required by controller based on SMC-FLC architecture is less and controlled transient as well as steady state response observed as compared to just Simple FLC architecture developed for joint motion control of ring finger. Control / contact forces for finger joints with SMC-FLC control is shown in Figure 4.26.

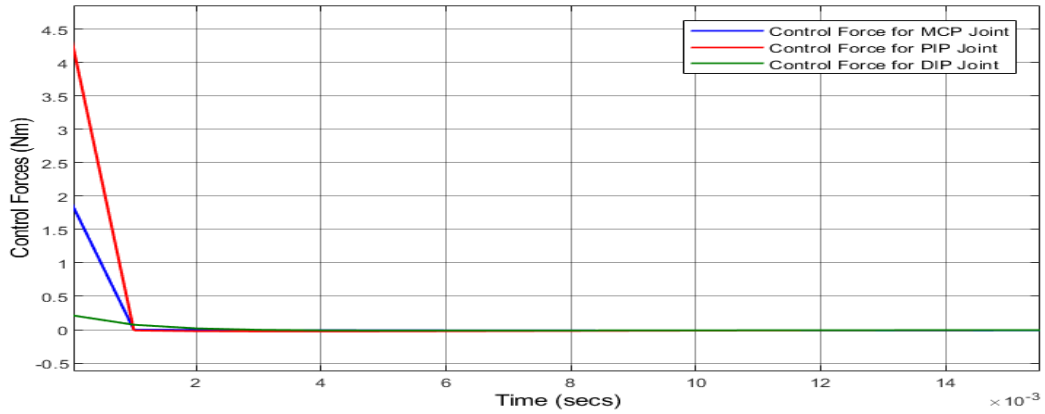

Figure 4.26: Control / contact forces for finger joints with SMC-FLC

4.15 Tracking Error History for Finger Joints with SMC-FLC

4.15.1 Tracking error history for ring finger position control with FLC-SMC controller

ZERO steady state error achieved quickly with fast transient response observed for developed system with SMC-FLC based control architecture. Tracking error history for ring finger position control with FLC-SMC controller is shown in Figure 4.27.

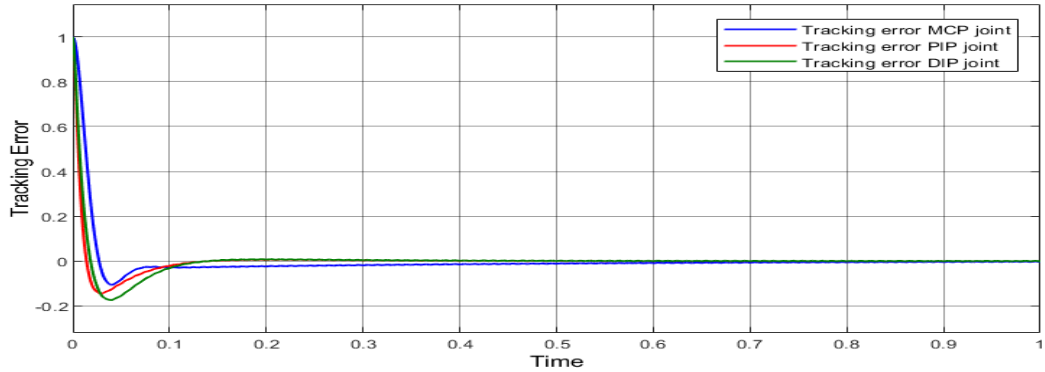

Figure 4.27: Tracking error history for ring finger position control with FLC-SMC controller

4.16 Phase portraits for Ring finger with SMC-FLC

4.16.1 Phase portrait for MCP joint of Ring finger with SMC-FLC

Position along y axis with respect to x axis change observed or phase portraits for the ring finger movement in geometrical view observed in above figure is constrained and confined, restricted and uniform for MCP joint of ring finger. The robustness is seen in Figures 4.28 , 4.29 and 4.30. By lowering the boundary layer, it is also possible to track under higher load. Nevertheless, λ must be more than 4 or equal to 4. Otherwise, the convergence will accelerate unintentionally. Recall that asymptotical convergence is best achieved with λ values between 4-6. As a result, λ affects the controller significantly and has the greatest potential for change.

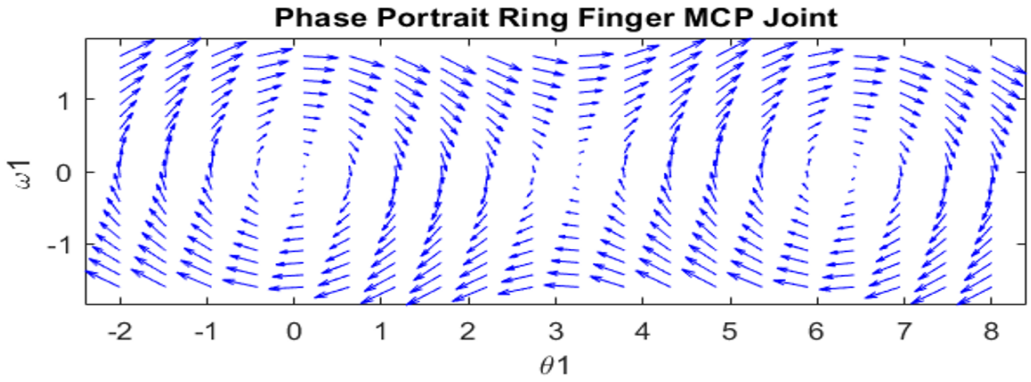

Figure 4.28: Phase portrait for MCP joint of Ring finger with SMC-FLC

4.16.2 Phase portrait for PIP joint of Ring finger with SMC-FLC

Position along y axis with respect to x axis change observed or phase portraits for the ring finger movement in geometrical view observed in above figure is constrained and confined, restricted and uniform for this joint of ring finger. Phase portraits for PIP joint of ring finger with FLC-SMC controller is shown in Figure 4.29.

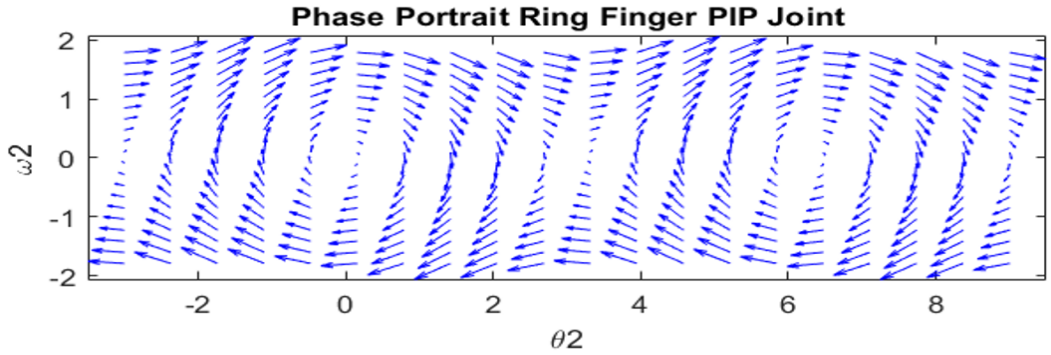

Figure 4.29: Phase portrait for PIP joint of Ring finger with SMC-FLC

4.16.3 Phase portrait for DIP joint of Ring finger with SMC-FLC

Position along y axis with respect to x axis change observed or phase portraits for the ring finger movement in geometrical view observed in above figure is constrained and confined, restricted and uniform for DIP joint of ring finger. Phase portraits for DIP joint of ring finger with FLC-SMC controller is shown in Figure 4.30.

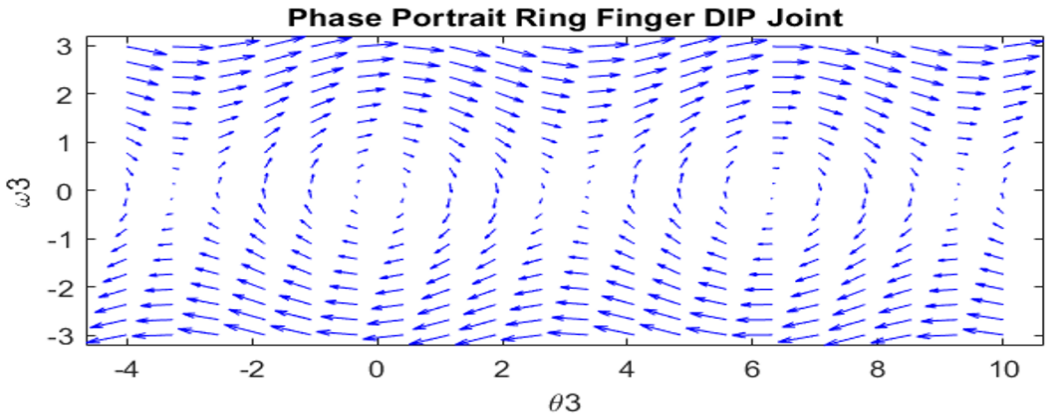

Figure 4.30: Phase portrait for DIP joint of Ring finger with SMC-FLC

4.17 Performance parameters of Ring Finger joints control motion with SMC-FLC

The %overshoot, which occurs when the system reaction surpasses the final steady-state value before reaching a stable level, is referred to when discussing the step response. The Figure 4.23 shows a 0.150 second rise time with an approximate 18% overshoot. After roughly one second of simulation, the plant output stabilizes. When the ring finger's DIP deflects, the plant response stabilises after about 0.2 seconds of simulation time. Above mentioned figure shows the rise time of 0.05 seconds or half of 0.1 second with an approximate overshoot of 21.3%.
The plant output stabilises after the simulation lasts for about one second. When the ring finger's DIP deflects, the plant's response is seen in the mentioned figure; the response stabilises after about 0.7 seconds of simulation time. When discussing the step response, overshoot refers to the percentage that the system reaction exceeds the final steady-state value prior to reaching a stable level.

Improved performance parameters for all of three joints movement-controlled output response observed for the system with control architecture of SMC-FLC controller.

4.18 Little Finger simulation with SMC-FLC control architecture

4.18.1 Joints Position Response for Little finger with SMC-FLC control

Obtained response for little finger joint position under Sliding Mode-Fuzzy logic controller design and implementation observed in mentioned figure. The response is smooth, uniform and steady state stable behavior as well as controlled transient as well as steady state performance parameters achieved as compared to just FLC control structure. The output results display a rise time that is 0.1 second with an approximate settling time of 2 seconds for MCP.
The rise time of 0.2 second approximately can be seen in Figure 4.31 with the approximately settling time of 2.3 second for PIP joint and 0.35 second rise time with an approximate settling time of 2.5 second for DIP joint. Joints Position Response for Little finger with SMC-FLC controller is shown in Figure 4.31.

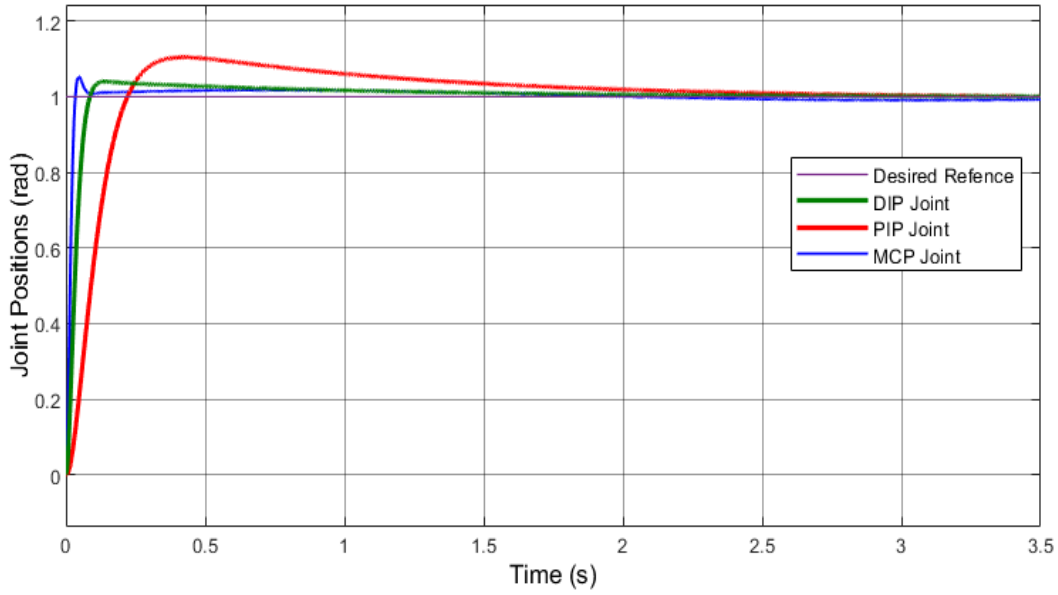

Figure 4.31: Joints Position Response for Little finger with SMC-FLC control

4.18.2 Joints Velocity Response for Little finger with SMC-FLC control

SMC- FLC controlled output response for joint velocities of MCP, PIP and DIP joints for little finger dynamic motion controlled for MCP, PIP and DIP joints observed.
Joints Velocity Response for Little finger with SMC-FLC controller is shown in Figure 4.32.

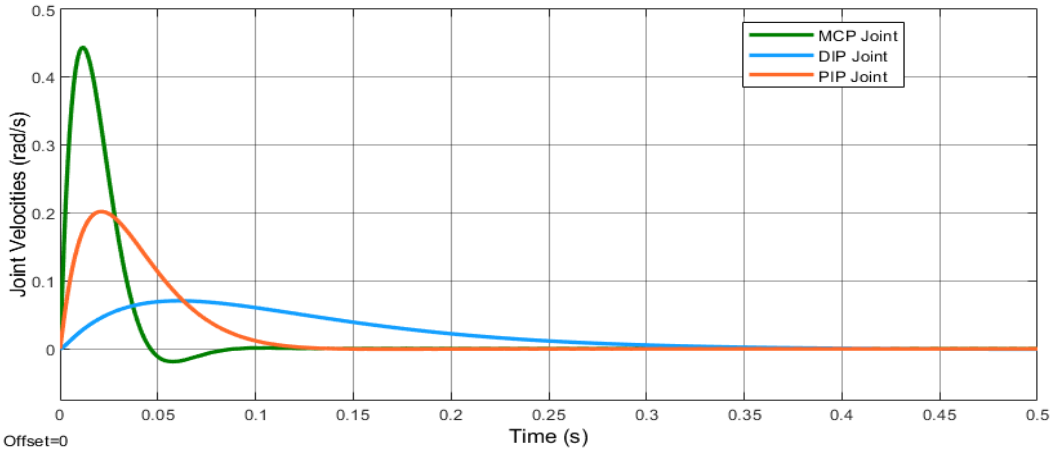

Figure 4.32: Joints Velocity Response for Little finger with SMC-FLC control

4.18.3 Joints Torque Response for Little finger with SMC-FLC control

Low torque offered by actuators controlled by SMC -FLC control architecture developed and implemented for little finger joint motion control as compared to simple FLC controller. Joints torque Response for Little finger with SMC-FLC controller is shown in Figure 4.33.

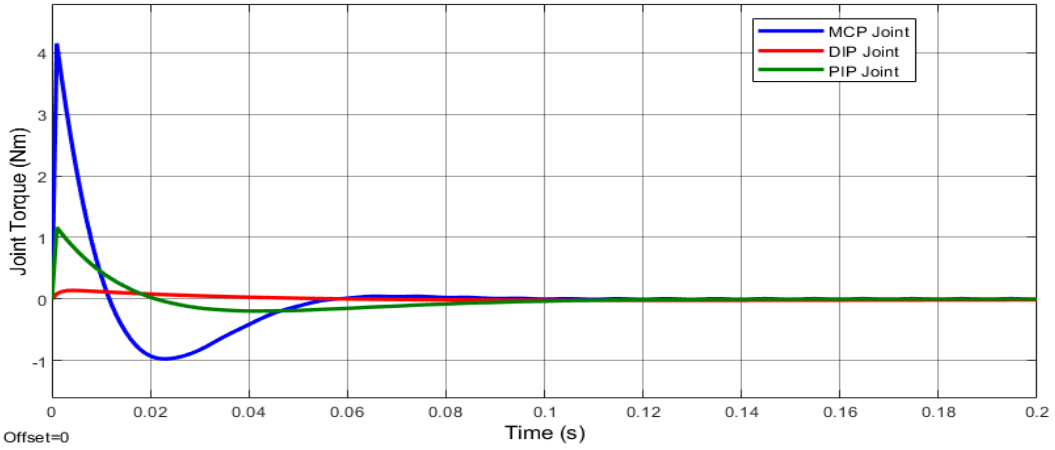

Figure 4.33: Joints Torque Response for Little finger with SMC-FLC control

4.19 Control / contact forces for finger joints with SMC-FLC

4.19.1 Control forces of joint position for Little finger with SMC-FLC

Compared to merely the Simple FLC design established for little finger joint motion control, less control effort is needed by the controller based on SMC-FLC architecture, and both regulated transient and steady state response are seen. Control / contact forces of joint position for little finger with SMC-FLC is shown in Figure 4.34.

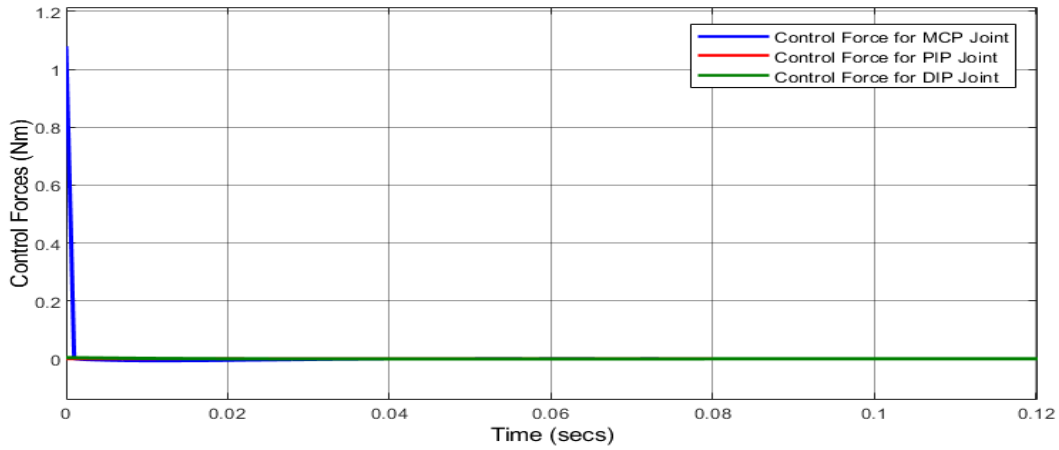

Figure 4.34: Control / contact forces of joint position for little finger with SMC-FLC

4.20 Tracking Error History for Finger Joints with SMC-FLC

4.20.1 Tracking error history for little finger position control with FLC-SMC controller

For the system that was created using an SMC-FLC based control architecture, ZERO steady state error was promptly attained with a fast transient response noted. Tracking error history for little finger position control with FLC-SMC controller is shown in Figure 4.35. If we set a time of three seconds, we can plainly observe the asymptotic convergence of the body joint through it. It will encompass its starting and ending positions.

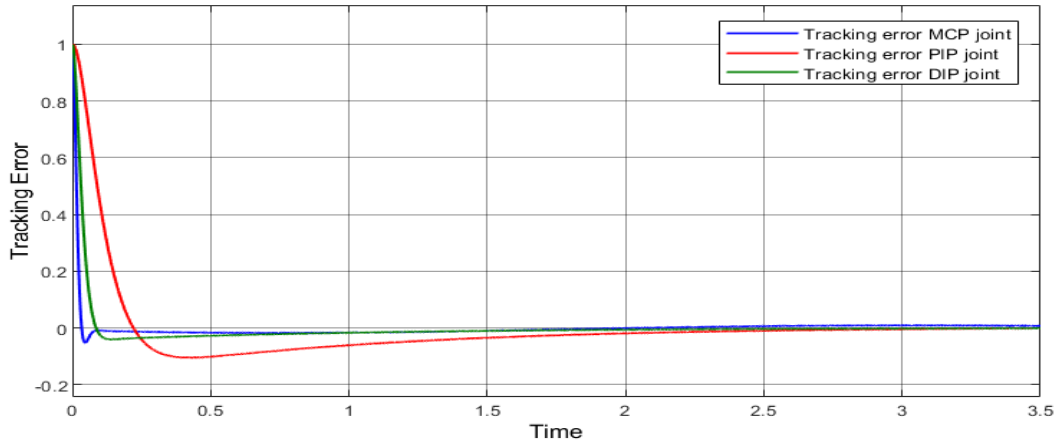

Figure 4.35: Tracking error history for little finger position control with FLC-SMC controller

4.21 Phase portraits for Little finger with SMC-FLC

4.21.1 Phase portrait for MCP joint of little finger with SMC-FLC

Position along y axis with respect to x axis change observed or phase portraits for the ring finger movement in geometrical view observed in above figure is constrained and confined, restricted and uniform for MCP joint of little finger. Phase portrait for MCP joint of little finger with SMC-FLC controller is shown in Figure 4.36.

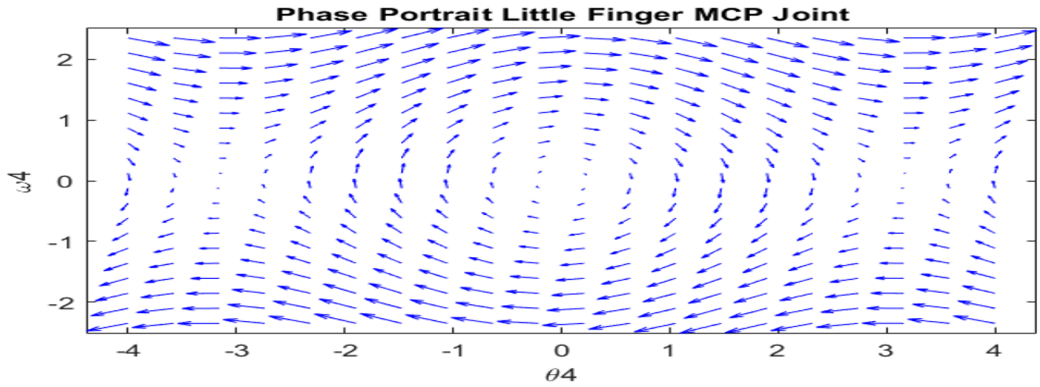

Figure 4.36: Phase portrait for MCP joint of little finger with SMC-FLC

4.21.2 Phase portrait for PIP joint of little finger with SMC-FLC

Position along y axis with respect to x axis change observed or phase portraits for the ring finger movement in geometrical view observed in above figure is constrained and confined, restricted and uniform for PIP joint of little finger. Phase portrait for PIP joint of little finger with SMC-FLC controller is shown in Figure 4.37.

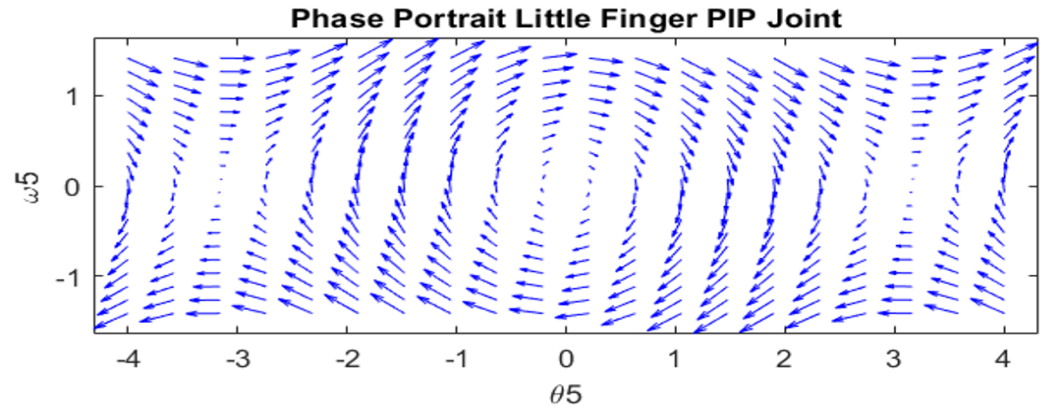

Figure 4.37: Phase portrait for PIP joint of little finger with SMC-FLC

4.21.3 Phase portrait for DIP joint of little finger with SMC-FLC

Position along y axis with respect to x axis change observed or phase portraits for the ring finger movement in geometrical view observed in above figure is constrained and confined, restricted and uniform for PIP joint of little finger. Phase portrait for DIP joint of little finger with SMC-FLC controller is shown in Figure 4.38.

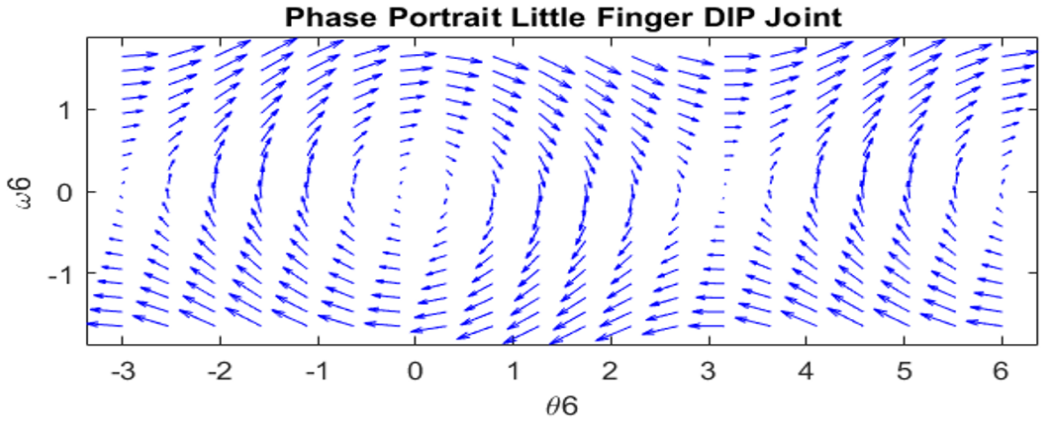

Figure 4.38: Phase portrait for DIP joint of little finger with SMC-FLC

4.22 Performance parameters of Little Finger joints control motion with SMC-FLC

The response of the plant stabilises after around 2.5 seconds of simulation time, as seen in the Figure 4.31 when the ring finger's MCP deflects. Overshoot, as it relates to the step response. Above mentioned figure displays the rise time of 0.1 second with an approximate % overshoot of 5.9%. The plant's output stabilises after about two and half seconds of simulation time. The plant's response to the ring finger's PIP deflection is seen in the Figure 4.31. The 0.2-second rising time and roughly 10.5% overshoot. The plant output stabilises at around 2.3 seconds into the experiment. The plant's reaction is depicted in the Figure 4.31 when the ring finger's DIP deflects; the response stabilizes after around 2.5 seconds of simulation time. The rise time of 0.35 seconds which is approximated with the % overshoot of 3.646% approximately. After approximately 3 seconds the plant output becomes stable.

Improved, robust, effective transient as well as steady state parameters values achieved and also minimized for MCP, PIP and DIP controlled motion of little finger controlled by SMC-FLC control architecture.

4.23 Mass Of Sample Human Finger Phalanges

Understanding the operation and limitations of the human body is made easier with the use of computational and mathematical models of bio-mechanical systems. The mass of the phalanx and the natural stiffness (K) and damping (B) values for this visco-elastic model are provided in Table 4.1 and Table 4.2, respectively, [61].

Table 4.1: Mass of Phalanges with units

Phalanx	Phalanx Human Mass	Units
Proximal	12.4	grams
Middle	3.6	grams
Distal	0.97	grams

4.23.1 Stifness And Damping Values Of Joints

Table 4.2: Joints and Corresponding Parameters

Joint	D (N-m-s/rad)	K (N-m/rad)	θ (radians)
DIP	0.0081	$0.384\theta^2 - 0.089\theta + 0.133$	θPIP
PIP	0.0105	$1.058\theta^2 - 0.760\theta + 0.396$	0.079
MCP	0.0142	$1.019\theta^2 - 0.541\theta + 0.454$	0.275

4.24 Performance Comparison

Table 4.3: Controller Performance Comparison

Approach/Technique	Percentage Overshoot	Rise Time	Steady State Error
Without Controller	Infinity	Infinity	Infinity
FLC	18.1%	169 milliseconds	0
SMC-FLC	10.5%	18.1 milliseconds	0

Regarding peak overshoot and stabilising duration, the efficiency of the FLC with SMC is indicated by comparing the reactions of plants under structured and unstructured uncertainty. Additionally, input reference tracking for the little and ring finger's DIP, PIP, and MCP joints were carried out. As a result, the output is shown to be exactly or partially matching the input's reference trajectory. The findings of the simulation, as discussed above, demonstrate how the model can be used in active prostheses and can be useful in simulating a hand that is partially disabled.

Table 4.4: Approach/Technique Stability Evaluation

Approach/Technique	**Stability**	**Disturbances**	**Stability Evaluation**
Without Controller	Not stable	Infinity	Infinity
FLC	Stable in 4-5 seconds	No jitters later 5 seconds	4-5 seconds
SMC-FLC	Stable in 3.5 seconds	Negligible jitters	3.5 seconds

It is evident that the plant response stabilises sooner once the real model's minimal realisation of state space is reached. Results for both controller are shown in Table 4.3 and 4.4. In simulation time, with FLC the response stabilizes at approximately 4 seconds while on the other hand the response stabilises at about 3.5 seconds with SMC-FLC which is better achievement.

Table 4.5: Compairing various control techniques

Author	**Control**	**Trajectories**	**Error**
Calderon et al. [62]	PI	Step 17 mm	SSE 0
Tasar et al. [63]	PID	Step (for three phalanxes)	0.255 deg (max)
Ghazali et al. [64]	Fuzzy-PID	Step 90 deg	0 deg
Ghazali et al. [64]	Fuzzy	Step 90 deg	0.12 deg
Rakovic´ et al. [65]	Fuzzy	Step 100 deg	SSE 0 rad
Jalani et al. [66]	PID	Sin [0–(1)] rad	0.0159 rad
Jalani et al. [66]	Adaptive	Sin [0–4] rad	0.0791 rad
Jalani et al. [66]	SMC	Sin [0–(1)] rad	0.0167 rad
Our proposed model	Optimized FLC	Step [0–1] rad	SSE 3.1352×10^{-4} rad
Our proposed model	SMC-FLC	Step [0–1] rad	SSE 3.1352×10^{-6} rad

It is evident from Table 4.5, which compares the current study with some previously published data, that nearly all finger models are underactuated. The response time in [62] is greater than 10 seconds. Less than five seconds are shown for the settling time in [64, 65], however, control settings must be manually established. Step response was provided as the desired input in [62, 64, 65], with steady-state error equal to zero. The main way that our work differs from others' is that we manually modify the controller parameters. We also achieve the lowest attainable error in all present trajectories by employing two non-linear controllers to provide regulated output. Both controllers generated a consistent and efficient output response by using controlled inputs.

Chapter 5

Conclusions & Future Recommendations

Conclusion:
Since everything in the world is nonlinear, using a nonlinear controller to control the nonlinearities of the two-finger model is more feasible. The precision and accuracy of the trajectory is the primary topic of this thesis. Computational and mathematical models of biomechanical systems are quite helpful to understand the constraints as well as functionality of human body. Two non-linear controllers are employed in this model: fuzzy logic controller and sliding mode. To produce controlled output, both controllers employed controlled input. By comparing their findings from the output graphs, it is evident that while sliding mode controller has eliminated uncertainty, it can also solve chattering by introducing boundary layer adaptive technique. In contrast, SMC is not as robust to uncertainties. The design, development as well as implementation of intelligent based control architecture based on fuzzy logic controller as well as Sliding mode Fuzzy logic architecture ensured and delivered the not only stable, controlled and robust performance for the joint motion of little as well as ring finger also ensured to minimize the energy loss by reducing the control efforts required to move each joint angular motion offered by actuators attached for MCP, PIP and DIP joints. The robust effective, uniform and desired output response and results achieved. The non-linear dynamic systems of the little finger and ring finger dynamic system control are stabilised by the efficient control strategy, which is based on a sliding mode fuzzy logic control architecture. The transient parameters and steady state parameters like settling time as well as steady state values are minimized with design, develop and implementation of effective and optimized controller of SMC-FLC structure. The control efforts reduced and minimized offered.

Future Recommendations:
Intelligent based Advanced control architecture, based on adaptive neuro fuzzy inference control structure ANFIS will be design developed and implementation will be ensured to deliver the controlled effective, desired and robust performance achieved for system linearization of dynamic behavior of two dependent moved finger.
The optimal controller based on optimal PID controller design, developed to minimize the cost function of controller effort of system to acquire the low energy minimization.
The entire thesis is composed of software, though it can also be extended to three, four, or even the entire hand with all five fingers. It can also be implemented on hardware. Further research can be conducted using additional non-linear controllers. Enhancing control will be the next step towards raising performance levels. When the model consists of five fingers, additional non-linear system techniques such as gain scheduling and back stepping control can be employed to achieve appropriate control at various operating points.Several observable variables, sometimes referred to as scheduling variables, are essentially used in gain scheduling to ascertain the system's operating status. Techniques for back stepping are intended to regulate dynamic systems that are not linear. Its recursive nature allows the designer to run the process at a known stable system and output a new controller that is used to achieve a stable external state. The procedure keeps going until the desired external control is attained. The best non-linear controllers for this model to use in order to ensure system stability are the ones listed above. I will recommend using them as an addition to this model by future researchers.

Appendix A

Appendix A

The attributes and their values for simulink model.

```
%% %%% Dynamic Parameters for RING Finger
clc;clear all;close all
l1=45/1000;    %%%% length of MP
l2=25/1000;    %%% length of DP
l3=20/1000;    %%% Length of D
m1=12.4/1000; %%% mass of Proximal Phalanges
m2=3.6/1000;  %%% mass of Middle Phalanges
m3=0.97/1000; %%% mass of Distal Phalanges
J1=m1*(l1^2);        %%% Moment of MCP joint
J2=m2*(l2^2);        %%% Moment of PIP joint
J3=m3*(l3^2);        %%% Moment of DIP joint
D1=0.0081;         %%% Damping of MCP and Reference
D2=0.0105;         %%% Damping of MCP-PIP
D3=0.0142;         %%% Damping of PIP-DIP
K1=0.384         %%% Stiffness of MCP and Reference
K2=1.058         %%% Stiffness of MCP-PIP
K3=1.019         %%% Stiffness of PIP-DIP
%%%% Dynamic Parameters for Little Finger
l4=40/1000;    %%%% length of MP
l5=20/1000;    %%% length of DP
l6=15/1000;    %%% Length of D
m4=10.4/1000; %%% mass of Proximal Phalanges
m5=2.9/1000;  %%% mass of Middle Phalanges
```

Figure A.1: MATLAB Modelling Code

```
m6=0.91/1000; %%% mass of Distal Phalanges
J4=m4*(l4^2);      %%% Moment of MCP joint
J5=m5*(l5^2);      %%% Moment of PIP joint
J6=m6*(l6^2);      %%% Moment of DIP joint
D4=0.0081      %%% Damping of MCP and Reference
D5=0.0101;      %%% Damping of MCP-PIP
D6=0.0139      %%% Damping of PIP-DIP
K4=0.344;      %%% Stiffness of MCP and Reference
K5=1.051;      %%% Stiffness of MCP-PIP
K6=1.011;      %%% Stiffness of PIP-DIP

%%
%%% State Space Model LINEARIZED Model of Ring Finger

%%% Define the system MATRIX A for Ring finger

A1=[0 0 0 1 0 0;0 0 0 0 1 0;0 0 0 0 0 1;(-K1-K2)/(m1*(l1^2)) K2/(m1*(l1^2)) 0 (-D1-D2)/(m1*(l1^2)) D2/(m1*(l1^2)) 0;
    0 (-K2-K3)/(m2*(l2^2)) K3/(m2*(l2^2)) 0 (-D2-D3)/(m2*(l2^2)) D3/(m2*(l2^2));
    0 K3/(m3*(l3^2)) -K3/(m3*(l3^2)) 0 D3/(m3*(l3^2)) -D3/(m3*(l3^2))]
%%% Define the Input Matrix B for Ring finger
B1=[0
    0
    0
```

Figure A.2: MATLAB Modelling

```
47        1/(m1*(l1^2))
48        1/(m2*(l2^2))
49        1/(m3*(l3^2))];
50    %%% Define the output Matrix C for Ring finger
51 -  C1 = [1 0 0 0 0 0;
52          0 1 0 0 0 0
53          0 0 1 0 0 0];
54    %%% Decoupling matrix D for Ring finger
55 -  D1 = [0;
56          0
57          0];
58 -  sys1=ss(A1,B1,C1,D1)  %%% Define the uncompensated system in state space model form
59    %%% State Space Model LINEARIZED of Little Finger
60
61    %%% Define the system MATRIX A for Little finger
62 -  A2=[0 0 0 1 0 0;0 0 0 0 1 0;0 0 0 0 0 1;(-K4-K5)/(m4*(l4^2)) K5/(m4*(l4^2)) 0 (-D4-D5)/(m4*(l4^2)) D5/(m4*(l4^2)) (
63        0 (-K5-K6)/(m5*(l5^2)) K6/(m5*(l5^2)) 0 (-D5-D6)/(m5*(l5^2)) D6/(m5*(l5^2));
64        0 K6/(m6*(l6^2)) -K6/(m6*(l6^2)) 0 D6/(m6*(l6^2)) -D6/(m6*(l6^2))]
65
66    %%% Define the Input Matrix B for Little finger
67 -  B2=[0
68        0
69        0
```

Figure A.3: MATLAB Modelling

```
70        1/(m4*(l4^2))
71        1/(m5*(l5^2))
72        1/(m6*(l6^2))];
73    %%% Define the output Matrix C for Little finger
74 -  C2 = [1 0 0 0 0 0;
75          0 1 0 0 0 0
76          0 0 1 0 0 0];
77    %%% Decoupling matrix D for Little finger
78 -  D2 = [0;
79          0
80          0];
81 -  sys2=ss(A2,B2,C2,D2)  %%% Define the uncompensated system in state space model form
82
83
```

Figure A.4: MATLAB Modelling

Editor - C:\Users\sabta\Downloads\Phase Portraits Ring and Little Finger With FLC\MATLAB_script_FLC_phase_Portraits.m

MATLAB_CODE_do.m | MATLAB_CODE_do.m | MATLAB_script_FLC_phase_Portraits.m

```
%% phase portrait FLC MCP Joint for Ring Finger
clc;close all;
mm=(max(phase_portrait_m)/1)
f = @(t,Y) [Y(2); -sin(Y(1))];
y1 = linspace(-2,8,20);
y2 = linspace((-1*mm),(1*mm),20);
[x,y] = meshgrid(y1,y2);
size(x)
size(y)
u = zeros(size(x));
v = zeros(size(x));
% one loop to each element to compute the derivatives at each point
t=0; % we want the derivatives at each point at t=0, i.e. the starting time
for i = 1:numel(x)
    Yprime = f(t,[x(i); y(i)]);
    u(i) = Yprime(1);
    v(i) = Yprime(2);
end
quiver(x,y,u,v,'b');
figure(gcf)
xlabel('theta1')
ylabel('w1')
axis tight equal;
title('Phase Portrait Ring Finger MCP Joint with FLC')

```

Figure A.5: MATLAB Modelling

```
%% phase portrait FLC PIP Joint for Ring Finger
clc;close all;
mp=(max(phase_portrait_p)/0.7)
f = @(t,Y) [Y(2); -sin(Y(1))];
y1 = linspace(-3,9,20);
y2 = linspace((-1*mp),(1*mp),20);
[x,y] = meshgrid(y1,y2);
size(x)
size(y)
u = zeros(size(x));
v = zeros(size(x));
% one loop to each element to compute the derivatives at each point
t=0; % we want the derivatives at each point at t=0, i.e. the starting time
for i = 1:numel(x)
    Yprime = f(t,[x(i); y(i)]);
    u(i) = Yprime(1);
    v(i) = Yprime(2);
end
quiver(x,y,u,v,'b'); figure(gcf)
xlabel('theta2')
ylabel('w2')
axis tight equal;
title('Phase Portrait Ring Finger PIP Joint with FLC')
```

Figure A.6: MATLAB Modelling

```
%% phase portrait FLC DIP Joint for Ring Finger
clc;close all;
md=(max(phase_portrait_p)/0.5)
f = @(t,Y) [Y(2); -sin(Y(1))];
y1 = linspace(-4,10,20);
y2 = linspace((-1*md),(1*md),20);
[x,y] = meshgrid(y1,y2);
size(x)
size(y)
u = zeros(size(x));
v = zeros(size(x));
% one loop to each element to compute the derivatives at each point
t=0; % we want the derivatives at each point at t=0, i.e. the starting time
for i = 1:numel(x)
    Yprime = f(t,[x(i); y(i)]);
    u(i) = Yprime(1);
    v(i) = Yprime(2);
end
quiver(x,y,u,v,'b'); figure(gcf)
xlabel('theta3')
ylabel('w3')
axis tight equal;
title('Phase Portrait Ring Finger DIP Joint with FLC')

```

Figure A.7: MATLAB Modelling

```
%%
%% phase portrait MCP Joint for Little Finger with FLC
clc;close all;
mml=(max(phase_portrait_m)/0.3)
f = @(t,Y) [Y(2); -sin(Y(1))];
y1 = linspace(-4,4,20);
y2 = linspace((-1*mml),(1*mml),20);
[x,y] = meshgrid(y1,y2);
size(x)
size(y)
u = zeros(size(x));
v = zeros(size(x));
% one loop to each element to compute the derivatives at each point
t=0; % we want the derivatives at each point at t=0, i.e. the starting time
for i = 1:numel(x)
    Yprime = f(t,[x(i); y(i)]);
    u(i) = Yprime(1);
    v(i) = Yprime(2);
end
quiver(x,y,u,v,'b'); figure(gcf)
xlabel('theta1')
ylabel('w1')
axis tight equal;
title('Phase Portrait Little Finger MCP Joint with FLC')
```

Figure A.8: MATLAB Modelling

```
%% phase portrait FLC PIP Joint for Little Fimger
clc;close all;
mpl=(max(phase_portrait_p)/0.4)
f = @(t,Y) [Y(2); -sin(Y(1))];
y1 = linspace(-4,4,20);
y2 = linspace((-1*mpl),(1*mpl),20);
[x,y] = meshgrid(y1,y2);
size(x)
size(y)
u = zeros(size(x));
v = zeros(size(x));
% one loop to each element to compute the derivatives at each point
t=0; % we want the derivatives at each point at t=0, i.e. the starting time
for i = 1:numel(x)
    Yprime = f(t,[x(i); y(i)]);
    u(i) = Yprime(1);
    v(i) = Yprime(2);
end
quiver(x,y,u,v,'b'); figure(gcf)
xlabel('theta2')
ylabel('w2')
axis tight equal;
title('Phase Portrait Little Finger PIP Joint with FLC')
```

Figure A.9: MATLAB Modelling

```
%% phase portrait FLC DIP Joint for Little Fimger
clc;close all;
mdl=(max(phase_portrait_d)/0.3)
f = @(t,Y) [Y(2); -sin(Y(1))];
y1 = linspace(-3,6,20);
y2 = linspace((-1*mdl),(1*mdl),20);
[x,y] = meshgrid(y1,y2);
size(x)
size(y)
u = zeros(size(x));
v = zeros(size(x));
% one loop to each element to compute the derivatives at each point
t=0; % we want the derivatives at each point at t=0, i.e. the starting time
for i = 1:numel(x)
    Yprime = f(t,[x(i); y(i)]);
    u(i) = Yprime(1);
    v(i) = Yprime(2);
end
quiver(x,y,u,v,'b'); figure(gcf)
xlabel('theta3')
ylabel('w3')
axis tight equal;
title('Phase Portrait Little Finger DIP Joint with FLC')
```

Figure A.10: MATLAB Modelling

Editor - C:\Users\sabta\Downloads\Phase Portraits\MATLAB_script.m

MATLAB_script.m

```
%% phase portrait SMC MCP Joint for Ring Fimger
clc;close all;
mm=(max(phase_portrait_m)/7)
f = @(t,Y) [Y(2); -sin(Y(1))];
y1 = linspace(-2,8,20);
y2 = linspace((-1*mm),(1*mm),20);
[x,y] = meshgrid(y1,y2);
size(x)
size(y)
u = zeros(size(x));
v = zeros(size(x));
% one loop to each element to compute the derivatives at each point
t=0; % we want the derivatives at each point at t=0, i.e. the starting time
for i = 1:numel(x)
    Yprime = f(t,[x(i); y(i)]);
    u(i) = Yprime(1);
    v(i) = Yprime(2);
end
quiver(x,y,u,v,'b'); figure(gcf)
xlabel('theta1')
ylabel('w1')
axis tight equal;
title('Phase Portrait Ring Finger MCP Joint')
```

Figure A.11: MATLAB Modelling

```
%% phase portrait SMC PIP Joint for Ring Fimger
clc;close all;
mp=(max(phase_portrait_p)/5)
f = @(t,Y) [Y(2); -sin(Y(1))];
y1 = linspace(-3,9,20);
y2 = linspace((-1*mp),(1*mp),20);
[x,y] = meshgrid(y1,y2);
size(x)
size(y)
u = zeros(size(x));
v = zeros(size(x));
% one loop to each element to compute the derivatives at each point
t=0; % we want the derivatives at each point at t=0, i.e. the starting time
for i = 1:numel(x)
    Yprime = f(t,[x(i); y(i)]);
    u(i) = Yprime(1);
    v(i) = Yprime(2);
end
quiver(x,y,u,v,'b'); figure(gcf)
xlabel('theta2')
ylabel('w2')
axis tight equal;
title('Phase Portrait Ring Finger PIP Joint')
```

Figure A.12: MATLAB Modelling

```
%% phase portrait SMC PIP Joint for Ring Fimger
clc;close all;
md=(max(phase_portrait_p)/3)
f = @(t,Y) [Y(2); -sin(Y(1))];
y1 = linspace(-4,10,20);
y2 = linspace((-1*md),(1*md),20);
[x,y] = meshgrid(y1,y2);
size(x)
size(y)
u = zeros(size(x));
v = zeros(size(x));
% one loop to each element to compute the derivatives at each point
t=0; % we want the derivatives at each point at t=0, i.e. the starting time
for i = 1:numel(x)
    Yprime = f(t,[x(i); y(i)]);
    u(i) = Yprime(1);
    v(i) = Yprime(2);
end
quiver(x,y,u,v,'b'); figure(gcf)
xlabel('theta3')
ylabel('w3')
axis tight equal;
title('Phase Portrait Ring Finger DIP Joint')

```

Figure A.13: MATLAB Modelling

```
%%
%% phase portrait SMC MCP Joint for Little Fimger
clc;close all;
mml=(max(phase_portrait_m)/0.3)
f = @(t,Y) [Y(2); -sin(Y(1))];
y1 = linspace(-4,4,20);
y2 = linspace((-1*mml),(1*mml),20);
[x,y] = meshgrid(y1,y2);
size(x)
size(y)
u = zeros(size(x));
v = zeros(size(x));
% one loop to each element to compute the derivatives at each point
t=0; % we want the derivatives at each point at t=0, i.e. the starting time
for i = 1:numel(x)
    Yprime = f(t,[x(i); y(i)]);
    u(i) = Yprime(1);
    v(i) = Yprime(2);
end
quiver(x,y,u,v,'b'); figure(gcf)
xlabel('theta1')
ylabel('w1')
axis tight equal;
title('Phase Portrait Little Finger MCP Joint')
```

Figure A.14: MATLAB Modelling

```
%% phase portrait SMC PIP Joint for Little Fimger
clc;close all;
mpl=(max(phase_portrait_p)/0.4)
f = @(t,Y) [Y(2); -sin(Y(1))];
y1 = linspace(-4,4,20);
y2 = linspace((-1*mpl),(1*mpl),20);
[x,y] = meshgrid(y1,y2);
size(x)
size(y)
u = zeros(size(x));
v = zeros(size(x));
% one loop to each element to compute the derivatives at each point
t=0; % we want the derivatives at each point at t=0, i.e. the starting time
for i = 1:numel(x)
    Yprime = f(t,[x(i); y(i)]);
    u(i) = Yprime(1);
    v(i) = Yprime(2);
end
quiver(x,y,u,v,'b'); figure(gcf)
xlabel('theta2')
ylabel('w2')
axis tight equal;
title('Phase Portrait Little Finger PIP Joint')
```

Figure A.15: MATLAB Modelling

```
%% phase portrait SMC DIP Joint for Little Fimger
clc;close all;
mdl=(max(phase_portrait_d)/0.3)
f = @(t,Y) [Y(2); -sin(Y(1))];
y1 = linspace(-3,6,20);
y2 = linspace((-1*mdl),(1*mdl),20);
[x,y] = meshgrid(y1,y2);
size(x)
size(y)
u = zeros(size(x));
v = zeros(size(x));
% one loop to each element to compute the derivatives at each point
t=0; % we want the derivatives at each point at t=0, i.e. the starting time
for i = 1:numel(x)
    Yprime = f(t,[x(i); y(i)]);
    u(i) = Yprime(1);
    v(i) = Yprime(2);
end
quiver(x,y,u,v,'b'); figure(gcf)
xlabel('theta3')
ylabel('w3')
axis tight equal;
title('Phase Portrait Little Finger DIP Joint')
```

Figure A.16: MATLAB Modelling

References

[1] Patel A. D. Murugesan T. Turini G. Young J. G. Riyal, R. Effect of control display transfer function on pointing performance for a hand/finger based touchless gestural controls: A preliminary investigation. proceedings of the human factors and ergonomics society. *arXiv preprint arXiv:1604.01485*, page 1085–1089, 2015. Cited on pp. 1 and 5.

[2] Li J. Zhao, X. Transfer of the index finger extensor digitorum communis tendon to the extensor pollicis longus tendon: A case report. plastic surgery case studies, 6. *arXiv preprint arXiv:1604.01485*, 2020. Cited on pp. 1 and 5.

[3] Budiarsa N. Widhiada W. Nindhia T. G. T. & Budiarsa N. Widhiada, W. Robust control for the motion five fingered robot gripper. 2015. Cited on pp. 1 and 5.

[4] Huang X. Lee J. Kambara H. Kang Y. Shin D. Narumi, S. A design of biomimetic prosthetic hand. actuators, 11(6). 2022. Cited on pp. 1 and 5.

[5] Queirós S. Fonseca J. Rodrigues P. L. Rodrigues N. F. Vilaça J. L. Moreira, A. H. J. Real-time hand tracking for rehabilitation and character animation. In *SeGAH 2014 - IEEE 3rd International Conference on Serious Games and Applications for Health, Books of Proceedings.*, 2014. Cited on pp. 2 and 6.

[6] Chen X. He Y. Zhao X. Cao, H. Dynamic adaptive hybrid impedance control for dynamic contact force tracking in uncertain environments. ieee access, 7, 83162–83174. 2019. Cited on pp. 2 and 6.

[7] Heung H. L. Tang Z. Q. Tong K. Y. Li Z. Shi, X. Q. Verification of finger joint stiffness estimation method with soft robotic actuator. frontiers in bioengineering and biotechnology, 8. 2020. Cited on pp. 2 and 6.

[8] Osorio A. Lopez R. Salazar S. Lozano R. Suárez, A. E. Z. Mathematical model and simulation of finger movement with electromyographic signals. In *2016 20th International Conference on System Theory, Control and Computing, ICSTCC 2016 - Joint Conference of SINTES 20, SACCS 16, SIMSIS 20 - Proceedings*, page 771–775, 2018. Cited on pp. 2 and 6.

[9] Muhammad Ajwad Wa'ie Hazman, Ili Najaa Aimi Mohd Nordin, Faridah Hanim Mohd Noh, Nurulaqilla Khamis, Muhammad Rusydi Muhammad Razif, Ahmad Athif Mohd Faudzi, and Asyikin Sasha Mohd Hanif. Imu sensor-based data glove for finger joint measurement. *Indonesian Journal of Electrical Engineering and Computer Science*, 20:82–88, 2020. Cited on pp. 2 and 12.

[10] Zhengwei Li L. Cheng, Miao Chen. Design and control of a wearable hand rehabilitation robot, 3 December 2018. Cited on pp. 2 and 6.

[11] Jamshed Iqbal, Hamza Khan, Nikos G. Tsagarakis, and Darwin Gordon Caldwell. A novel exoskeleton robotic system for hand rehabilitation - conceptualization to prototyping. *Biocybernetics and Biomedical Engineering*, 34:79–89, 2014. Cited on pp. 3 and 7.

[12] Jeffrey T. Spooner, Manfredi Maggiore, Raúl Ordóñez, and Kevin M. Passino. Control of nonlinear systems. 2002. Cited on p. 3.

[13] M. E. Griess, B Reilmann, and M Chanavaz. The multi-modal prosthetic treatment of mentally handicapped patients–necessity and challenge. *The European journal of prosthodontics and restorative dentistry*, 6 3:115–20, 1998. Cited on p. 4.

[14] Parag Bharadwaj and Katherine T. Ward. Ethical considerations of patients with pacemakers. *American family physician*, 78 3:398–9, 2008. Cited on p. 4.

[15] Katarina Dathe and Christof Schaefer. The use of medication in pregnancy. *Deutsches Arzteblatt international*, 116 46:783–790, 2019. Cited on p. 4.

[16] Guillermo Linares and Stephan A. Mayer. Hypothermia for the treatment of ischemic and hemorrhagic stroke. *Critical Care Medicine*, 37:S243–S249, 2009. Cited on p. 4.

[17] J. Biggs and K. Horch. A three-dimensional kinematic model of the human long finger and muscles that actuate it, medical engineering and physics,. *21*, page 625–639, 2018. Cited on p. 7.

[18] T.J. Armstrong and D.B. Chaffin. An investigation of the relationship between displacements of the finger and wrist joints and the extrinsic finger flexor tendons. *Journal of Biomechanics, 11 (3)*, page 119–128, 2016. Cited on p. 7.

[19] Anu Polvinen and Mikko Laaksonen. Determinants of transition from partial to full disability pension: A register study from finland. scandinavian journal of public health. *Journal of Public Health*, page 14034948211020172, 2021. Cited on p. 7.

[20] Yasuyoshi Yokokohji, Takashi Imaida, and Tsuneo Yoshikawa. Bilateral control with energy balance monitoring under time-varying communication delay. *Proceedings 2000 ICRA. Millennium Conference. IEEE International Conference on Robotics and Automation. Symposia Proceedings (Cat. No.00CH37065)*, 3:2684–2689 vol.3, 2000. Cited on p. 7.

[21] J.L. Banks. Design and control of an anthropomorphic robotic finger with multi-point tactile sensation. mit ai lab technical report aitr-2010-005. 2014. Cited on p. 7.

[22] Eugene F Murphy. The challenge of replacing human parts and functions. bull. pros. res. page pages 10–3, 2020. Cited on p. 7.

[23] Lee H. N. Sclabassi R. J. Sun M. Mao, Z. H. Information capacity of the thumb and the index finger in communication. In *2019 IEEE Transactions on Biomedical Engineering, 56(5)*, page 1535–1545, 2019. Cited on p. 8.

[24] Schieber M. H. Lang, C. E. Human finger independence: Limitations due to passive mechanical coupling versus active neuromuscular control. Number 92(5), page 2802–2810, 2004. Cited on p. 8.

[25] Chen-Hua Chiu Mao-Cheng Hsu Yang Chen Tzu-Yang Pai Wei-Geng Peng Chih-Hsing Liu, Ta-Lun Chen and Yen-Pin Chiang. Optimal design of a soft robotic gripper for grasping unknown objects,. 28 Aug 2018. Cited on p. 8.

[26] A. Mahmood M. Iqbal. H2 optimal control of a minimal space realization model of coordinated finger movement"17th ieee international conference on science and techniques of automatic control and computer engineering, sousse, tunisia,. pages 19–21, 2016. Cited on p. 8.

[27] Maryam Iqbal and A. Mahmood. Structured uncertainty modeling, control synthesis tracking of coordinated fingers movement. In *2018 14th International Conference on Emerging Technologies (ICET)*, pages 1–6, 2018. Cited on p. 8.

[28] Erik D. Engeberg and Sanford G. Meek. Backstepping and sliding mode control hybridized for a prosthetic hand. *IEEE Transactions on Neural Systems and Rehabilitation Engineering*, 17:70–79, 2009. Cited on p. 8.

[29] Elisabetta Punta Giorgio Bartolini, Alessandro Pisano and Elio Usai. A survey of applications of second-order sliding mode control to mechanical systems. *International Journal of Control*, 76(9-10):875–892, 2003. Cited on p. 8.

[30] A. Bartoszewicz. A comment on a time-varying sliding surface for fast and robust tracking control of second-order uncertain systems, automatica,31 (12). *31*, 2015. Cited on p. 9.

[31] Suzuki Y. Ganesh G. Miyawaki Y. Umezawa, K. Bodily ownership of an independent supernumerary limb: an exploratory study. scientific reports, 12(1). *Journal of Disability Religion*, page 1–31, 2022. Cited on p. 9.

[32] Aranya Chakrabortty; Murat Arcak. Robust stabilization and performance recovery of nonlinear systems with unmodeled dynamics,. pages 1351 – 1356, 27 May 2009. Cited on p. 9.

[33] TW Williams. Clinical application of the improved boston arm. proc. cant syst. devices for the disabled. *European Journal of Public Health*, page pages 109–113, 2018. Cited on p. 9.

[34] Steinar Krokstad Roar Johnsen Gunnhild Åberge Vie, Kristine Pape and Johan Håkon Bjørngaard. Temporal changes in health within 5 years before and after disability pension–the hunt study. european journal of public health. *European Journal of Public Health*, 2017. Cited on p. 9.

[35] Donald R Taylor Roy W Wirta and F Ray Finley. Pattern-recognition arm prosthesis: a historical perspective-a final report. bull. prosthet. res 10(30). *European Journal of Public Health*, page 8–35, 2019. Cited on p. 9.

[36] E.Y. Chao W.P. Cooney An, K.N. and R.L. Linscheid. Normative model of human hand for biomechanical analysis, journal of biomechanics , 12 (10). Cited on p. 9.

[37] Carolina Pereira Abud Maria Helena Naves Inácio Pedroso Kamila Seidel Albuquerque Natália Borges Nunes Gomes Ana Cláudia Vincenzi Raduan Uski, Luciana Maksoud Piccolo and José de Ávila Fernandes. Mri of penile prostheses: The challenge of diagnosing postsurgical complications. radiographics, 42(1). Cited on p. 9.

[38] Arif Ankaralı and Murat Çilli. Anfis inverse kinematics and hybrid control of a human leg gait model. 2013. Cited on p. 10.

[39] Nur Nabilah Mohd Yusof, Yan Chai Hum, Nur Azah Hamzaid, and Khin wee Lai. Adaptive network based fuzzy inference system (anfis) for an active transfemoral prosthetic leg by using in-socket sensory system. 2017. Cited on p. 10.

[40] Jiahao Fan and Xiaogang Hu. Towards efficient neural decoder for dexterous finger force predictions. *IEEE Transactions on Biomedical Engineering*, pages 1–10, 2024. Cited on p. 10.

[41] Theodore E. Milner and David W. Franklin. Characterization of multijoint finger stiffness: dependence on finger posture and force direction. *IEEE Transactions on Biomedical Engineering*, 45:1363–1375, 1998. Cited on p. 10.

[42] Shuchen Ding, Xianlin Huang, Xiaojun Ban, Hongqian Lu, and Hongyang Zhang. Type-2 fuzzy logic control for underactuated truss-like robotic finger with comparison of a type-1 case. *J. Intell. Fuzzy Syst.*, 33:2047–2057, 2017. Cited on p. 10.

[43] Haoyan Zhang, Ning Xu, Guangdeng Zong, and Abdulhameed F. Alkhateeb. Adaptive fuzzy hierarchical sliding mode control of uncertain under-actuated switched nonlinear systems with actuator faults. *International Journal of Systems Science*, 52:1499 – 1514, 2021. Cited on p. 11.

[44] Yue ying Wang, Bin Jiang, Zhengguang Wu, Shaorong Xie, and Yan Peng. Adaptive sliding mode fault-tolerant fuzzy tracking control with application to unmanned marine vehicles. *IEEE Transactions on Systems, Man, and Cybernetics: Systems*, 51:6691–6700, 2021. Cited on p. 11.

[45] Francisco J. Espinosa Garcia, Esther Lugo-González, Arturo Téllez-Velázquez, Manuel Arias-Montiel, and Marco Ceccarelli. Optimal position fuzzy control of an underactuated robotic finger. *Mathematical Problems in Engineering*, 2022. Cited on p. 11.

[46] Jérôme Coupier, Samir Hamoudi, Sonia Telese-Izzi, Véronique Feipel, Marcel Rooze, and Serge Van Sint Jan. A novel method for in-vivo evaluation of finger kinematics including definition of healthy motion patterns. *Clinical biomechanics*, 31:47–58, 2016. Cited on p. 12.

[47] Peter Braido and Xudong Zhang. Quantitative analysis of finger motion coordination in hand manipulative and gestic acts. *Human movement science*, 22 6:661–78, 2004. Cited on p. 12.

[48] William T. Coffey, Yu. P. Kalmykov, and Serguey V. Titov. Inertial effects in the nonlinear transient relaxation of brownian particles in strong external electric fields. *Journal of Chemical Physics*, 115:9895–9904, 2001. Cited on p. 14.

[49] Theodore E. Milner and Caroline Cloutier. Damping of the wrist joint during voluntary movement. *Experimental Brain Research*, 122:309–317, 1998. Cited on p. 14.

[50] Anthony Unsworth, Patrick Bey, and I. B. Haslock. Stiffness in the metacarpophalangeal joints of young adults. *Clinical physics and physiological measurement : an official journal of the Hospital Physicists' Association, Deutsche Gesellschaft fur Medizinische Physik and the European Federation of Organisations for Medical Physics*, 2 2:123–33, 1981. Cited on p. 14.

[51] Marcelo H. Stoppa and João Carlos Mendes Carvalho. Kinematic modeling of a multi-fingered hand prosthesis for manipulation tasks. 2015. Cited on p. 14.

[52] John C. Herrera. Equation of motion in classical electrodynamics. [poymting momentum]. *Physical Review D*, 1977. Cited on p. 14.

[53] Irfan Hussain, Zubair Iqbal, Monica Malvezzi, Lakmal D. Seneviratne, Dongming Gan, and Domenico Prattichizzo. Modeling and prototyping of a soft prosthetic hand exploiting joint compliance and modularity. *2018 IEEE International Conference on Robotics and Biomimetics (ROBIO)*, pages 65–70, 2018. Cited on p. 17.

[54] A. van der Wegen. Representing a nonlinear state space system as a set of higher-order differential equations in the inputs and outputs. *Systems & Control Letters*, 12:151–160, 1989. Cited on p. 17.

[55] van der Arjan Schaft. Representing a nonlinear state space system as a set of higher-order differential equations in the inputs and outputs. 2002. Cited on p. 17.

[56] George C. Verghese, Bernard C. Levy, and Thomas Kailath. Generalized state-space systems. *1978 IEEE Conference on Decision and Control including the 17th Symposium on Adaptive Processes*, pages 518–520, 1978. Cited on p. 17.

[57] David Wright. The jacobian conjecture: linear triangularizatlon for cubics in dimension three. *Linear & Multilinear Algebra*, 34:85–97, 1993. Cited on p. 17.

[58] Waleed Mohamed Abd-Elhameed, Eid H. Doha, and Hany M. Ahmed. Linearization formulae for certain jacobi polynomials. *The Ramanujan Journal*, 39:155–168, 2016. Cited on p. 17.

[59] Boon Teck Ooi and Marcel Ivanès. Stiffness and damping matrices in free-body translational electromechanics. *Electric Machines and Power Systems*, 5:15–23, 1980. Cited on p. 20.

[60] Hyo-Jeong Cha, Kyoung Chul Koh, and Byung ju Yi. Stiffness modeling of a soft finger. *International Journal of Control, Automation and Systems*, 12:111–117, 2014. Cited on p. 20.

[61] Michael Vande Weghe, Matthew Rogers, Michael Weissert, and Yoky Matsuoka. The act hand: design of the skeletal structure. *IEEE International Conference on Robotics and Automation, 2004. Proceedings. ICRA '04. 2004*, 4:3375–3379 Vol.4, 2004. Cited on p. 63.

[62] Kevin Hung, Ho-Yuen Cheung, Nathan Wan, Eva Lee, C N Lai, Kun Pan, Rongle Liang, Carlin Chu, Sheung-On Choy, Douglas Ng, and D.H.K. Chow. Design, development, and evaluation of upper and lower limb orthoses with intelligent control for rehabilitation. *IET Science, Measurement & Technology*, 2021. Cited on p. 64.

[63] Long Wang, Joseph DelPreto, Sampriti Bhattacharyya, Jonathan Weisz, and Peter K. Allen. A highly-underactuated robotic hand with force and joint angle sensors. *2011 IEEE/RSJ International Conference on Intelligent Robots and Systems*, pages 1380–1385, 2011. Cited on p. 64.

[64] Xin hua Liu, Xiao hu Chen, Xian hua Zheng, Sheng peng Li, and Zhongbin Wang. Development of a ga-fuzzy-immune pid controller with incomplete derivation for

robot dexterous hand. *The Scientific World Journal*, 2014, 2014. Cited on p. 64.

[65] Konstantinos Andrianesis and Anthony Tzes. Development and control of a multifunctional prosthetic hand with shape memory alloy actuators. *Journal of Intelligent & Robotic Systems*, 78:257–289, 2015. Cited on p. 64.

[66] Kaiji Sato and Guilherme J. Maeda. A practical control method for precision motion—improvement of nctf control method for continuous motion control. *Precision Engineering-journal of The International Societies for Precision Engineering and Nanotechnology*, 33:175–186, 2009. Cited on p. 64.